AFRL-RV-HA-TR-2009-1013

Empirical Calibration of Small Explosion Seismic And Acoustic Phenomenology in New England

James Britton
Mark Leidig
Jessie Bonner
James Lewkowicz

Weston Geophysical Corporation
181 Bedford St., Suite 1
Lexington, MA 02420

Final Report

31 October 2008

APPROVED FOR PUBLIC RELEASE; DISTRIBUTION UNLIMITED.

AIR FORCE RESEARCH LABORATORY
Space Vehicles Directorate
29 Randolph Rd
AIR FORCE MATERIEL COMMAND
HANSCOM AFB, MA 01731-3010

NOTICES

Using Government drawings, specifications, or other data included in this document for any purpose other than Government procurement does not in any way obligate the U.S. Government. The fact that the Government formulated or supplied the drawings, specifications, or other data does not license the holder or any other person or corporation; or convey any rights or permission to manufacture, use, or sell any patented invention that may relate to them.

This report was cleared for public release and is available to the general public, including foreign nationals. Qualified requestors may obtain additional copies from the Defense Technical Information Center (DTIC) (http://www.dtic.mil). All others should apply to the National Technical Information Service.

AFRL-RV-HA-TR-2009-1013 HAS BEEN REVIEWED AND IS APPROVED FOR PUBLICATION IN ACCORDANCE WITH ASSIGNED DISTRIBUTION STATEMENT.

//Signature//	//Signature//
ROBERT J. RAISTRICK Contract Manager	Domenic Thompson, Maj, USAF, Acting Chief Battlespace Surveillance Innovation Center

This report is published in the interest of scientific and technical information exchange, and its publication does not constitute the Government's approval or disapproval of its ideas or findings.

REPORT DOCUMENTATION PAGE

Form Approved
OMB No. 0704-0188

1. REPORT DATE *(DD-MM-YYYY)*	2. REPORT TYPE	3. DATES COVERED *(From - To)*
10-31-2008	Final Report	08-30-2005 to 09-30-2008

4. TITLE AND SUBTITLE
Empirical Calibration of Small Explosion Seismic and Acoustic Phenomenology at Local and Regional Distances in New England

5a. CONTRACT NUMBER
FA8718-05-C-0073

5b. GRANT NUMBER
N/A

5c. PROGRAM ELEMENT NUMBER
62601F

6. AUTHOR(S)
James Britton, Mark Leidig, Jessie Bonner, and James Lewkowicz

5d. PROJECT NUMBER
1010

5e. TASK NUMBER
SM

5f. WORK UNIT NUMBER
A1

7. PERFORMING ORGANIZATION NAME(S) AND ADDRESS(ES)

Weston Geophysical Corporation
181 Bedford St., Suite 1
Lexington, MA 02420

8. PERFORMING ORGANIZATION REPORT NUMBER

9. SPONSORING / MONITORING AGENCY NAME(S) AND ADDRESS(ES)

Air Force Research Laboratory
29 Randolph Rd.
Hanscom AFB, MA 01731-3010

10. SPONSOR/MONITOR'S ACRONYM(S)
AFRL/RVBYE

11. SPONSOR/MONITOR'S REPORT NUMBER(S)
AFRL-RV-HA-TR-2009-1013

12. DISTRIBUTION / AVAILABILITY STATEMENT

Approved for Public Release; Distribution Unlimited.

13. SUPPLEMENTARY NOTES

14. ABSTRACT

Sparse station distribution, broad areas with few prior calibration events, complex paths, and a variety of seismic sources, both man-made and natural, are problems plaguing seismic monitoring in many regions of Europe and Asia. Added to these complexities are a lack of a physical understanding and empirical calibration data for small explosion sources in a variety of different crystalline media, including granitic and metamorphic terranes.

We conducted the experimental phase of the New England Damage Experiment in a granite quarry near Barre, VT. The goal of this experiment was to characterize the rock damage from an explosive source and to identify the source(s) of shear wave generation. We quantified crack nucleation and growth as a possible *S*-wave generation mechanism in the far field and mapped the cone of damage above a source, modeled by a compensated linear vector dipole. The velocity of explosive detonation (VOD) influences the amount of damage. A faster VOD generates higher pressures that crush the rock into a powder, which inhibits the explosive gasses from driving long cracks. We detonated black powder, ANFO/Emulsion, and COMP B, which have significantly different VOD so we could compare and contrast the damage from each source. Five shots were detonated ranging in size from 134 to 270 lbs of explosives. Over 140 seismic sensors were installed from less than 5 m to 30 km from the blasts specifically to record this experiment. Pre- and post-blast studies of the source rock properties were conducted using acoustic and optical borehole televiewers, coring, laboratory measurements for rock core properties, and cross-hole tomography.

15. SUBJECT TERMS
Explosions, Shear-wave generation, Nuclear monitoring, Rock damage, Infrasound, seismology

16. SECURITY CLASSIFICATION OF:			17. LIMITATION OF ABSTRACT	18. NUMBER OF PAGES	19a. NAME OF RESPONSIBLE PERSON
a. REPORT	b. ABSTRACT	c. THIS PAGE			Robert Raistrick
UNCLASSIFIED	UNCLASSIFIED	UNCLASSIFIED	SAR	118	19b. TELEPHONE NUMBER *(include area code)* 781-377-3726

Table of Contents

LIST OF FIGURES

List of Tables

1. SUMMARY

This contract (FA8718-05-C-0073) included the following tasks:

1. Quantify the source physics of small chemical explosions in a variety of crystalline media.

2. Study the regional phase energy partitioning of explosion-generated acoustic and seismic phases on permanent stations of the New England Seismic Network.

3. Predict the capabilities of regional seismic and acoustic discriminants for identification of earthquakes, mining explosions, and small explosions, with emphasis on extrapolating the results to the Korean Peninsula.

This report describes Tasks 1 and 2.

A related contract (FA8718-08-C-0044) included the following tasks:

1. Develop and design a "Pilot Study" to relate damage caused by small explosions (in the immediate and surrounding source region) to seismic phase generation.

2. Analysis of experimental program data.

Some of these objectives in these two contracts overlap. For example, Task 1 in Contract FA8718-05-C-0073 and Tasks 1 and 2 in Contract FA8718-08-C-0044, i.e., specifically the design, execution and analysis of data from an explosive field program to better understand the relationship of damage caused by the explosion in the source region to the propagated seismic energy. The field acquisition program, which addresses Task 1 in both contracts, was conducted under Contract FA8718-05-C-0073; while the preliminary data analysis is currently being conducted Contract FA8718-08-C-0044.

Therefore, what is described in this report is:

1) the design, deployment and preliminary data analysis for the Hanscom seismo-acoustic array (HANS) and

2) the field acquisition experiment to study the generation of seismic waves form damaged zones near the source region (The preliminary analysis of these data will be completed as Task 2 under contract FA8718-08-C-0044)

Sparse station distribution, broad areas with few prior calibration events, complex paths, and a variety of seismic sources, both man-made and natural, are problems plaguing seismic and acoustic monitoring in many regions of the Middle East and Asia. Added to these complexities are a lack of a physical understanding and empirical calibration data for small explosion sources in a variety of different crystalline media, including granitic and metamorphic terranes. We have

formed a consortium of industry and academic institutions to investigate these research topics by conducting a series of coordinated seismic experiments in the northeastern corridor of the United States (New England and New York). This region is predominantly composed of "hard" rocks consisting of granitic and metamorphic terranes that can be considered analogues for regions of monitoring concerns.

During the first year of this project, we found quarries and mines that were willing to detonate explosions in a variety of crystalline rock to help us accomplish our objectives. We also located sites for the deployment of temporary seismic and acoustic sensors. Our research effort shifted focus during the second year of this contract, and we have designed, deployed, and operated an infrasonic array near the Hanscom Air Force Base near Bedford, MA. The array consists of four (4) Chaparral 2 acoustic gauges in a 100 meter aperture with a broadband three-component Guralp CMG-3T seismometer located at the central element. The array became operational in December 2006 and continues to operate as of the publication of this report. During that time, we have collected a variety of seismic and infrasonic signals in this semi-urban setting, ranging from military and civilian aircraft (infrasound data only) to construction and mining explosions (both seismic and acoustic data).

During the final year of the project, we shifted our research focus back to active explosion source studies. Weston Geophysical Corp., New England Research, Inc., and a variety of blasting and geotechnical consultants conducted the experimental field phase of the New England Damage Experiment (NEDE) in a granite quarry near Barre, VT, during the first three weeks of July 2008. The goal of this experiment was to characterize the damage around an explosion and to identify possible source(s) of shear wave generation. The velocity of explosive detonation (VOD) and resulting borehole pressures have been shown to influence the amount of damage from an explosion[1]. A faster VOD generates higher pressures that crush the rock into a powder, which inhibits the explosive gasses during the crack forming processes. We detonated various types of explosives with significantly different VOD so we could examine the quantity of damage from each source. Seismic sensors were installed specifically to record this experiment. Pre-blast studies of the source rock properties were conducted and will be compared to currently on-going post-blast studies so that the damage generated by the explosions can be quantified.

2. INTRODUCTION

Few calibration data from previous nuclear or chemical explosions may exist in some regions of monitoring concern. Mining explosion data from such regions are rarely supported by ground truth information that can be used to improve the knowledge base. In some areas, earthquakes could be used to develop research and operational tools that increase the Air Force's capacity to detect nuclear explosions in these regions. However, other important regions may be relatively aseismic and have no calibration information. Therefore, numerous questions still remain as to the exact seismic and infrasonic nature of small explosions in regions of monitoring concern.

[1] http://www.johnex.com.au/index.php?section=105 (last accessed in July 2008).

Weston Geophysical and New England Research, Inc. formed a consortium to attack this problem from a unique direction. We built upon the similarities in the geographic, topographic, geologic, and geophysical characteristics between New England (including New York) and different regions of monitoring concern and developed a unique seismic and infrasonic database. The database will allow us to obtain an improved understanding of the characteristics of small explosions in a variety of different crystalline rock emplacement media.

While the database developed from this project is not be a direct substitute for the calibration information that could be gained from in-country explosion data, we do believe it will improve the Air Force's monitoring mission in a variety of different ways. The explosions we have conducted as part of the third year of this project will help:

- Quantify the source physics of small chemical explosions in a variety of crystalline media,

- Study the local and regional phase energy partitioning of explosion-generated seismic phases on temporary and permanent stations of the New England Seismic Network (NESN), and

- Predict the capabilities of regional discriminants for identification of earthquakes, mining explosions, and small explosions, with emphasis on extrapolating the results to current monitoring concerns.

Additionally, the database has infrasound signals from a variety of sources in a semi-urban environment. This project resulted in a three-year effort that provides the Air Force with a unique dataset for improved characterization of nuclear explosions in emplacement media and propagation path terranes similar to the Korean Peninsula and other regions of monitoring concern.

3. PRELIMINARY RESEARCH AND ARRAY INSTALLATION

During the first two years of this research project, we determined the optimal explosion source locations at mines in New England, obtained site permissions for deploying near-source, local, and regional seismic and acoustic stations, deployed a seismo-acoustic array in a semi-urban setting, and recorded seismic and infrasound data from a variety of man-made sources.

3.1 Mine Locations

Weston Geophysical Corporation (WGC), with help from Father James W. Skehan, S.J., Boston

College (BC), located active mines and quarries in New England. We completed a study of the explosion seismicity to identify possible mines that could be locations for the source phenomenology experiments. We used single- and multiple-station methods to locate four clusters of mining events (Table 1) using seismic data from the United States Geological Survey and New England Seismic Network.

Examples of data for a suspected mining explosion near Littleton, MA are shown in Figure 1. After the preliminary locations had been formed, we used Google Earth and land use geographic information system (GIS) databases to pinpoint the mines. Examples of the images of these mines are shown in Figures 2-16.

Table 1. Cluster coordinates represent the median location for the events in each cluster.

Cluster No.	Cluster Coordinates	Nearest Quarry(s)	Quarry Location	Quarry Coordinates	Dist from Cluster
1a	42.55, -71.51	Aggregate Industries	Littleton, MA	42.55, -71.52	<1 km
1b	42.19, -71.22	Sam White & Sons	Medfield, MA	42.18, -71.32	8 km
		S.M. Lorusso & Sons	Walpole, MA	42.14, -71.27	7 km
1c	42.61, -71.08	Benevento Sand & Stone	Wilmington, MA	42.58, -71.13	5 km
		Heffron Materials	Wilmington, MA	42.58, -71.13	5 km
1d	42.89, -71.11	Galloway Trucking, Inc.	Plaistow, NH	42.86, -71.09	3-4 km
1e	42.45, -71.84	Pandolf-Perkins	Sterling, MA	42.43, -71.77	6 km
2a	42.01, -71.44	Kimball Sand Co, Inc.	Blackstone, MA	42.06, -71.52	5 km
		unknown #1	Slatersville, RI	41.99, -71.59	8 km
		unknown #2	Primrose, RI	41.95, -71.55	9 km
		Aggregate Industries	Wrentham, MA	42.03, -71.36	11 km
2b	41.70, -71.54	P.J. Keating	Cranston, RI	41.77, -71.44	9 km
3	42.11, -71.72	Percy Guiou Excavating	Douglas, MA	42.06, -71.73	5 km
		Aggregate Industries	Sutton, MA	42.17, -71.73	7 km
		unknown #3*	Sutton, MA	42.10, -71.71	<1 km
4	42.07, -71.49	Kimball Sand Co, Inc.	Blackstone, MA	42.06, -71.52	2-3 km

* Several pits are in the area along Route 495. It is not clear to which company they belong.

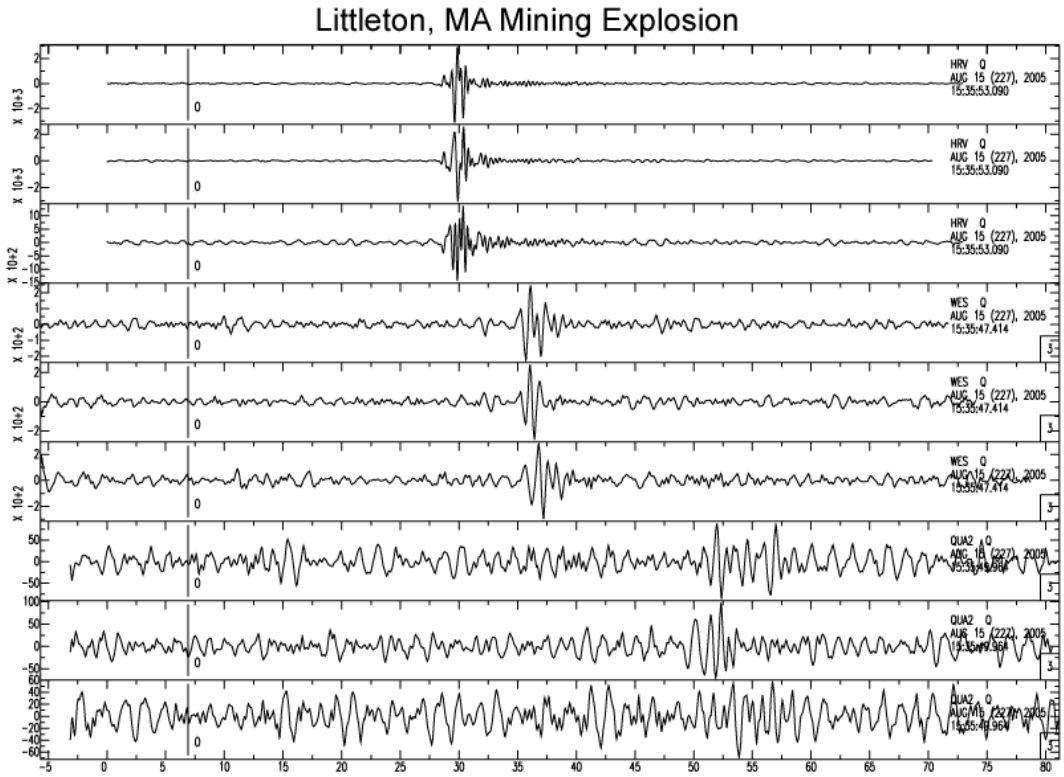

Figure 1. Examples of waveforms recorded on the New England Seismic Network for a mining explosion near Littleton, MA. Overhead imagery of the mine is shown in Figure 9.

Quarry Associated with Cluster 1a

Figure 2. Aggregate Industries, Littleton, MA – Photo from Google Earth

Quarries Associated with Cluster 1b

Figure 3. Sam White & Sons, Medfield, MA – Photo from Google Earth

Quarries Associated with Cluster 1b

Figure 4. S.M. Lorusso & Sons, Walpole, MA – Photo from Google Earth

Quarries Associated with Cluster 1c

Figure 5. Heffron Materials and Benevento Sand & Stone Co. are adjacent to one another. It is not clear which property belongs to which company. – Photo from Google Earth

Quarry Associated with Cluster 1d

Figure 6. Galloway Trucking, Inc., Plaistow, NH. The imagery for this part of New Hampshire is of much poorer resolution than the imagery of Massachusetts (bottom right of picture). – Photo from Google Earth.

Quarry Associated with Cluster 1e

Figure 7. Pandolf-Perkins, Sterling, MA – Photo from Google Earth

Quarries Associated with Cluster 2a

Figure 8. Kimball Sand Co, Blackstone, MA – Photo from Google Earth

Quarries Associated with Cluster 2a

Figure 9. Unknown Quarry #1, Slatersville, RI – Photo from Google Earth

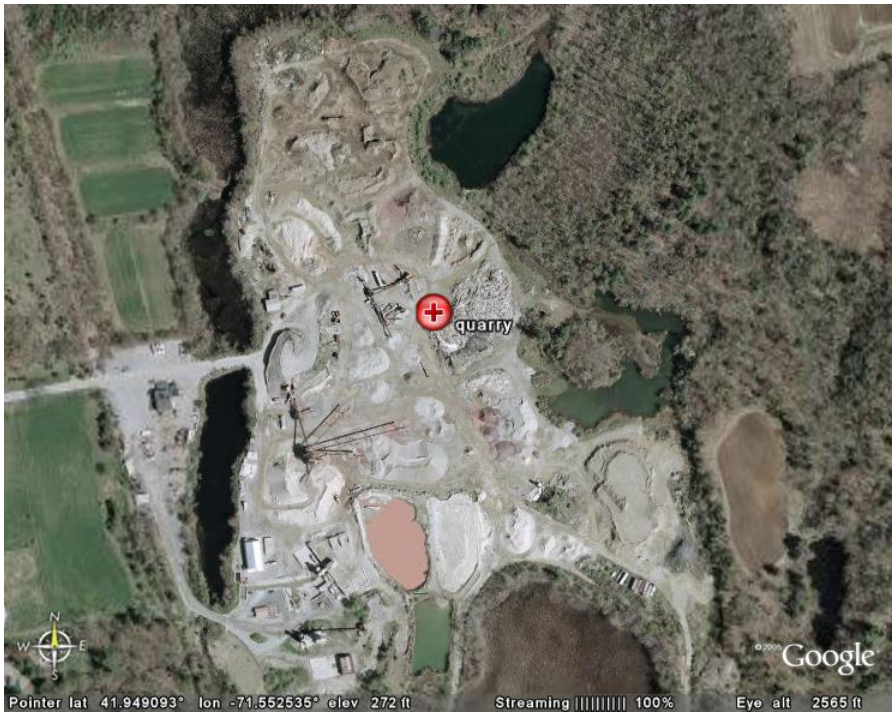

Figure 10. Unknown Quarry #2, Primrose, RI – Photo from Google Earth

Quarries Associated with Cluster 2a

Figure 11. Aggregate Industries, Wrentham, MA – Photo from Google Earth

Quarry Associated with Cluster 2b

Figure 12. P.J. Keating, Cranston, RI – Photo from Google Earth

Quarries Associated with Cluster 3

Figure 13. Percy Guiou Excavating, Douglas, MA – Photo from Google Earth

Figure 14. Aggregate Industries, Sutton, MA – Photo from Google Earth

Quarries Associated with Cluster 3

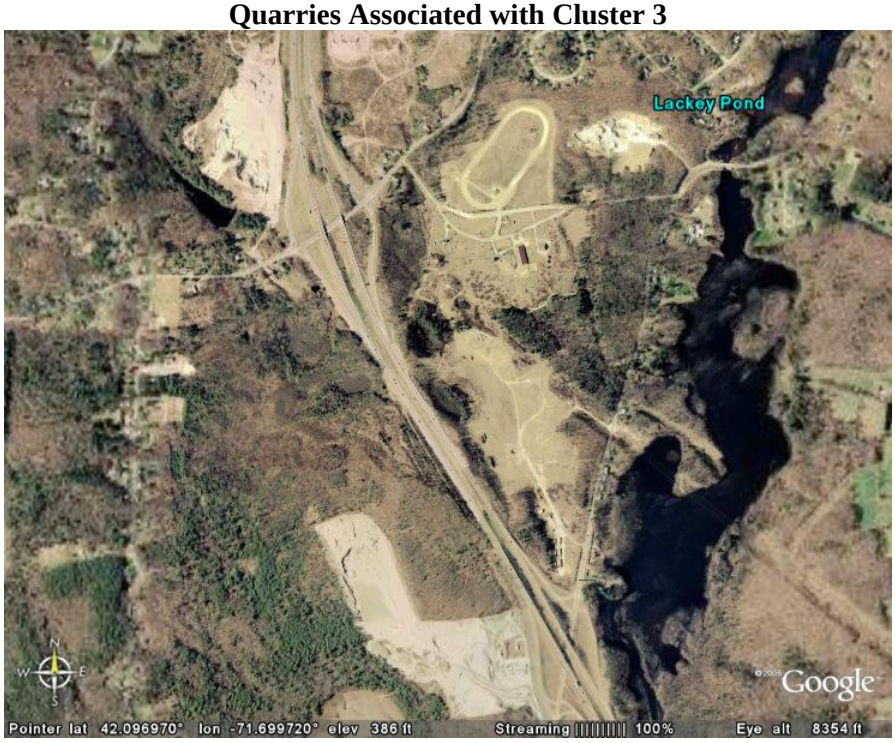

Figure 15. Unknown Quarry #3, Sutton, MA. The photo shows two pits alongside Route 495. There are others in the same area. – Photo from Google Earth

Quarry Associated with Cluster 4

Figure 16. Kimball Sand Co, Blackstone, MA – Photo from Google Earth

3.2 Mine Collaboration

Weston Geophysical contacted mines in New England to enter into collaborative agreements to conduct the single-fired experiments in either Summer 2006 or 2007. We found several mines willing to participate, including gravel and basalt quarries in central and northeastern Massachusetts, gravel quarries in northern Connecticut, and garnet quarries in eastern New York.

3.2.1 Central and Eastern Massachusetts

A gravel quarry in the town of Leominster, Massachusetts is one property that agreed to shoot a series of tests for us. The quarry is located in a quartzite and typically shoots 1-2 production shots per week (Figure 17a). At this quarry, they agreed to drill to the appropriate depths in the pit floor (Figure 17b) and to detonate the shots for our project. We also contacted other mines in Sterling, Holden, and Littleton Massachusetts and had success in getting the mining engineers to consider cooperating with the proposed tests.

Figure 17. a) Fractured rock from a production shot at a quartzite mine in Leominster, Massachusetts. b) Entrance to pit where explosion tests were to be conducted. The rock below the basal level of the pit is undamaged by previous explosions.

3.2.2 Connecticut

We also met with the blasting engineers at Vets Explosives in northwest Connecticut. They agreed to conduct explosives experiments at the Burrville No. 4 quarry (Figures 18-21). The mine was located in a granite and metamorphic complex with competent crystalline rock for the explosions.

Figure 18. Entrance to the Burrville Quarry, No. 4 north of Torrington, CT.

Figure 19. Pit in the Burrville No. 4 quarry.

Figure 20. Preparing for a blast in the metamorphic complex at Burrville.

Figure 21. Crystalline rock at the Burrville quarry.

Quarry blast logs from the Burrville Quarry #4 were obtained for year 2005 shots 22 through 35, excluding 24 and 28. This quarry is located in a very dense, strong granite and metamorphic complex. Waveform data from nearby stations were downloaded from IRIS and examined for phase arrivals at various distances. The small shot sizes, both total yield and yield per delay, in combination with an inexact shot time made it difficult detect the explosions at most stations.

Station LSCT (25 km from the mine) recorded the blasts well at all recordable frequencies, but data were only available for a limited period in 2005. Data from these shots were available from IRIS and are shown in Figure 22. Rayleigh waves are evident in the 0.8-2 Hz passband, but are only slightly dispersed at 25 km distance. The *P* and *S* phases tend to be emergent and scattered due to the delay-fired nature of the explosions.

Figure 23 shows waveforms from station MANY, 75 km distance from the Burrville Quarry. Body wave arrivals are buried in the noise and only Rayleigh waves can be observed. Although, the first two shots have two sets of large amplitude arrivals and the cause of this is not known. The largest amount of explosives fired per delay is 900 lbs. The experiment explosions at Burrville would have ranged from 500 to 2000 lbs single-fired.

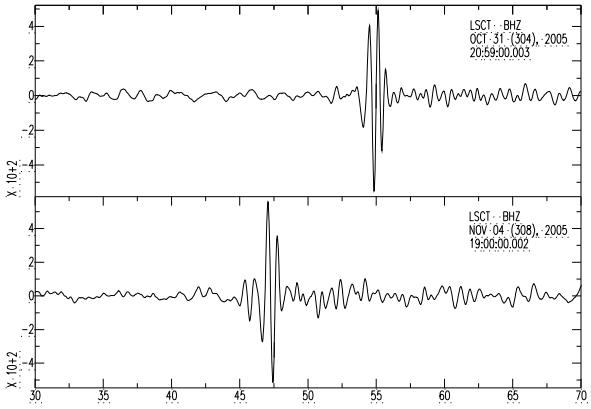

Figure 22. Station LSCT, 25 km from Burrville Quarry. BHZ components band passed from 0.8-2 Hz. Only the 10/31/2005 & 11/04/2005 events had data available from IRIS.

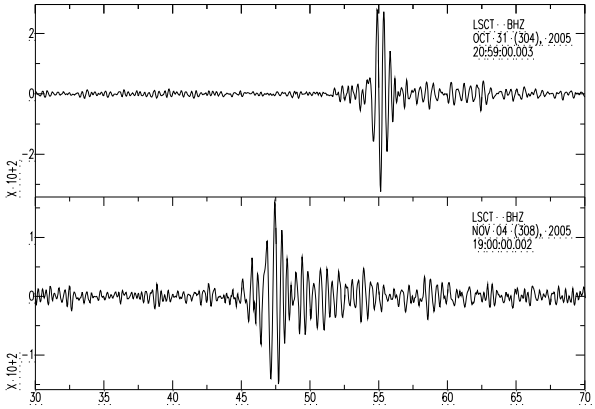

LSCT BHZ 2-4 Hz

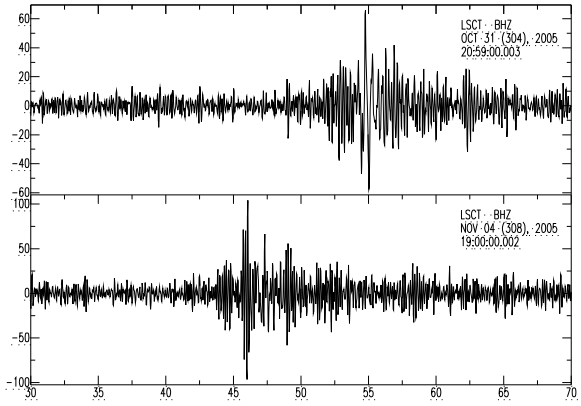

LSCT BHZ 4-8 Hz

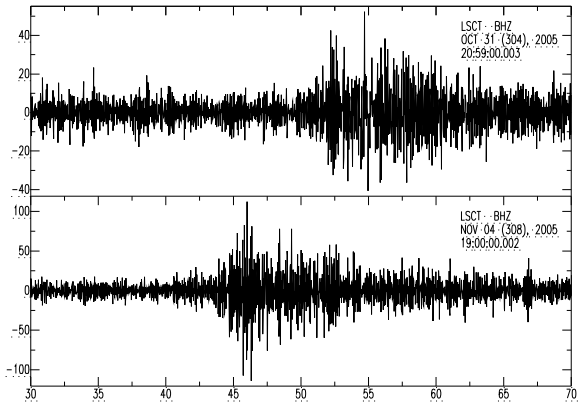

LSCT BHZ 8-16 Hz

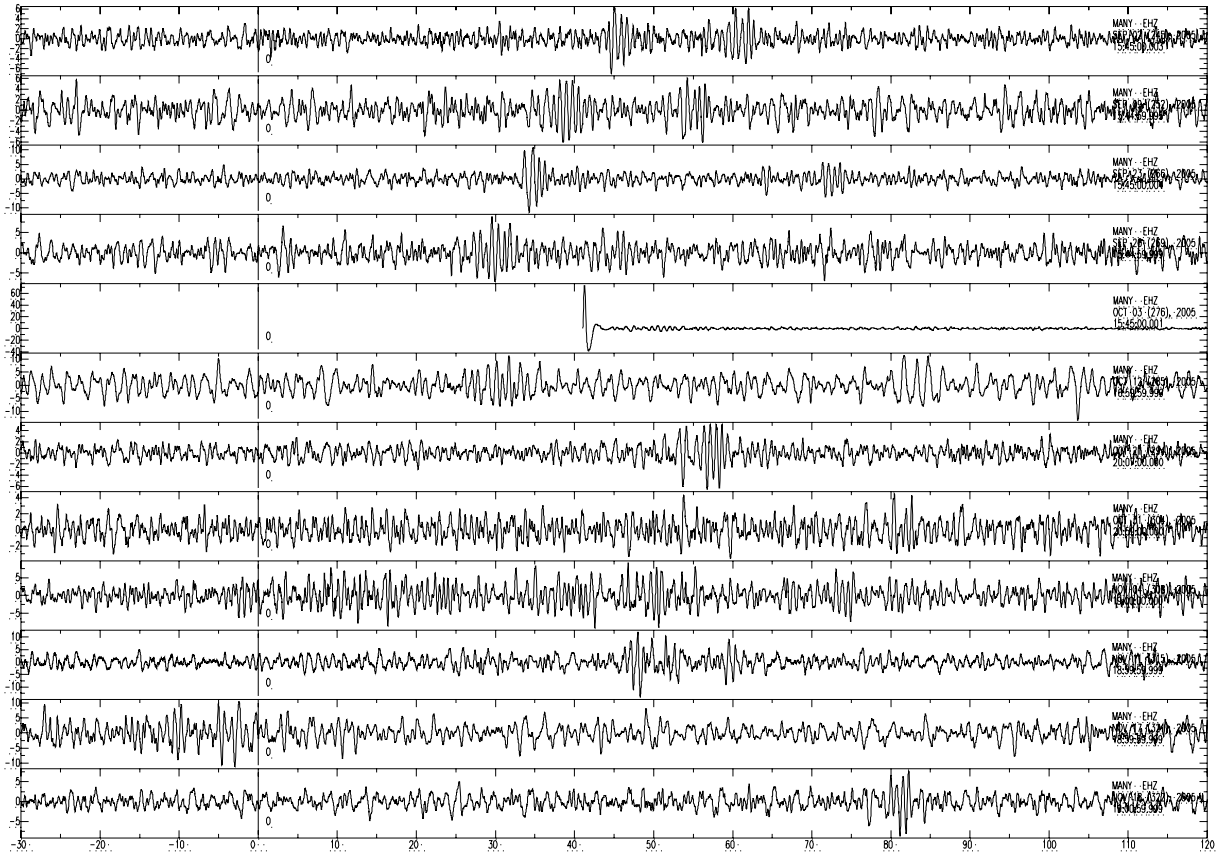

Figure 23. Mining events recorded at station MANY, 97 km SSW of Burrville Quarry. EHZ components band passed at 0.5-2 Hz.

3.3 Station Locations

We scouted locations to deploy our seismic instruments for the New England Source Phenomenology Experiment. Because we planned to deploy these sensors for at least one year, we chose locations that had on-site security or with limited public access. As a result, most of our stations were in state parks in Connecticut, New Hampshire, Massachusetts, and New York. Weston Geophysical worked with these state parks to obtain permits to deploy the instruments for the duration of the experiment. Examples of the localities are shown in Figures 24 and 25. Figure 26 provides the final network design together with the location of the collaborating mines.

Figure 24. Burrville Pond State Park in CT.

Figure 25. Mohawk Trail State Forest in Massachusetts.

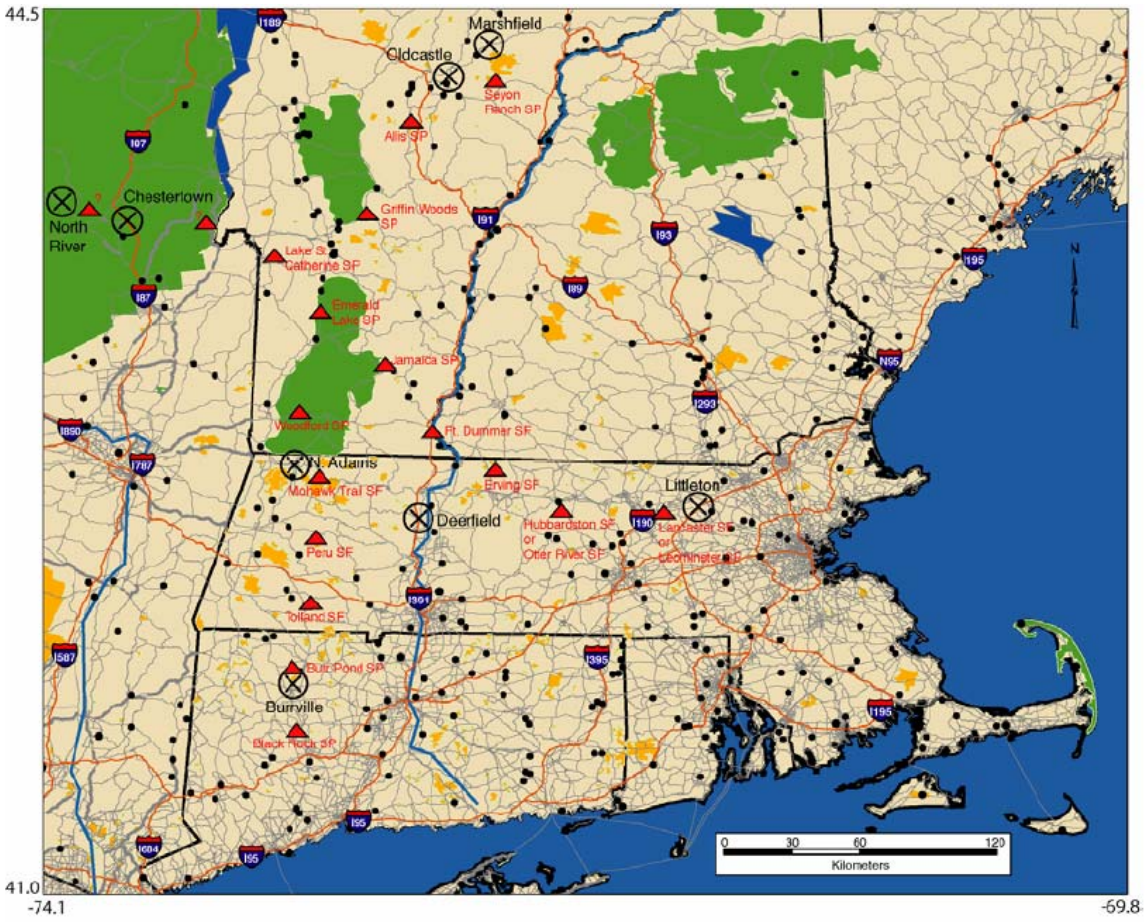

Figure 26. Locations of mines (circles with x) and seismometers (▲) for the New England Source Phenomenology Experiments.

3.4 Seismo-Acoustic Array

The Hanscom Seismo-Acoustic Array, codename HANS, is located in a hay field just to the southwest of Hanscom Field, a regional airport in Bedford, Massachusetts (Figure 27). The coordinates for the array are: 42.4611° N Latitude and 71.2996° W Longitude. The seismo-acoustic array is arranged in a "Y"-shaped pattern with Chaparral acoustic sensors located at the center and ends of the "Y" (Figure 28). The outlying acoustic elements are located 100 meters from the center, connected to the center of the array by three 100-meter cables joined together at one end with a single connector. Six 25-foot (Apex brand) soaker hoses are attached to each of the acoustic elements, as shown in Figure 29. The sample rate for the acoustic sensors is 100 samples per second.

Figure 27. Google Earth image of Hanscom Field in Bedford, MA. The red circle shows the location of the seismo-acoustic array.

Figure 28. Google Earth image showing the locations of the seismo-acoustic array in relation to Runway 5 at Hanscom Field. The seismic instrument is co-located with the central acoustic element acou5.

Figure 29. A Chaparral acoustic sensor with attached soaker hoses for wind noise reduction.

A Guralp 3C broadband seismometer was installed near the center of the array within two meters of the central acoustic element. The broadband seismometer was later replaced in July 2008 with a short-period Sercel (formerly Mark Products) 1 Hz L4-3D seismometer. The digital acquisition systems (Reftek 72A-08 DAS prior to July 2008; Reftek RT-130 DAS thereafter) and power supply are also located in the center of the array. An inverted beverage cooler is used to provide the seismometer with protection from the wind, rain, and daily thermal fluctuations (Figure 30). The sample rate was initially set to 40 sps for the seismic instrument, but was increased to 100 sps in Fall 2007. The array is powered by a solar panel system consisting of two deep-cycle batteries and a 110W Mitsubishi solar panel (Figure 31).

Figure 30. Placement of seismometer on concrete surface before being enclosed by the insulating cooler.

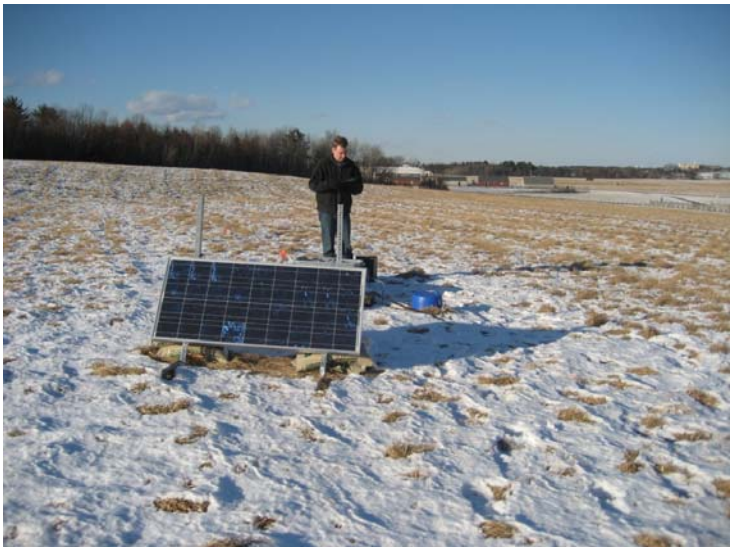

Figure 31. Solar panel that powers the HANS seismo-acoustic array at Hanscom Air Force base.

3.4.1 Noise Studies

We compared the seismic noise at the Hanscom (HANS) seismic station to the Peterson (1993) Low Noise Models. The results shown in Figure 32 suggest the station is relatively quiet at higher frequencies, but has increased longer-period noise and microseisms. We also examined the acoustic noise spectra recorded at the array. Comparisons of median spectra for night and day and varying wind conditions are shown in Figure 33.

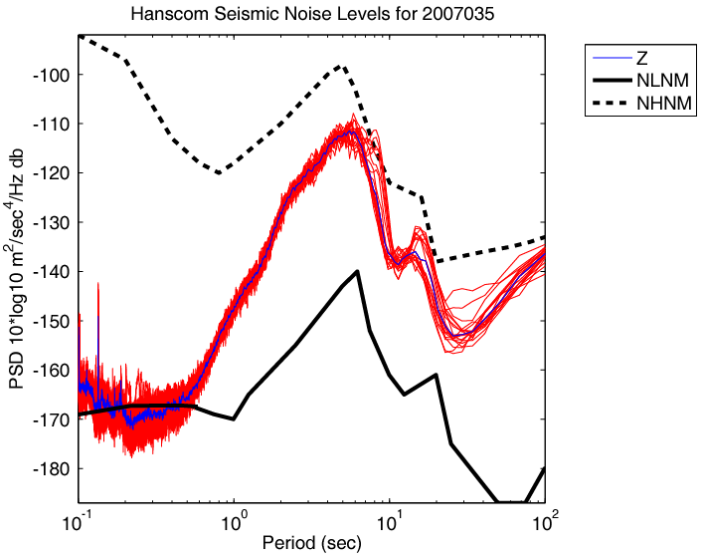

Figure 32. Hourly noise spectra (red lines) and median spectrum (blue) for seismic data recorded at HANS. Also shown are the new low and high noise models for comparison to the observed spectra.

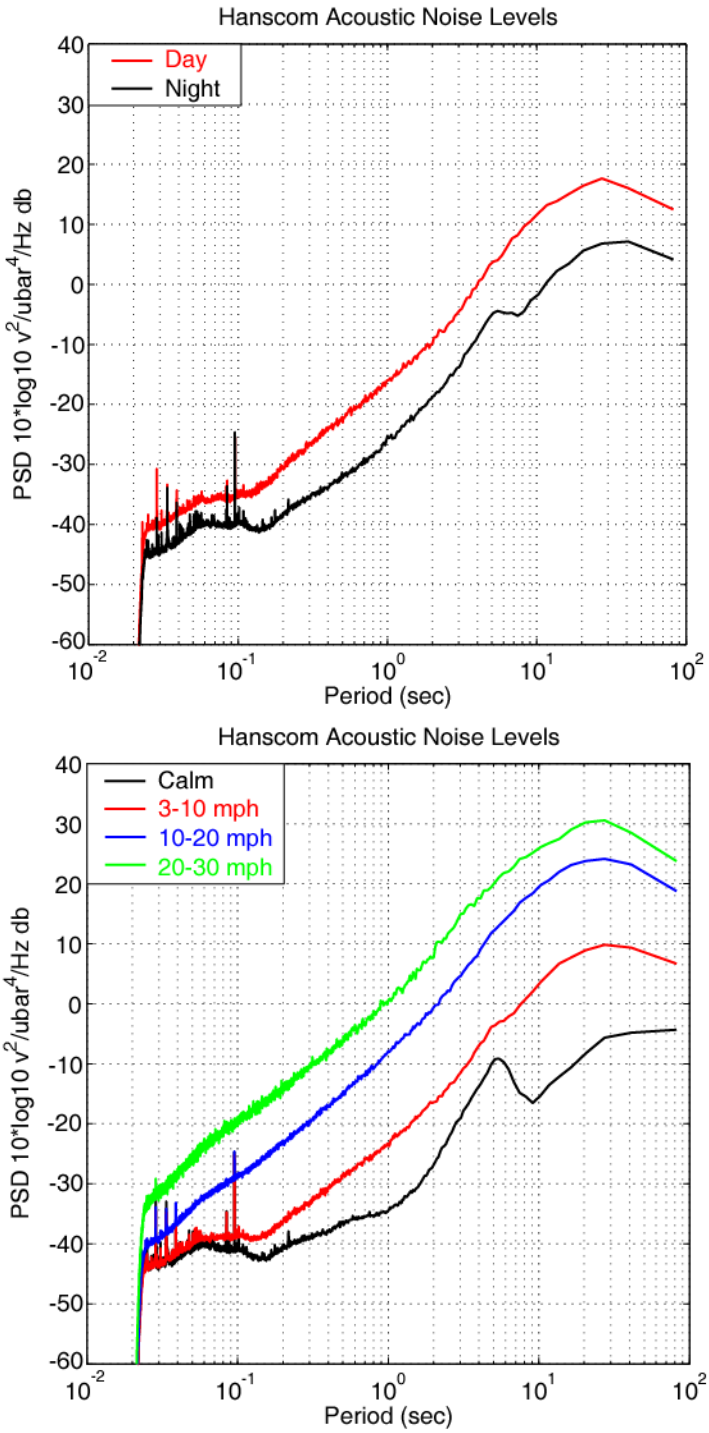

Figure 33. Acoustic noise at HANS. (Top) Median noise spectra for night (black) and day (red) at the HANS acoustic array. (Bottom) Median noise spectra for varying wind speeds at the HANS acoustic array. We note that for the calm winds, we observe 5-second microbarom noise generated from distant marine storms.

3.4.2 Earthquakes

The HANS seismic array recorded numerous small magnitude earthquakes in New England (Figure 34) since its start date in December 2006. The magnitudes reported for these events range from 1.1 to 3.6. Table 2 provides a list of local- to near-regional distance events contained in our current waveform database. We supplemented the HANS data with waveform data from nearby stations (Table 3) from the New England Seismic Network (NESN) and a United States Geological Survey network (USGS). Examples of waveforms for the events listed in Table 2 are shown in Figure 35.

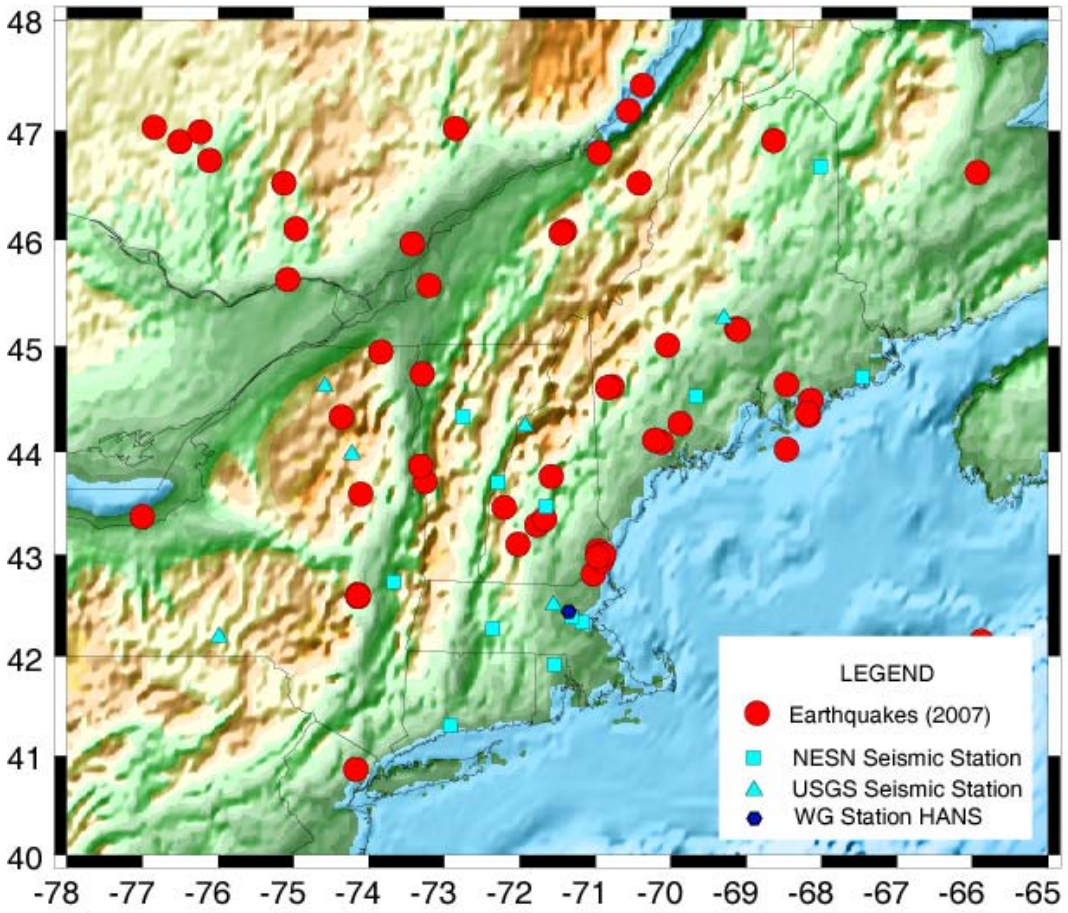

Figure 34. Local earthquakes (red circles) occurring in New England since the on-date (December, 2006) of the HANS seismo-acoustic array (blue circle) until October 2007. Also shown are the locations of the seismic stations of the NESN and USGS National Earthquake Information Center (NEIC).

Table 2. Earthquakes sorted by epicentral distance. Bulletin sources: NESN and NEIC.

Mon	Day	Year	Time	Mag	Lat	Lon	Loc	Dist
10	19	2007	05:23	2.5	42.54	-71.50	Littleton, MA	20
10	19	2007	10:04	0.9	42.55	-71.48	Littleton, MA	20
10	08	2007	11:15	1.3	42.81	-71.02	Merrimac, MA	45
06	21	2007	00:31	1.0	43.04	-70.96	Exeter, NH	65
06	03	2007	03:08	1.1	42.94	-70.91	Exeter, NH	65
06	03	2007	02:35	1.4	42.99	-70.93	Exeter, NH	65
06	02	2007	23:56	1.9	43.00	-70.88	Exeter, NH	65
06	01	2007	14:10	1.4	42.98	-70.96	Exeter, NH	65
10	21	2007	23:46	1.7	43.02	-71.86	Bennington, NH	77
03	13	2007	05:21	1.5	43.37	-71.62	Franklin, NH	104
03	21	2007	15:55	2.6	43.76	-71.57	Laconia, NH	146
02	01	2007	01:04	1.5	43.86	-73.31	Middlebury, VT	226
02	01	2007	16:48	2.1	44.27	-69.87	Augusta, ME	232
12	29	2006	21:21	3.1	44.35	-68.17	Bar Harbor, ME	329
12	18	2006	19:53	2.3	44.37	-68.16	Bar Harbor, ME	331

Table 3. Seismic stations near the Hanscom Array

Code	Network	Name	Location	Distance from HANS	Lat	Lon	Elev [m]
HANS	WG	Hanscom Seismic	Bedford, MA	0 km	42.4611	-71.2996	43
FHL	WG	Fiske Hill (temporary)	Lexington, MA	3.6 km	42.4464	-71.2608	67
WES	NE	Weston Observatory	Weston, MA	8.7 km	42.3848	-71.3218	60
HRV	US	Harvard	Harvard, MA	21.8 km	42.5063	-71.5583	178
BRYW	NE	Bryant College	Smithfield, RI	63.4 km	41.9178	-71.5388	116
QUA2	NE	Quabbin Reservoir	Belchertown, MA	89.0 km	42.2788	-72.3525	168
FFD	NE	Franklin Falls Dam	Franklin Falls, NH	115.6 km	43.4701	-71.6533	131

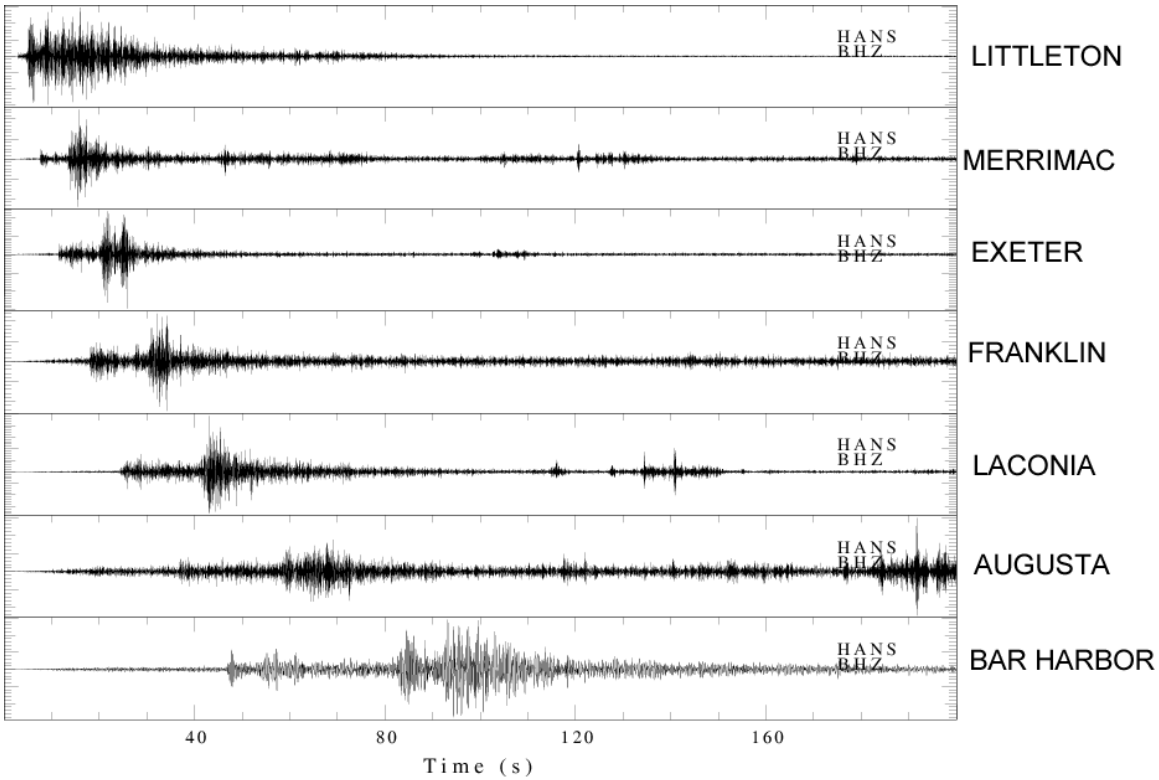

Figure 35. Record section of select events listed in Table 2 as recorded at the Hanscom seismic station (HANS) near the Hanscom Air Force Base in Bedford, MA.

3.4.3 Blasting at Starwood Hotels

In addition to natural seismicity, signals from local quarries and construction sites were routinely detected at HANS. Blasting activity occurred 3.6 km from the Hanscom Array on the Starwood Hotels property site in Lexington, MA from 2/5/07 until 4/10/07 (Figures 36 and 37). Permission was granted by the National Park Service on 3/20/07 to place a near-source seismometer (station FHL) on their property, Fiske Hill, located directly across the road from the blasting activity. The average distance from FHL to the blasts was about 200 meters. The instrument used was a Mark L4-3D short-period seismometer with a sampling rate of 250 Hz. Park regulations prohibited the digging of holes for archeological reasons. The L4-3D seismometer was placed above-ground on a small stone slab (Figure 38) and covered by a plastic bin weighted down by sand bags.

Blast reports were obtained from the Lexington Fire Department. These reports are on file for a minimum of 5 years following blasting activity. According to the reports, the types of explosives used included: cast boosters, Hydromite 860, ANFO, and a bulk emulsion. Blasting mats were used in at least some of the shots to reduce flyrock. Table 4 lists the most recent of the 33 blasts detonated at this site, and which data are available for these shots.

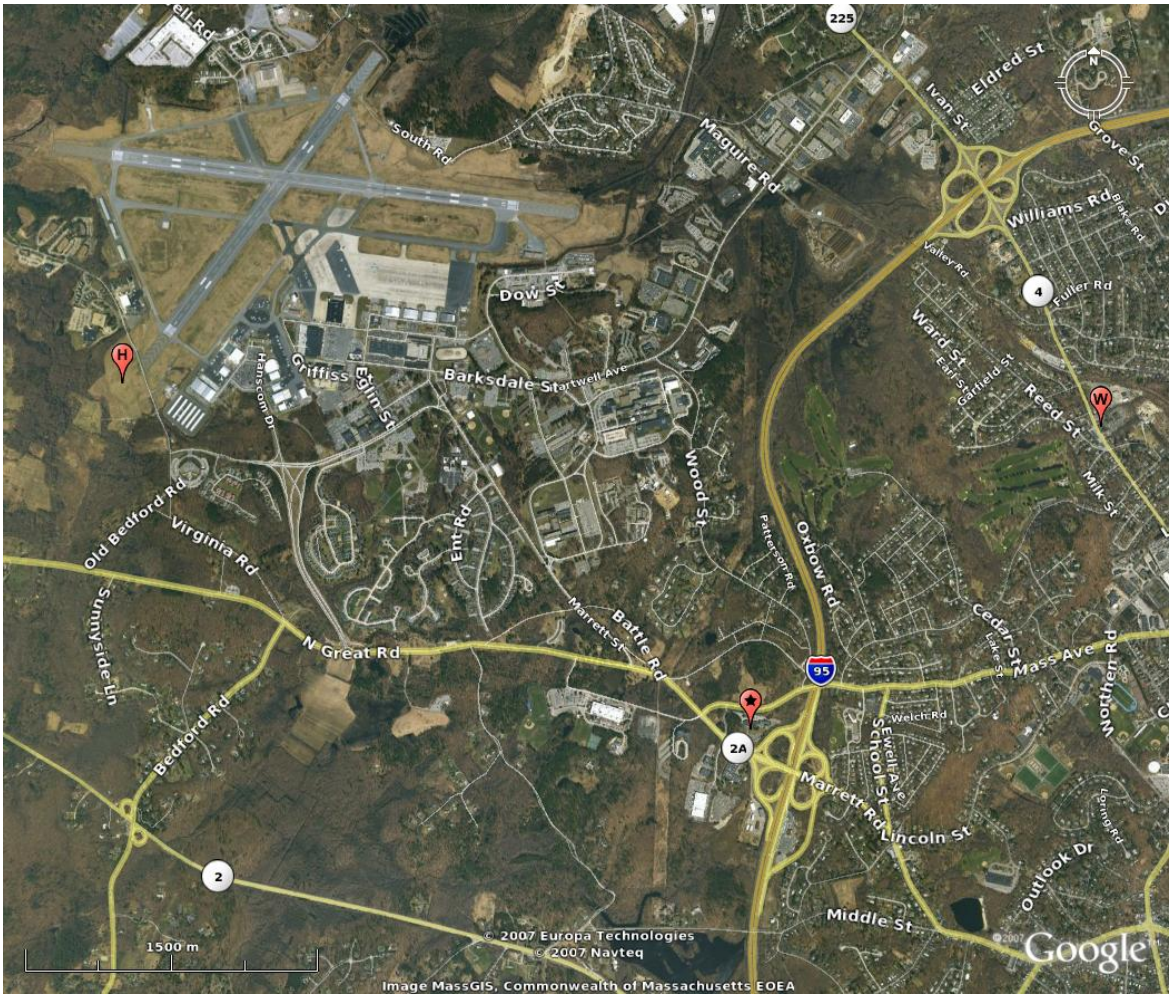

Figure 36. Locations of blast site (star), Hanscom Array (H), and Weston Geophysical home office (W). Scale bar in lower left corner is 1.5 km.

Figure 37. Google Earth map showing the locations of station FHL (white diamond) and approximate blasting area (red rectangle).

Figure 38. Temporary short-period seismic station FHL consisting of an L4-3D seismometer set up on a stone pad.

Table 4. Events with blast confirmation from near-source instrument or blasting report.

Date	Time [UTC]	Near-Source (FHL)	Seismic (HANS)	Acoustic (HANA)	Total pounds per shot	Shot No.
03/12/2007	16:59	NA	?	?	275	18
03/13/2007	17:18	NA	yes	yes	2234	19
03/14/2007	17:23	NA	yes	yes	3000	20
03/15/2007	17:18	NA	yes	yes	2491.5	21
03/19/2007	17:25	NA	NA	?	1805.3	22
03/20/2007	17:39	NA	yes	?	3430	23
03/21/2007	17:47	yes	yes	NA	2108.36	24
03/22/2007	17:36	yes	yes	NA	3931.5	25
03/23/2007	17:13	yes	yes	NA	1655	26
03/27/2007	17:38	yes	yes	NA	3951	27
03/29/2007	16:51	yes	NA	NA	3838	28
04/02/2007	16:47	NA	yes	NA	2460	29
04/03/2007	17:58	yes	yes	yes	2614	30
04/05/2007	17:30	NA	yes	yes	2276	31
04/06/2007	17:02	yes	yes	yes	2207.5	32
04/10/2007	17:21	yes	yes	yes	1355.5	33

An example of one of these events (4/10/2007) recorded on the near-source, broadband, and acoustic instruments is shown in Figure 39 (unfiltered) and Figure 40 (bandpass filtered from 0.8 to 19.9 Hz). The acoustic signal arrives just over 10 seconds after the seismic signal at Hanscom, and is visible on both the unfiltered and filtered waveforms.

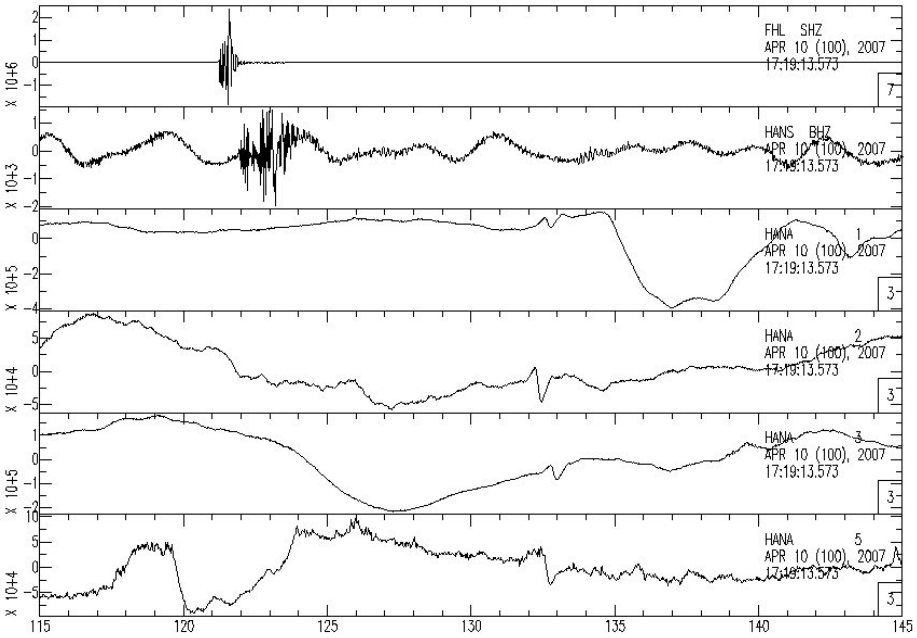

Figure 39. Unfiltered seismic and acoustic data from Starwood Hotels blasting.

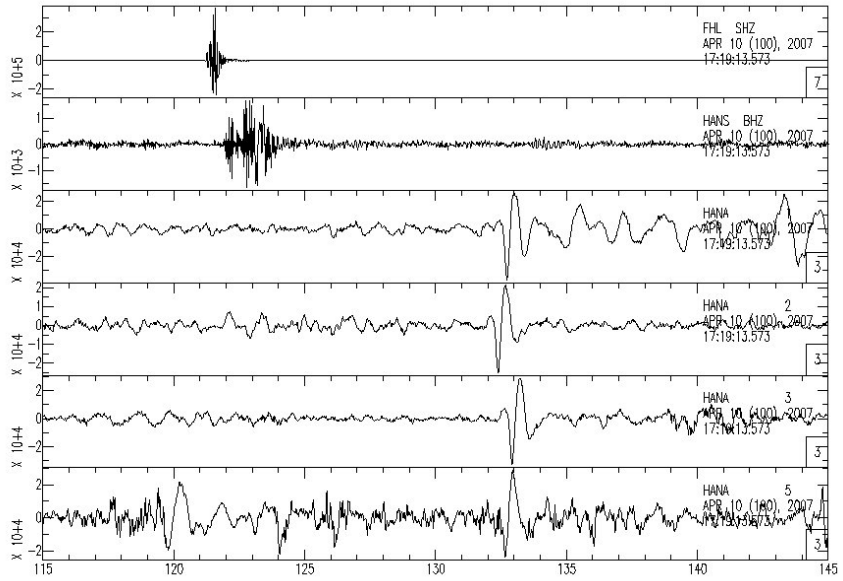

Figure 40. Bandpass filtered (0.8 to 19.9 Hz) seismic and acoustic data from Starwood Hotels blasting.

3.4.4 Blasting at Aggregate Industries, Littleton, MA

Blasting is routinely conducted at the Aggregate Industries quarry in Littleton, MA (Figure 41), located approximately 20 km northwest (42.55N, 71.52W) of the Hanscom Array. The quarry operators have been cooperative with providing blast information (Table 5).

Figure 41. Aggregate Industries (formerly San Vel Quarry) in Littleton, MA.

Table 5. Blasting times and explosive weights for blasts at Aggregate Industries

Date	Local Time [EST]	Explosive Weight [lbs]
3/15/2007	11:38 AM	20,160
4/2/2007	1:11 PM	19,111
4/6/2007	1:12 PM	18,455
4/25/2007	1:07 PM	23,320
5/1/2007	11:37 AM	22,940
5/7/2007	11:00 AM	23,700
5/11/2007	11:07 AM	20,990
5/17/2007	11:11 AM	24,616

On October 19, 2007, a 2.5 Mn earthquake occurred within 2 km of the quarry, and was later followed by a 0.9 Mn aftershock (Table 6). The two earthquakes and one of the quarry blasts are shown in Figure 42. All events exhibit a large *Rg* signal (Figure 43), signifying shallow depths. The acoustic instruments lost power during the time span of the earthquakes, so it is not known if the shallow earthquakes produced an acoustic signal. A preliminary assessment of *P/S* ratios shows a distinct difference between the blasts and earthquakes at frequencies greater than 8 Hz (Figure 44).

Table 6. Earthquakes located near Littleton quarry (source: NESN bulletin)

Date	Time [UTC]	Latitude	Longitude	Magnitude
10/19/2007	05:23:52.96	42.54	-71.50	2.5 Mn
10/19/2007	10:04:47.04	42.55	-71.48	0.9 Mn

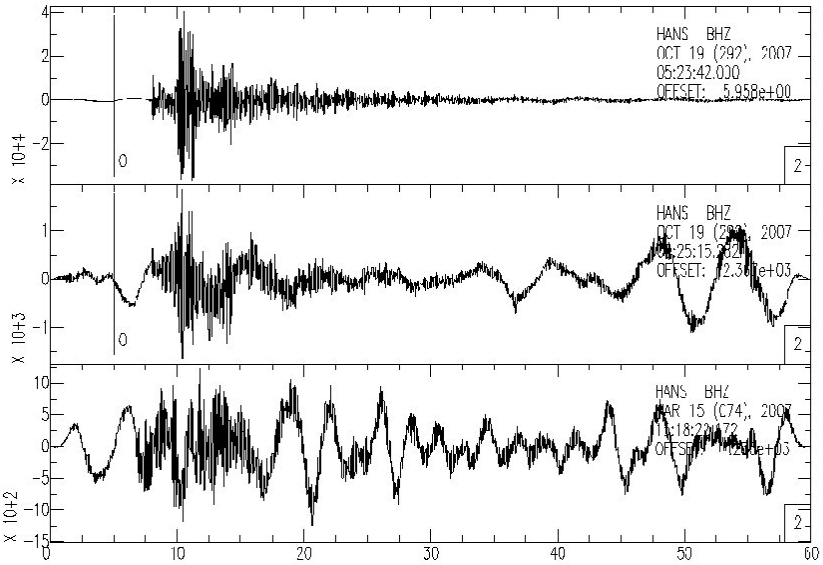

Figure 42. Un-filtered waveforms recorded at HANS. From top to bottom: 2.5 Mn earthquake, 0.9 Mn earthquake, 03/15/07 quarry blast.

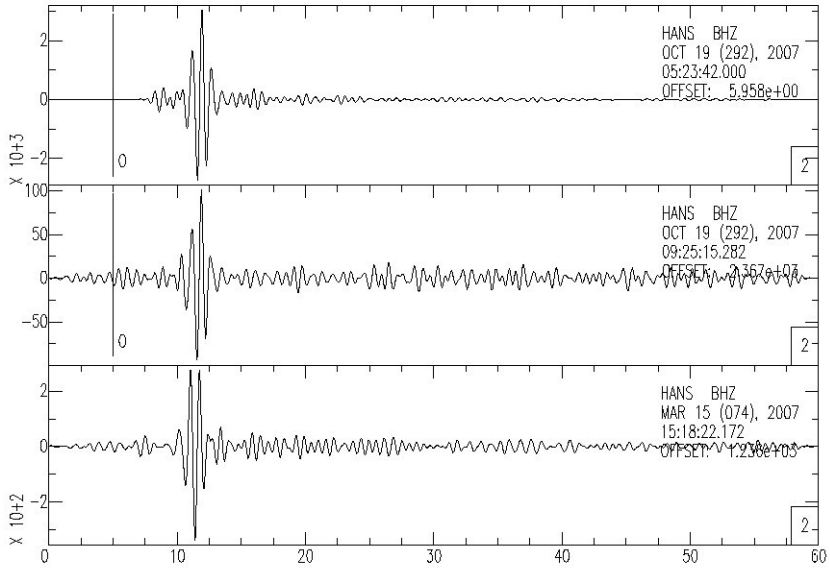

Figure 43. Same waveforms as previous figure but bandpass filtered from 1 to 2 Hz.

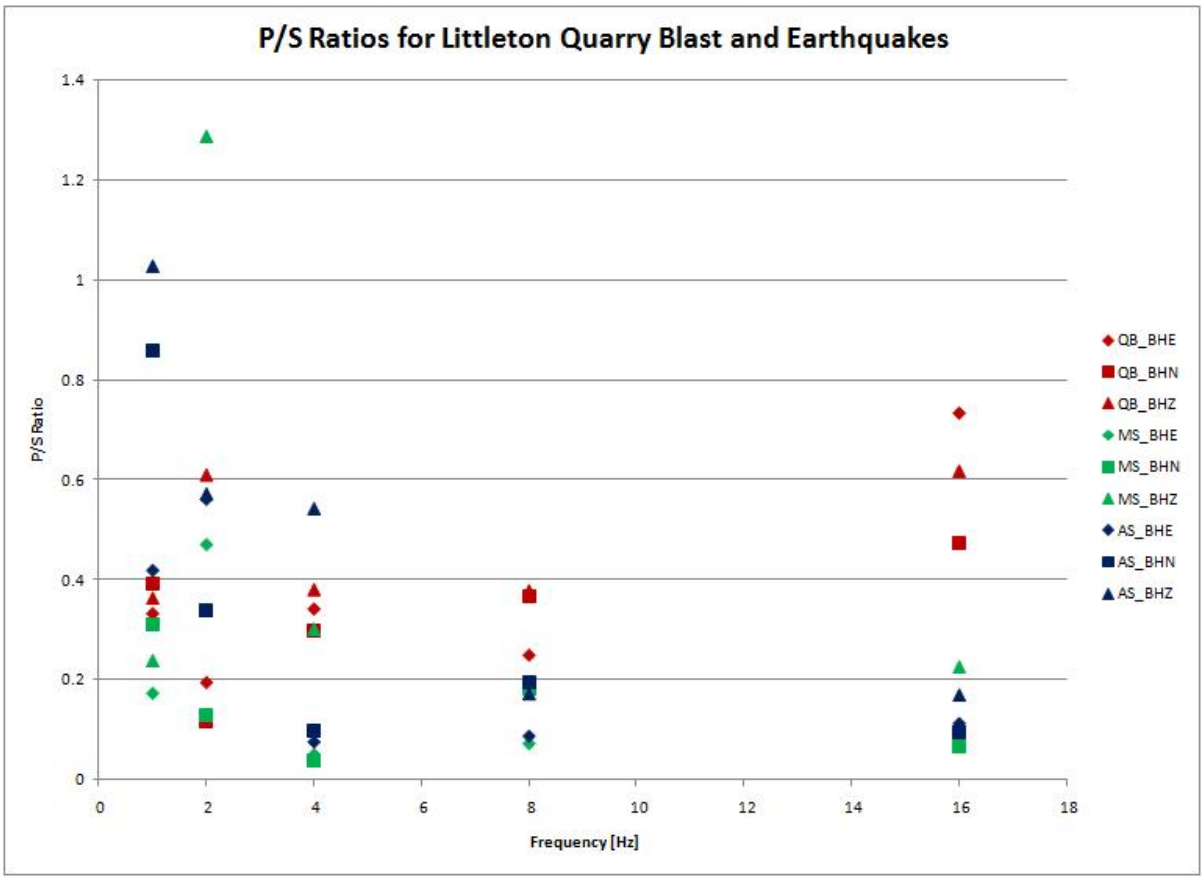

Figure 44. Preliminary *P/S* ratio analysis for quarry blast (red), mainshock (green), and aftershock (blue). A clear separation of earthquakes from the quarry blast is apparent above 8 Hz.

3.4.5 F-16 Flyovers

Tuesday April 10, 2007 marked Opening Day for the Boston Red Sox at Fenway Park. Four F-16 fighter jets from the Vermont Air National Guard flew over the baseball park, located 21 km to the south of the Hanscom Array site. Minutes later, at around 1:56pm local time, the F-16's approached the Hanscom array from the south and proceeded to make seven clockwise loops around Hanscom Field before landing on Runway 29 from the east (Figure 45). The F-16's flew in two separate pairs until the final loop where they joined up in a single line and then broke off one by one from this formation to land (Figure 46). Examples of the acoustic signals generated by these jets are illustrated in Figures 47 and 48.

Figure 45. Four F-16 jets over Hanscom Seismo-Acoustic Array

Figure 46. Left) Four F-16 jets above Hanscom Field with the seismo-acoustic array in the foreground; Right) One by one the jets broke from their formation to land.

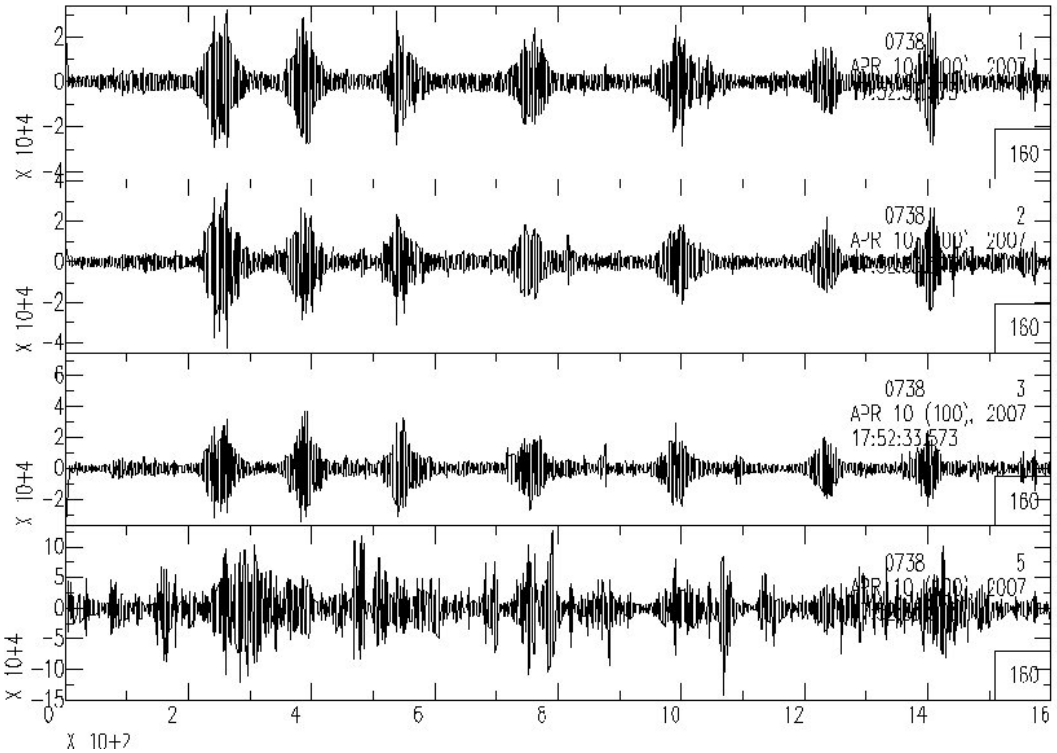

Figure 47. Bandpass-filtered acoustic data of the F-16 jets flying overhead.

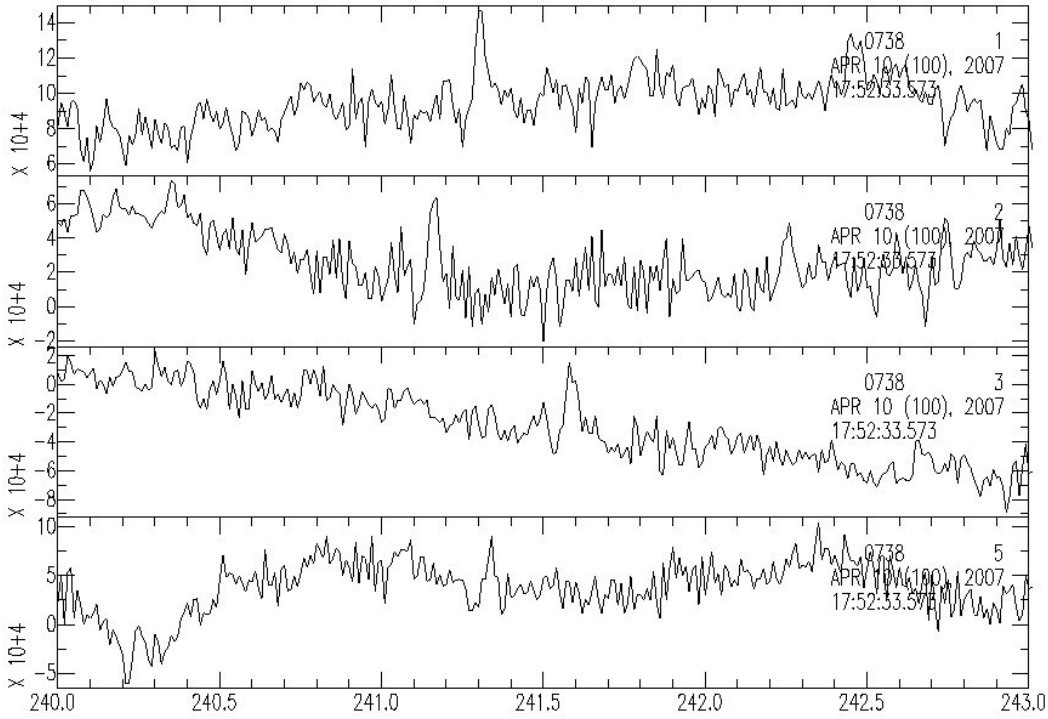

Figure 48. Close-up of the first of seven flyovers. A spike centered around 241.5 seconds is visible on all four acoustic elements.

4. VERMONT DAMAGE PROJECT

4.1 Introduction

4.1.1 Objective

Recent advances in explosion source theory indicate that the damage that occurs near an explosion is a prominent source of *S*-wave energy. The Ashby and Sammis (1990) model for crack nucleation and growth predicts *S*-wave generation in the far field (Figure 49; Sammis, 2002). Modeling by Patton *et al.* (2005) and Stevens *et al.* (2003) have shown the importance of the cone of damage above a source, modeled by a compensated linear vector dipole (CLVD), in generating *Rg* in the near field and *S (Lg)* in the far field, respectively. The phenomenology in the CLVD regime includes block motions, crack damage, and spallation. The New England Damage Experiment (NEDE) was conducted to test these theories and provide empirical data to aid in answering questions regarding shear wave generation mechanism(s).

4.1.2 Location

The NEDE was conducted in the Barre granite, a homogenous hard rock with low fracture density (Figure 50), to allow study of the damage zones and fractures created by a fully confined and contained explosion. Figure 51 shows a general geologic map of Vermont with a black box showing the location of the Barre granite. The geology of Vermont is an extension of the Appalachian Mountains with structural trends that generally run in a north to northeast orientation. The Barre granite is a felsic intrusion into Silurian to Devonian age rocks of the Connecticut Valley-Gaspe Basin caused by melting due to closing of a basin and collision of continental landmasses (Doolan, 1996). Significant reshaping of the land occurred under thick ice sheets.

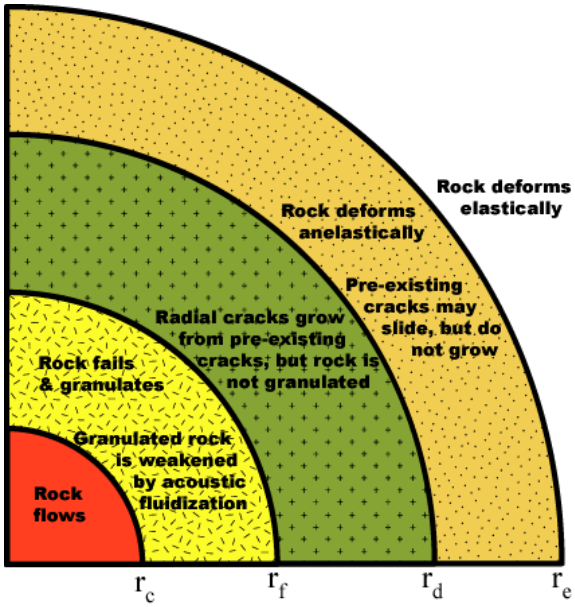

Figure 49. Rheology surrounding an underground explosion (after Rodean (1971) and modified by Sammis for acoustic fluidization from Melosh, 1979).

The fine-grained Barre grey granite has been quarried for over 100 years as a monument stone due its low fracture density and homogeneous composition. While coring the granite for our test applications, the driller often had to snap the core from the bottom of the hole due to a lack of naturally occurring fractures. A further discussion of the Barre granite and its rock properties can be found later in this chapter. A site near the active quarry pit was originally chosen for the blasts (Figure 52). The upper 50 feet of fractured and weathered granite had been stripped off at this site, which allowed us to be closer in depth to the relatively-unfractured, monument-quality Barre granite. Unfortunately, this site was too close to a nearby cell/radio tower and the active quarry wall to detonate our planned 400 lb explosions.

Core drilling at an alternative test site (Figure 52) was conducted further away from the active quarry wall and a nearby cell/radio tower. The alternative site would be far enough away from the sensitive structures so that the planned 400 lb blasts could be safely detonated. Unfortunately, the granite had a much higher fracture density (it was quarried for aggregate stone) and drilling encountered large schistosic xenoliths (Figure 53). This site was abandoned and the experiment was returned into the original location (Figure 52). In order to reduce the projected ground vibrations at the cell/radio tower and high wall of the active quarry to safe limits, we scaled the planned explosions down to ~200 lbs.

Figure 50. Photograph of 3-5 m thick relatively-unfractured sections of Barre granite. The test site was located behind this granite ledge.

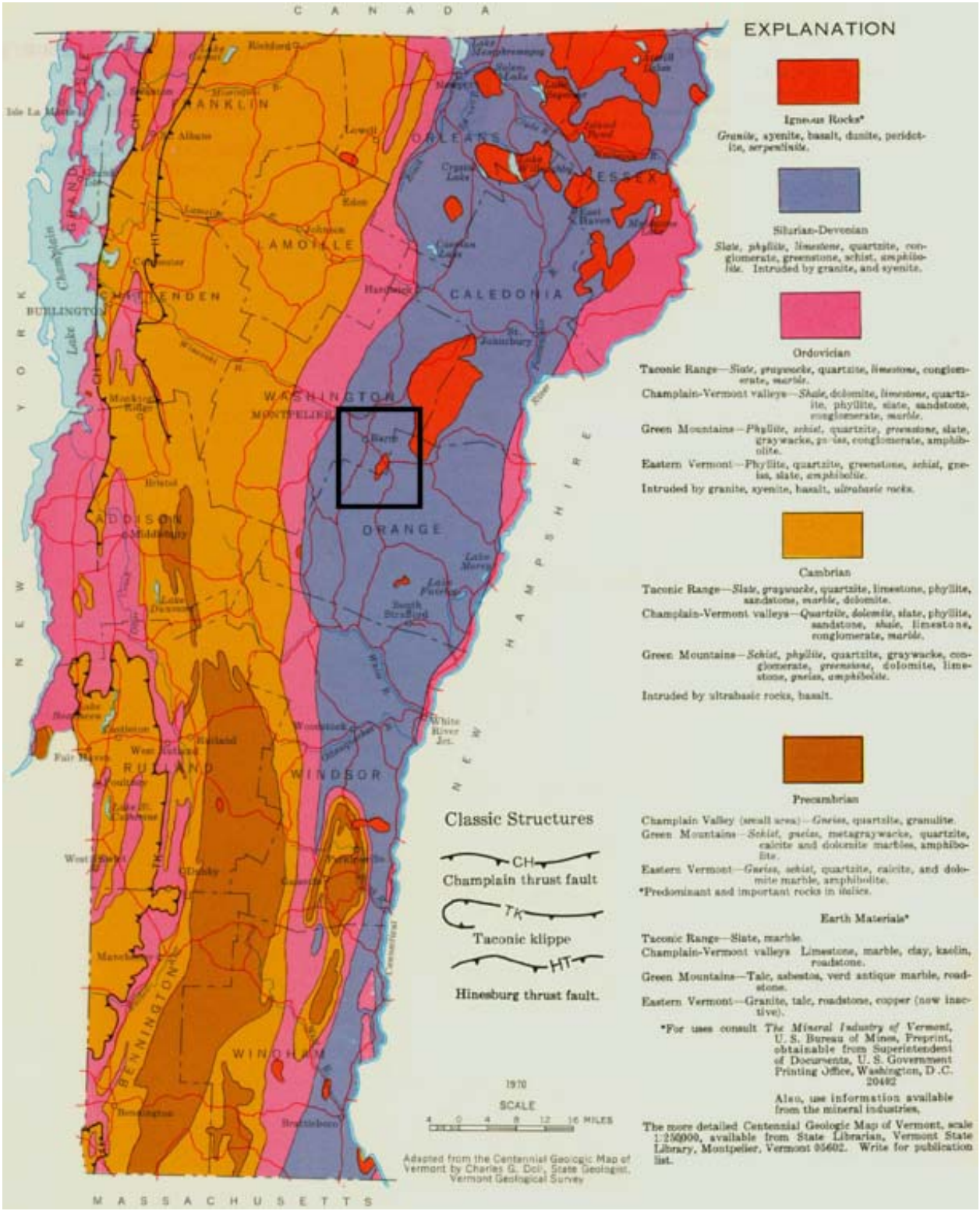

Figure 51. Geologic map (modified) from the Vermont Geological Survey. The black box highlights Barre, VT and the Barre granite igneous intrusion to the southeast. Source: http://www.anr.state.vt.us/DEC/GEO/images/geo5.JPG

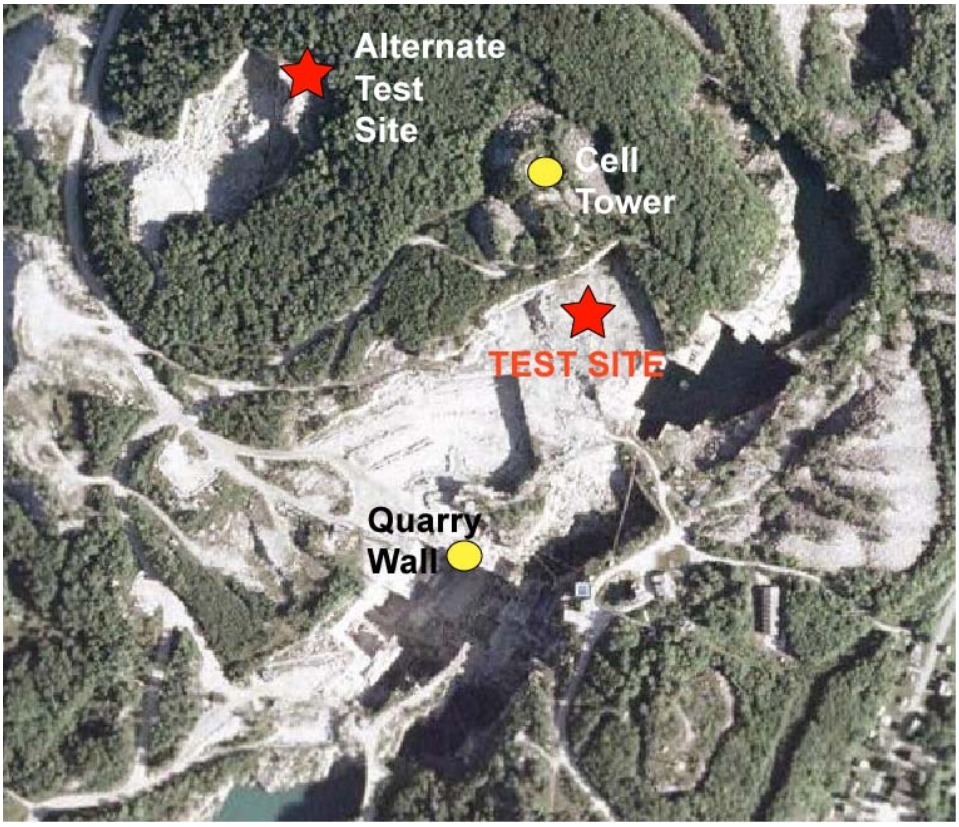

Figure 52. Location of the test site and alternative test site in relation to nearby structures.

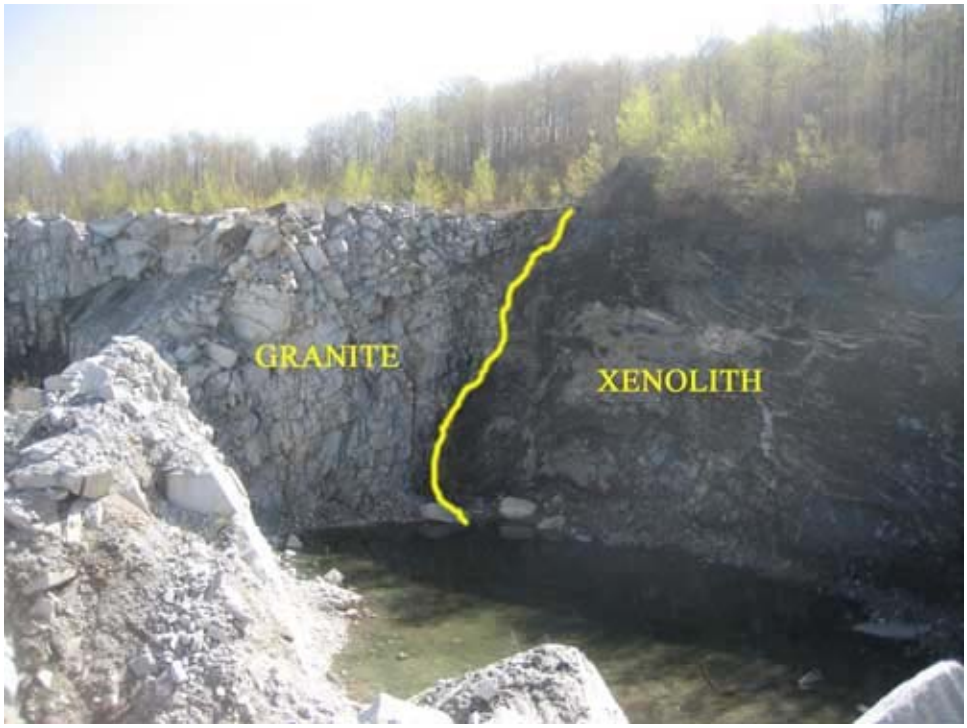

Figure 53. Photo of the highly-fractured nature of the granite at the alternative test site (see Figure 52) and a contact with large xenoliths at the abandoned test site.

4.2 Seismic Deployments

The NEDE explosions were recorded on over 140 seismic instruments, including short-period seismometers, high-g accelerometers, and a high-resolution video camera, deployed at distances of less than 5 m to 30 km from the explosions. We recovered 99.7% of the data.

4.2.1 Near-Source Array

Jessie Bonner, James Britton, Katherine Murphy, Sam Huffstetler, Delaine Reiter, and Mark Leidig (Weston) deployed 6 short period Mark Product L4-3D seismometers, 2 Endevco 100 g accelerometers, and 5 TerraTek 40 g accelerometers in close proximity to the explosions to record the source phenomenology. All of these instruments recorded three components (3C) of motion. One of the accelerometers (N1B) was moved before each shot to be less than 5 m from the borehole to record shot time. Table 7 lists the locations and instrumentation deployed for the three-component near-source array. Figure 54 shows the locations of the very close-in sensors and the shot locations. The remainder of the near-source stations, at distances of less than 1 km, can be seen in Figure 55.

Station N5 was across an 80 m deep quarry pit (Don Murray, pers. comm.), now filled with water. This pit may have an effect on the data at station N5 and the data for some shots at station N4. Station N2 was deployed above the test site on the edge of a high wall.

Table 7. Near-source 3C Sensors.

Station	Latitude	Longitude	Elev (m)	Channels 1-3	S/N	Channels 4-6	S/N	DAS	DISK	GPS
N1A	44.15785	-72.47808	503	Endevco	6			734	5715	663
N1B Shot 1	44.15782	-72.47852	501			Endevco	2	734	5715	663
N1B Shot 2	44.15803	-72.47814	508			Endevco	2	734	5715	663
N1B Shot 3	44.15783	-72.47773	507			Endevco	2	734	5715	663
N1B Shot 4	44.15749	-72.47793	506			Endevco	2	734	5715	663
N1B Shot 5	44.15752	-72.47753	503			Endevco	2	734	5715	663
N2	44.15826	-72.47862	533	L4-3D	189	TerraTek	7	738	87	664
N3	44.15724	-72.47930	492	L4-3D	257	TerraTek	9	716	5106	248
N4	44.15642	-72.47736	500	L4-3D	619	TerraTek	8	733	5959	669
N5	44.15687	-72.47575	506	L4-3D	37	TerraTek	6	739	5247	674
N6	44.15967	-72.48204	489	L4-3D	L41168			940F		4196
N7	44.15637	-72.47913	502	L4-3D	628	TerraTek	4	743	5713	244

The near-source accelerometers and seismometers were placed in a shallow hole, oriented to true north, and lightly covered with dirt. True north was 16° west of magnetic north at our location for the experiment. For placement of the Endevco accelerometers, very shallow holes were dug into the granite with a rock bar. The sensors were coupled to the granite with dirt and granite flour from the drilling. Data were recorded at 250 sps on 24-bit Reftek 72A-08 DAS for all stations except N6, which was digitized on a Reftek RT130. More recording parameters can be found in Table 8. The DAS and GPS clock were placed in a plastic tub and covered by a garbage bag. The external GPS clock acquired GMT time. A 17 Ah deep-cycle battery powered each station. Figure 56 and Figure 57 show examples of the sensor installation and the plastic tub with

recording equipment. Information on the near-source vertical-component only sensors shown in Figure 55 can be found in the following "Texan Network" section.

Table 8. Near-Source Recording Parameters.

Parameter	Value
Digitizer	Reftek 72A-08 (N1-N5, N7) Reftek RT130 (N6)
Channels	Reftek 72A-08 – 6 Reftek RT130 – 3
Resolution	24-bit
Gain	1
Sample Rate	250
Record Mode	Continuous
Data Format	Reftek 72A-08 – PASSCAL† 32 bit Reftek RT130 – PASSCAL Compressed

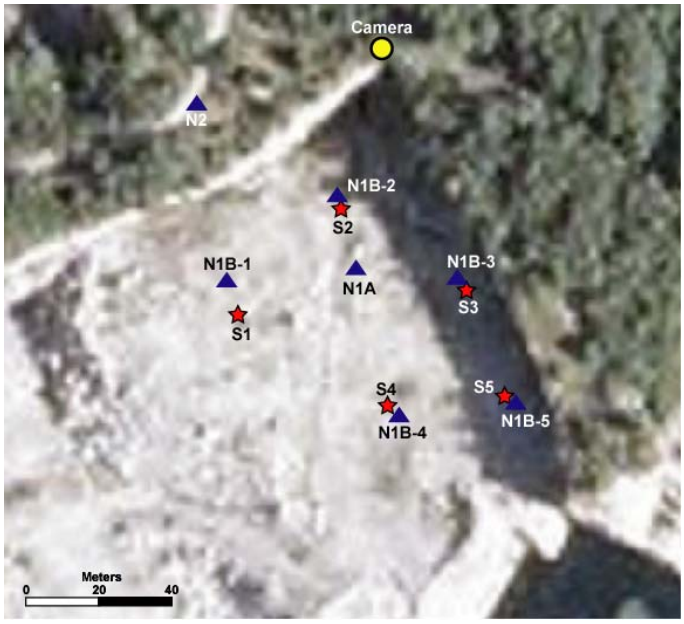

Figure 54. Test site station N1 (blue triangles) and shots (red stars). N1 consisted of two Endevco accelerometers. N1A remained stationary for all 5 shots, while N1B moved to be less than 5 m from each shot. Station N2 and the camera are also shown on a hill overlooking the test site. (Google Earth Background)

† PROGRAM FOR ARRAY SEISMIC STUDIES OF THE CONTINENTAL LITHOSPHERE

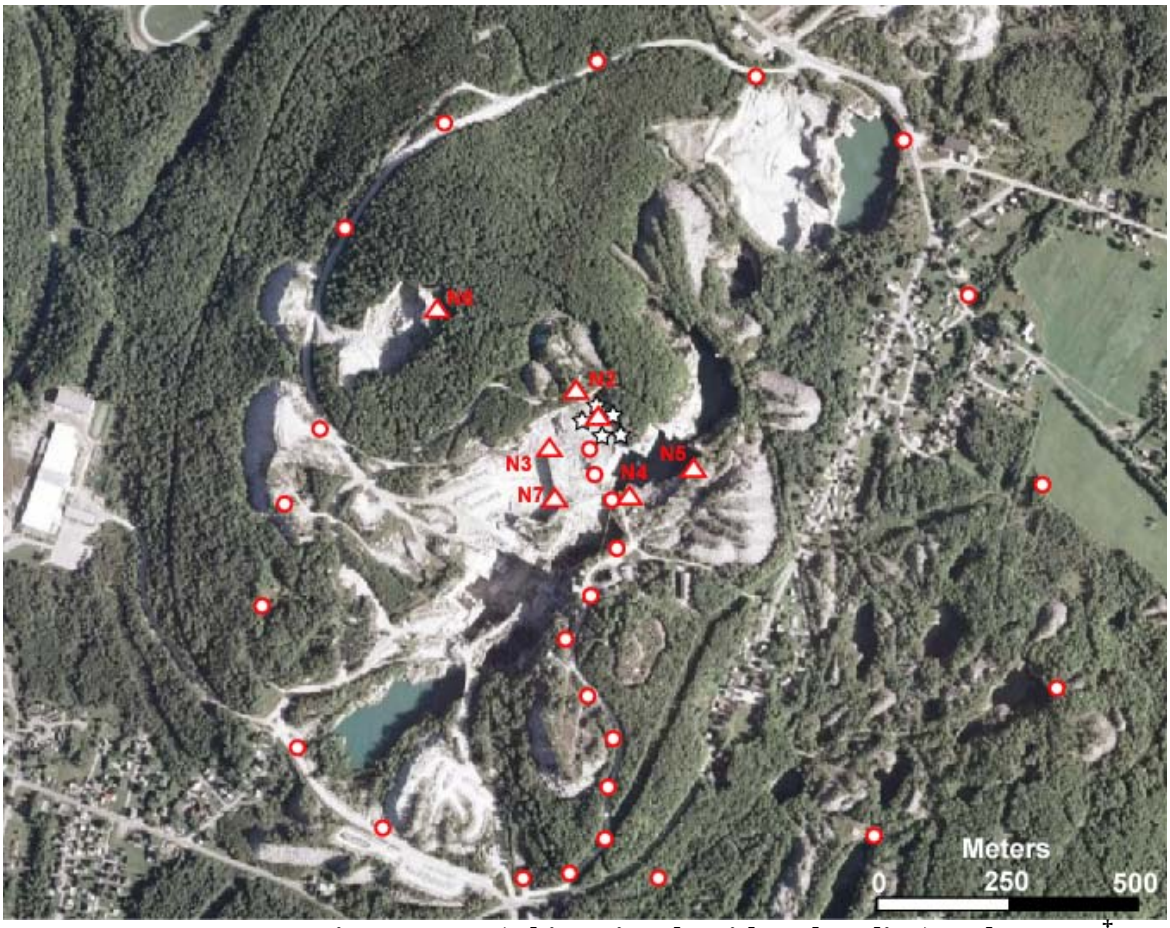

Figure 55. Near-source stations N1-N7 (white triangle with red outline) and Texans[‡] NT01-NT27 (white dot with red outline). N1 consisted of two sensors, one of which moved for each shot (Figure 54). The shots (white stars with black outline) can be seen in the middle of the image. (Google Earth Background)

[‡] "Texans" refer to single-component geophones recorded on a small digitizer with internal memory and power. The name "Texan" refers to the original design by Stever Harder, who worked for a university in Texas.

Figure 56. Example of near-source instrument installation. Katherine Murphy levels and orients a TerraTek accelerometer to true north while Sam Huffstetler installs the Reftek 72A-08 digitizer and battery.

Figure 57. A second example of installing a near-source accelerometer and seismometer (Delaine Reiter, Sam Huffstetler, and Mark Leidig).

Station N3 had a timing issue. It is unclear whether this was a problem with the DAS or clock, but at the beginning of a new data file, the time would jump 1 second forward and then back. This would happen a few times for each file. Arrivals at N3 came in late by an increasing number of seconds with respect to the other near-source stations. The offsets seem to be in terms of full seconds as the millisecond accuracy appears to be correct, but we cannot verify this. Corrections to the processed data have been applied by the amounts shown in Table 9. Station N3 should not be used in the development of the velocity model.

Table 9. Station N3 Timing Corrections.

Shot	Correction (sec)
1	3
2	5
3	7
4	11
5	14

4.2.2 Short Period 3C Linear Arrays

Two linear arrays of short-period 3C seismometers were deployed extending away from the test site for 30 km in two directions as shown in Figure 58 and Table 10. Station spacing was designed to be every 3 km "as the crow flies" from the test site. A lack of roads and many inaccessible areas, particularly along the NE line, made maintaining station spacing and a straight line difficult. Station NE06 was not deployed due to a 6 km region void of any roads. The NE line followed the trend of the granite intrusives and the structural trend of the region (Figure 51), while the SE line cut across the structural trend. The stations were generally located along dirt roads that only saw local resident traffic. Vehicle traffic can be seen in the recordings, and passing cars interfered with a few recordings. Permissions were obtained to install these sensors from the local Vermont towns, but several stations along the NE line required landowner permission as well (Figure 59).

Nine Sercel (formerly Mark Products) 1 Hz L4-3D short period seismometers with Reftek RT130 digitizers were installed along the NE line by Mark Leidig, James Britton, and Katherine Murphy (Weston) and Lisa Foley (PASSCAL). Along the SE line, ten Mark Products 2 Hz L22 short period seismometers were installed by Jessie Bonner, Sam Huffstetler, Delaine Reiter (Weston) and Willie Zamora (PASSCAL). All stations had an external GPS clock for recording GMT time and recorded at 250 sps. More recording information can be found in Table 11.

The sensors were oriented to truth north, placed in a shallow hole, leveled, and loosely covered with soil (Figure 60). The soil was generally an organic rich dense soil, but sometimes had large amounts of decaying plant matter that left the site somewhat "spongy". No solid bedrock was found at the sites within a foot of the surface. Therefore, it is expected that site responses will have some variation. A huddle test was conducted prior to the experiment and that information can be found in Appendix A. PASSCAL collected *in-situ* response information for each of the L22s on the SE line. This information can be found in Appendix B. Lisa Foley examined the *in-*

situ response data and found sensor 496L (SE02) had a "bad" channel 2 and thinks that a faulty internal connection is the cause. Initial examination of the experiment data did not show any abnormalities with this sensor. She also noted that the 462L (SE08) sensor had swapped and reversed cables, which made the north/south channel into the east/west channel and vice versa. The polarity on each channel was also flipped. Factory response information for the Sercel L4-3Ds can be found in Appendix C.

The RT130 digitizer, GPS clock, and 79 AH deep-cycle battery were placed in a black plastic bag and hidden behind bushes or covered with grass and leaves for camouflage. The GPS clock was held upright by attaching the sensor cable to the DAS through the metal clock loop. At a couple sites, tall grass interfered with satellite reception and the clock was elevated by placing it on top of foam pads that were placed on the battery box.

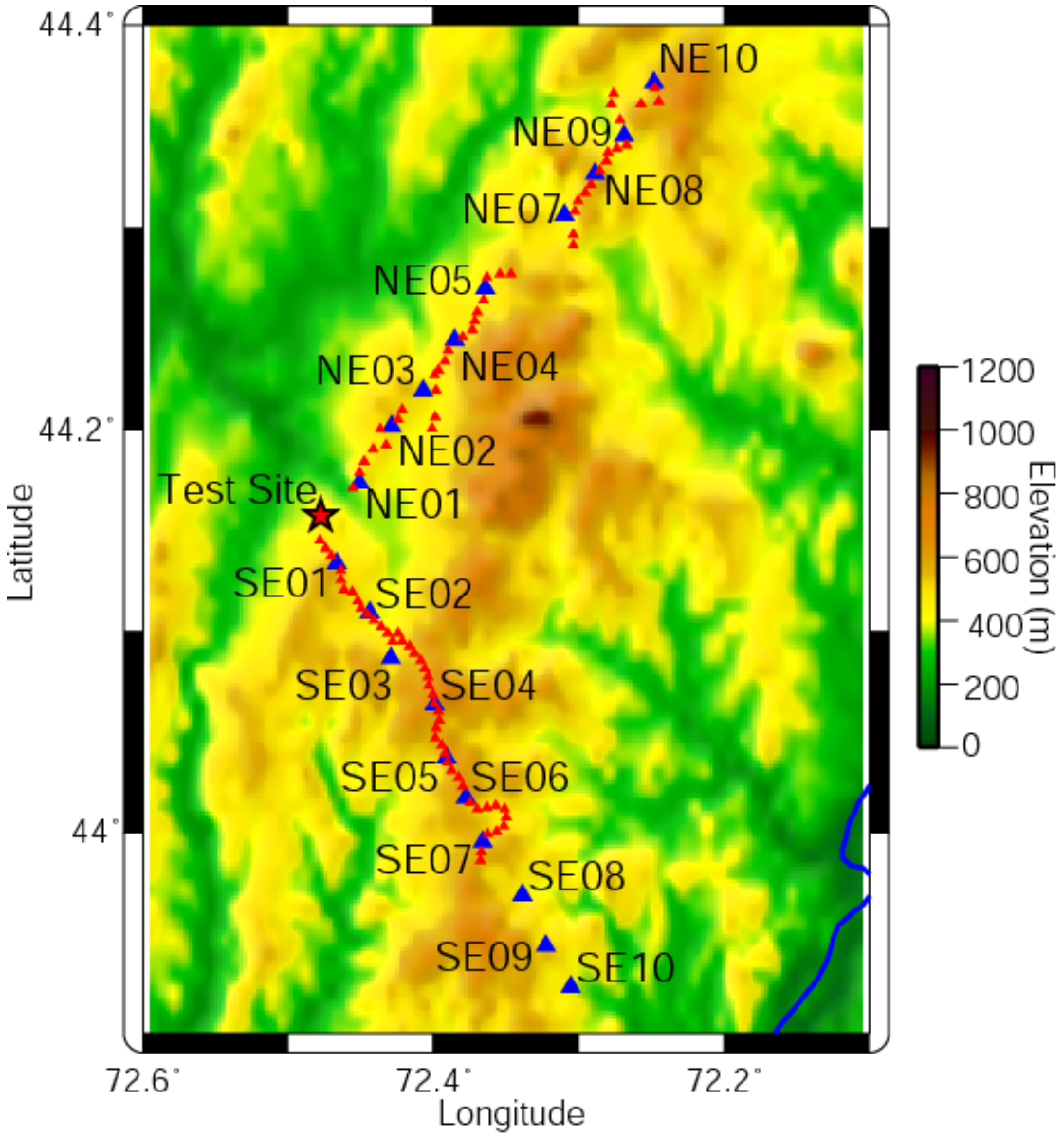

Figure 58. Linear array short period stations (blue triangles) and Texans (red triangles).

Table 10. Short Period Linear Array Stations.

Station	Latitude	Longitude	Elev (m)	Channels 1-3	S/N	DAS	GPS
SE01	44.13362	-72.46659	514	L22	459L	9D63	5155
SE02	44.10946	-72.44367	475	L22	496L	A198	4161
SE03	44.08698	-72.42968	470	L22	479L	9669	4188
SE04	44.06350	-72.39923	595	L22	494L	9E50	4176
SE05	44.03733	-72.39093	588	L22	720L	939E	4175
SE06	44.01771	-72.37772	514	L22	643L	930E	3890
SE07	43.99543	-72.36589	556	L22	449L	9E45	4194
SE08	43.96925	-72.33883	456	L22	462L	9D42	4198
SE09	43.94373	-72.32292	507	L22	642L	9312	4179
SE10	43.92329	-72.30565	369	L22	468L	9E40	4189
NE01	44.17376	-72.45101	420	L4-3D	L41167	9E4B	2449
NE02	44.20178	-72.42899	511	L4-3D	L41166	9D8F	2565
NE03	44.21921	-72.40699	474	L4-3D	L41169	9DEA	2514
NE04	44.24436	-72.38558	462	L4-3D	L41162	9E18	2711
NE05	44.26989	-72.36425	447	L4-3D	L41164	9E1B	2531
NE07	44.30621	-72.30992	436	L4-3D	L41161	9E42	2661
NE08	44.32654	-72.28904	541	L4-3D	L41165	9E4F	2665
NE09	44.34530	-72.26903	461	L4-3D	L41170	9DAA	2516
NE10	44.37157	-72.24832	542	L4-3D	L41163	9E17	2520

Table 11. Short Period Recording Parameters.

Parameter	Value
Digitizer	Reftek RT130
Channels	3
Resolution	24-bit
Gain	32
Sample Rate	250
Record Mode	Continuous
Data Format	PASSCAL Compressed
Sensor	1 Hz Sercel L4-3D (NE01-NE10) 2 Hz Mark L22 (SE01-SE10)
Sensitivity	Appendices B and C

Figure 59. Discussing where to place the station with the landowner of Carrier's Sky Park.

Figure 60. Example of orienting to true north and leveling an L4-3D sensor on the NE line.

4.2.3 Texan Network

Weston Geophysical and IRIS PASSCAL split into three teams and deployed 112 Reftek RT-125 “Texans” (Figure 61) along the NE and SE short period array lines and around the test site (Figure 55 and Figure 58). Two of the 112 Texans deployed either had a cable or geophone problem. Data were successfully retrieved from every other instrument in the experiment. The Texan stations are single channel sensors with a 4.5 Hz 3” spike vertical geophone and were installed every 0.5 km along the short period array lines. Willie Zamora and Lisa Foley scouted a possible third line to the west of the test site, but found the road and traffic conditions unfavorable.

The team along the SE line (Sam Huffstetler, Delaine Reiter, and Willie Zamora) installed sensors every 0.5 km of driving mileage, including in close proximity to the short period sensors. Therefore, they installed 45 Texans in about 22 km. Their stations are designated ST01-ST45.

The NE line Texan team (Mark Leidig, Katherine Murphy, and James Britton) installed Texans every 0.5 km (“as the crow flies”) with respect to the test site and skipped sites that were near the already installed short period sensors. They were only able to install 40 Texans (NT01-NT40) along their 30 km line with this method because they were confronted with inaccessible regions where no Texans could be placed.

Jessie Bonner, Lisa Foley, and Sam Huffstetler formed the third team and installed 27 Texans around and in the test region (NT01-NT27). These Texans will be helpful in examining any possible radiation patterns generated by the shots.

Table 12 lists the Texan locations and Table 13 details the recording parameters. The Texans were programmed the morning of installation by Willie Zamora to record during specified time intervals for 4 days at 250 sps (Table 13). The recorder was placed in a small plastic bag, to keep it clean, and then placed in a shallow trench. The geophone was placed vertically in the ground using a bubble level and everything was covered with dirt to hide them and provide thermal stability. The recorders were powered by two internal Duracell Procell D size batteries that were installed prior to programming. Since all shots were completed in one day, the sensors were pulled on day two of recording, acquisition was stopped, and the data were downloaded.

Figure 61. (Left) RT-125 "Texan" seismic recorder and attached 4.5 Hz vertical spike geophone (orange). For the experiment, the recorder was placed in a plastic bag, laid on its side in a trench, and everything was buried. (Right) Texans in their carrying crates being programmed prior to deployment.

Table 12. RT-125 "Texan" Sensors.

Station	Latitude	Longitude	Elev (m)	Geophone	S/N
NT01	44.14975	-72.47660	439	4.5 Hz	1847
NT02	44.15050	-72.47139	474	4.5 Hz	1817
NT03	44.15306	-72.46688	469	4.5 Hz	2185
NT04	44.15661	-72.46726	433	4.5 Hz	2988
NT05	44.15994	-72.46902	419	4.5 Hz	2137
NT06	44.16267	-72.47063	399	4.5 Hz	2148
NT07	44.16375	-72.47424	402	4.5 Hz	2087
NT08	44.16403	-72.47813	411	4.5 Hz	3003
NT09	44.16295	-72.48178	446	4.5 Hz	2455
NT10	44.16111	-72.48428	450	4.5 Hz	2218
NT11	44.15758	-72.48488	483	4.5 Hz	2237
NT12	44.15627	-72.48574	471	4.5 Hz	2703
NT13	44.15452	-72.48631	445	4.5 Hz	2464
NT14	44.15202	-72.48542	415	4.5 Hz	1910
NT15	44.15061	-72.48338	424	4.5 Hz	2450
NT16	44.14973	-72.47993	436	4.5 Hz	2161
NT17	44.14983	-72.47882	430	4.5 Hz	2465
NT18	44.15044	-72.47791	441	4.5 Hz	2459
NT19	44.15135	-72.47785	469	4.5 Hz	1919
NT20	44.15220	-72.47769	478	4.5 Hz	2142
NT21	44.15300	-72.47834	481	4.5 Hz	2589
NT22	44.15392	-72.47892	485	4.5 Hz	1555
NT23	44.15469	-72.47827	488	4.5 Hz	2564

Station	Latitude	Longitude	Elev (m)	Geophone	S/N
NT24	44.15552	-72.47762	491	4.5 Hz	2179
NT25	44.15637	-72.47777	489	4.5 Hz	1923
NT26	44.15683	-72.47819	488	4.5 Hz	1683
NT27	44.15724	-72.47828	508	4.5 Hz	1522
ST01	44.14481	-72.47836	415	4.5 Hz	2155
ST02	44.14083	-72.47468	470	4.5 Hz	2089
ST03	44.13749	-72.47077	501	4.5 Hz	1649
ST04	44.12999	-72.46384	527	4.5 Hz	1739
ST05	44.12524	-72.46401	508	4.5 Hz	2253
ST06	44.12048	-72.46160	525	4.5 Hz	1697
ST07	44.11936	-72.45598	517	4.5 Hz	1836
ST08	44.11476	-72.45226	487	4.5 Hz	1941
ST09	44.11152	-72.45009	476	4.5 Hz	1884
ST10	44.10815	-72.44569	453	4.5 Hz	1718
ST11	44.10532	-72.44118	431	4.5 Hz	1694
ST12	44.10210	-72.43603	432	4.5 Hz	2044
ST13	44.09886	-72.43151	456	4.5 Hz	1868
ST14	44.09502	-72.42836	451	4.5 Hz	2362
ST15	44.09881	-72.42456	480	4.5 Hz	1676
ST16	44.09485	-72.42188	502	4.5 Hz	2990
ST17	44.09256	-72.41641	516	4.5 Hz	2234
ST18	44.08877	-72.41341	528	4.5 Hz	1746
ST19	44.08528	-72.40897	555	4.5 Hz	2476
ST20	44.08119	-72.40638	569	4.5 Hz	1706
ST21	44.07713	-72.40380	598	4.5 Hz	2994
ST22	44.07272	-72.40329	641	4.5 Hz	2153
ST23	44.06861	-72.40077	616	4.5 Hz	1815
ST24	44.06423	-72.39933	605	4.5 Hz	2091
ST25	44.06016	-72.39693	587	4.5 Hz	2477
ST26	44.05563	-72.39617	595	4.5 Hz	2480
ST27	44.05147	-72.39829	599	4.5 Hz	2479
ST28	44.04698	-72.39883	623	4.5 Hz	1790
ST29	44.04327	-72.39462	611	4.5 Hz	1808
ST30	44.03915	-72.39230	600	4.5 Hz	2475
ST31	44.03485	-72.39060	606	4.5 Hz	2566
ST32	44.03075	-72.38752	595	4.5 Hz	2474
ST33	44.02710	-72.38279	604	4.5 Hz	2612
ST34	44.02293	-72.38020	618	4.5 Hz	2837
ST35	44.01464	-72.37524	576	4.5 Hz	2461
ST36	44.01176	-72.37000	535	4.5 Hz	2463
ST37	44.01231	-72.36317	520	4.5 Hz	1655
ST38	44.01310	-72.35706	513	4.5 Hz	2451
ST39	44.01176	-72.35107	474	4.5 Hz	1841
ST40	44.00738	-72.34996	483	4.5 Hz	1784
ST41	44.00307	-72.35169	490	4.5 Hz	2458
ST42	44.00023	-72.35682	505	4.5 Hz	2452

Station	Latitude	Longitude	Elev (m)	Geophone	S/N
ST43	43.99909	-72.36286	518	4.5 Hz	2453
ST44	43.99044	-72.36703	549	4.5 Hz	2457
ST45	43.98604	-72.36784	560	4.5 Hz	2230
TN01	44.17101	-72.45563	357	4.5 Hz	1827
TN02	44.17853	-72.45098	461	4.5 Hz	1702
TN03	44.18431	-72.44757	460	4.5 Hz	1762
TN04	44.19030	-72.44159	464	4.5 Hz	1835
TN05	44.19208	-72.43277	490	4.5 Hz	1899
TN06	44.20009	-72.43657	490	4.5 Hz	1934
TN07	44.20498	-72.42451	486	4.5 Hz	2017
TN08	44.20959	-72.42144	475	4.5 Hz	1634
TN09	44.20053	-72.40111	429	4.5 Hz	1652
TN10	44.20614	-72.39907	419	4.5 Hz	1682
TN11	44.21946	-72.39829	417	4.5 Hz	1750
TN12	44.22675	-72.39961	428	4.5 Hz	1569
TN13	44.22939	-72.39684	463	4.5 Hz	2113
TN14	44.23362	-72.39248	452	4.5 Hz	1567
TN15	44.23918	-72.39013	473	4.5 Hz	1570
TN16	44.24562	-72.38012	470	4.5 Hz	1578
TN17	44.24944	-72.37331	476	4.5 Hz	1612
TN18	44.25382	-72.37190	476	4.5 Hz	1520
TN19	44.25821	-72.36987	455	4.5 Hz	1789
TN20	44.26419	-72.36535	437	4.5 Hz	2478
TN21	44.27529	-72.36361	436	4.5 Hz	1972
TN22	44.27692	-72.35464	493	4.5 Hz	2573
TN23	44.27680	-72.34652	524	4.5 Hz	1677
TN24	44.29133	-72.30389	454	4.5 Hz	1736
TN25	44.29651	-72.30374	445	4.5 Hz	2991
TN26	44.30800	-72.30269	454	4.5 Hz	2562
TN27	44.31292	-72.30035	492	4.5 Hz	2561
TN28	44.31717	-72.29567	523	4.5 Hz	2560
TN29	44.32093	-72.29184	537	4.5 Hz	2572
TN30	44.32799	-72.28578	537	4.5 Hz	2563
TN31	44.33274	-72.28131	504	4.5 Hz	2924
TN32	44.33710	-72.27986	469	4.5 Hz	2927
TN33	44.33886	-72.27404	453	4.5 Hz	2926
TN34	44.34054	-72.26735	441	4.5 Hz	2920
TN35	44.35288	-72.27189	431	4.5 Hz	2902
TN36	44.36076	-72.27804	394	4.5 Hz	2901
TN37	44.36620	-72.27633	437	4.5 Hz	2904
TN38	44.36110	-72.25740	518	4.5 Hz	2874
TN39	44.36218	-72.24525	594	4.5 Hz	2921
TN40	44.36885	-72.24784	565	4.5 Hz	2923

Table 13. Texan Recording Parameters.

Parameter	Value
Digitizer	Reftek RT125
Channels	1 - vertical
Resolution	24-bit
Gain	32
LSB (nV/count)	57.37
Sample Rate	250
Record Mode	Time Windows
Window 1 (UTC)	2008:194:14:00 to 2008:194:24:00
Window 2 (UTC)[§]	2008:195:14:00 to 2008:195:24:00
Window 3 (UTC)	2008:196:19:00 to 2008:196:24:00
Window 4 (UTC)	2008:197:19:00 to 2008:197:24:00
Sensor	4.5 Hz vertical 3” spike

4.2.4 Video Camera

A Sony Hi-8 video camera recorded all of the explosions in order to study the surface manifestations of the explosions. A picture of the camera overlooking the test site is shown in Figure 62. The camera needed to be moved a few feet for Shot 3 to avoid the vantage angle being blocked by vegetation. The camera was moved back to its initial location for shots 4 and 5. The locations of the camera are listed in Table 14 and plotted in Figure 54. The Hi-8 analog videos were digitized to small computer movies. Jessie Bonner also recorded many of the explosions using his personal hand held video camera placed on a tripod near the blasts. Those videos provide a view of the blasts from a different angle.

Table 14. Camera Locations.

Station	Latitude	Longitude	Elev (m)	Shots Recorded
Camera1	44.15837	-72.47800	541	1, 2, 4, 5
Camera2	44.15842	-72.47816	538	3

Figure 62. Camera overlooking the test site.

4.3 Explosions in Barre Granite

4.3.1 Shot Characteristics

Five explosions were detonated at the test site on 12 July 2008 (Table 15). A delay-fired production shot was conducted on 11 July 2008, and we have the blasters information for this shot (Appendix E). A goal of this experiment was to examine how the velocity of detonation (VOD) affects the damage and shear wave generation. Three explosives with dramatically different VOD were used to compare these effects. Our planned single-fired blasts ranged in yield from 134 to 270 lbs of explosives with the first three being ~135 lbs of black powder, ANFO/Emulsion (Heavy ANFO), and Composition B (COMP B), respectively. The blast plan was designed and executed by Mr. Tim Rath of Maxam-North America who was assisted by Peter West and Jason Trippiedi.

Table 15. Origin Characteristics for NEDE Shots.

Shot	Date	Origin Time (GMT)	Latitude	Longitude	Elevation (m)	Borehole/ Centroid Depth (m)	Stemming (m)	Yield (lbs)	Explosive
1	7/12/2008 (194)	14:37:42.160	44.15774	-72.47848	509	9.1/8.5	7.3	134	Black Powder
2	7/12/2008 (194)	16:02:05.020	44.15800	-72.47813	509	11.3/10.7	10.1	135.5	ANFO/Emul 50:50
3	7/12/2008 (194)	17:30:40.730	44.15780	-72.47770	503	11.3/10.7	10.4	136	COMP B
4	7/12/2008 (194)	19:16:15.010	44.15751	-72.47797	508	13.7/12.8	11.6	269.5	ANFO/Emul 50:50
5	7/12/2008 (194)	20:50:12.770	44.15754	-72.47757	503	13.7/12.8	11.9	270	COMP B
P1	7/11/2008 (193)	~19:33:54	-	-	-	-	-	1934	ANFO

Note: Yield is based on explosives + detonators.
Lat/Long/Elevation error was 4+ meters according to the GPS unit.

Black powder is traditionally used for firearms and fireworks because its slow burn rate produces gases that can propel a bullet but not damage the barrel. It has a low brisance, the rate at which an explosive reaches maximum pressure, which means it generates relatively fewer fractures in the rock around the explosive source. The fractures generated will be longer due to the escape of the explosive gasses. Occasionally, it is used to break monument stone, such as granite, without damaging the stone itself due to properties of gas expansion only along pre-existing cracks.

ANFO/Emulsion (Figure 63) is the primary blasting agent used in the mining industry due to its stability, low cost, easy production as well as optimum blast effects for rock fracturing. ANFO is considered a high explosive when properly confined and especially when mixed with an emulsion. We use the phrase “Heavy ANFO” to describe the 50:50 ANFO:Emulsion mix used for the NEDE.

Composition B (Figure 64) is a military grade explosive composed of RDX and TNT. It is primarily used in military applications such as munitions. COMP B is a shapeable charge and was cast specifically to fit our boreholes. One cast charge was used for Shot 3 and two were used for Shot 5. The high VOD of this explosive allowed it to be used in the first nuclear weapons. During the experiment, increased care was required handling this explosive due to its increased sensitivity and the booster being strapped to the charge as it was being lowered down the hole (Figure 65). A small amount of ANFO/Emulsion was poured in the hole prior to loading the COMP B charge to increase explosive coupling to the borehole.

Figure 63. Loading of ANFO/Emulsion explosive.

Figure 64. COMP B charge and the tube taped on to hold the detonator.

Figure 65. Lowering the COMP B charge into the hole.

Table 15 lists the total depth of the boreholes, the centroid depths of the explosive column, and the amount of stemming. Stemming consisted of granite flour from drilling, a blast plug (Figure 66) designed to lock into the borehole walls, and ½" gravel. The boreholes had a 9" diameter as logged by Hager-Richter Geoscience (Figure 67).

The shot time was determined by placing an Endevco accelerometer (N1B) within 5 m of the borehole and examining the first large positive break on the vertical component. With the explosives at a maximum depth of 13 m, the compressional wave took less than three milliseconds to reach the sensor. The origin time is accurate to better than 0.05 seconds.

4.3.2 Velocity of Detonation

The velocity of detonation (VOD; Table 16) was measured using a MREL HandiTrap II. A resistance wire is taped to the booster and lowered down the hole. As the explosives burn up the

borehole, the resistance wire is melted and the recorder measures the decreasing resistance at 1 million samples per second. The resistance was then converted to distance and a velocity calculated.

Black powder burns the slowest with a VOD of 0.49 km/s (1608 ft/s; Figure 68). The ANFO/Emulsion (Figure 69) and COMP B (Figure 70) explosives are considered high explosives due to their 5.26 and 8.31 km/s VOD, respectively. The first ANFO/Emulsion shot detonated with a VOD of 5.06 km/s. It is not clear why there is a VOD difference between these two shots. Explosive confinement can play an important role in explosive performance and may have been a factor. The blaster forgot to attach the VOD resistance wire to Shot 3, the first COMP B charge, as he was focused on safely handling the charge.

Figure 66. Blast plug (white ball) used to help stem the holes.

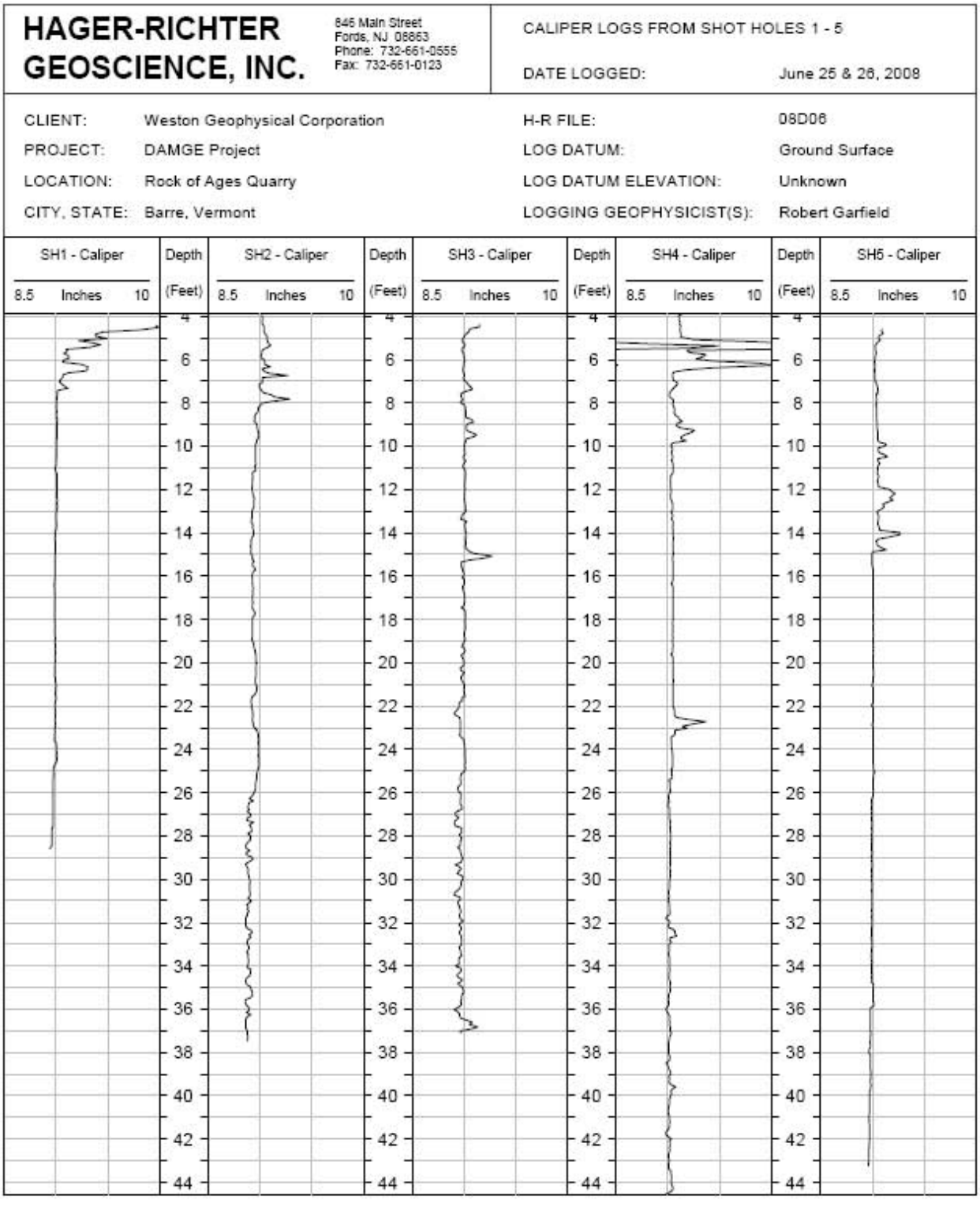

Caliper Logs from Shot Holes 1 - 5

Figure 67. Caliper logs from each blast borehole.

Table 16. Velocity of Detonation.

Shot	Explosive	VOD (km/sec)
1	Black Powder	0.49
2	ANFO/Emul 50:50	5.06
3	COMP B	-
4	ANFO/Emul 50:50	5.26
5	COMP B	8.31

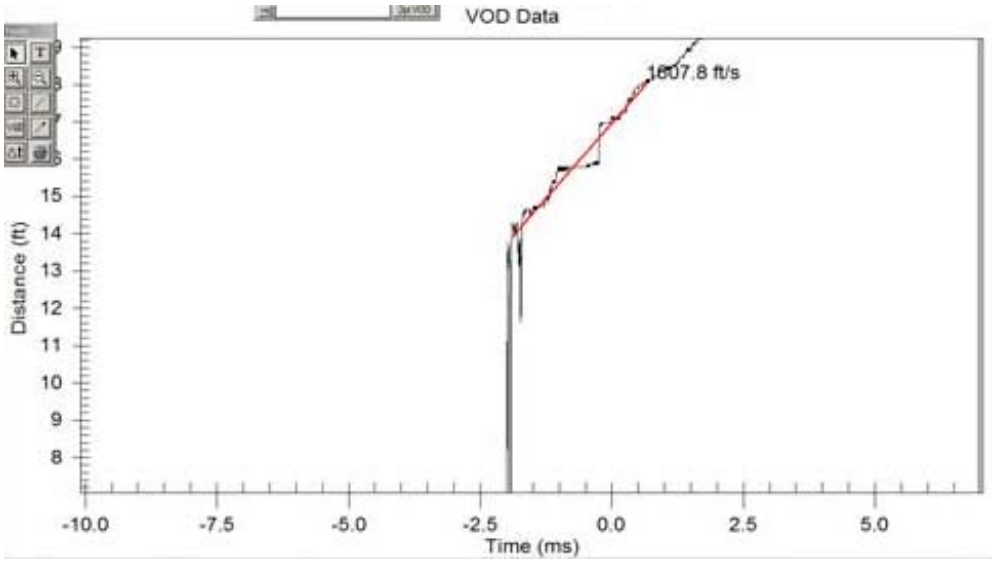

Figure 68. Black powder VOD of 0.49 km/s (1608 ft/s) from Shot 1.

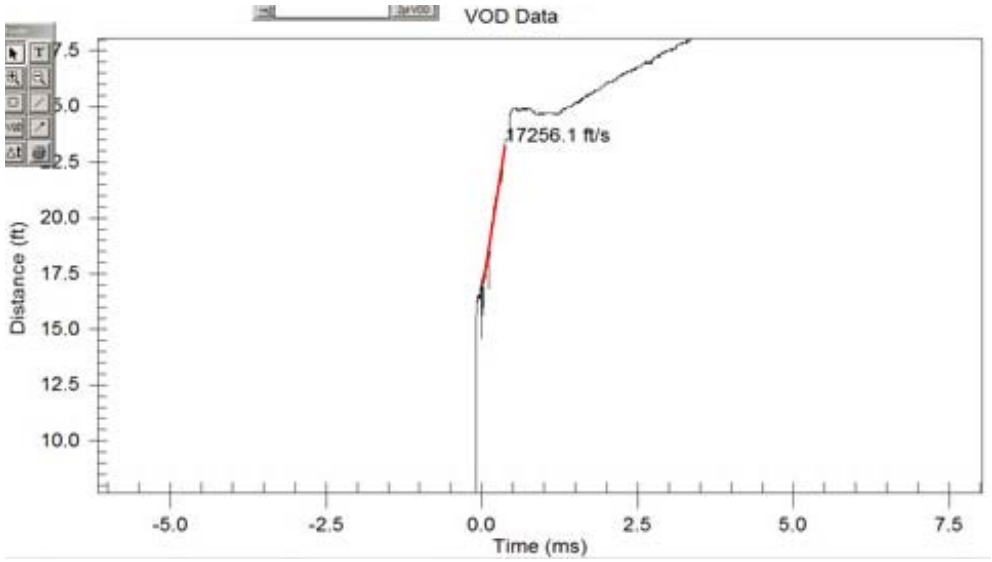

Figure 69. ANFO/Emulsion VOD of 5.26 km/s (17256 ft/s) from Shot 4.

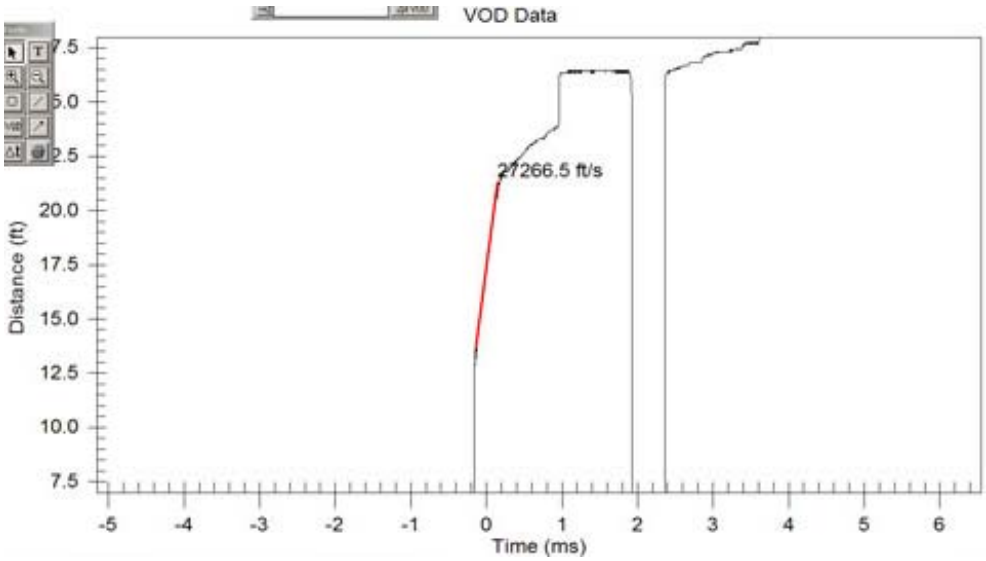

Figure 70. COMP B VOD of 8.31 km/s (27267 ft/s) from Shot 5.

4.3.3 Surface Effects

A Sony Hi-8 video camera (Figure 62) recorded each explosion. The analog video was digitized into mpeg movies available via e-mail from Weston Geophysical Corporation. The video data show the surface processes that occurred during the explosion so that secondary effects of the source can be modeled. All shots spalled, but no shots cratered or produced fly rock. Shot 1 generated the most observable surface fracturing and still video images are shown in Figure 71. A photo of the largest crack generated by Shot 1 is shown in Figure 72. This crack both opened and had vertical displacement of a few centimeters.

Along with the black powder shot, the small ANFO/Emulsion Shot 2 produced some surface fracturing (Figure 73), although the extent was not the same as from Shot 1. Neither Shot 3 (Figure 74) or Shot 4 (Figure 75) produced any surface fracturing visible in the video, although small cracks were observed on the ground after the Shot 4 (Figure 76). The two larger shots, shots 4 and 5, produced significantly more dust.

Figure 71. Digitized still images of the Shot 1 detonation. Note the two fractures developing after 0.8 s and the further fractures after 1.2 s in the red ellipses.

Figure 72. Largest crack generated by Shot 1.

Figure 73. Digitized still images of the Shot 2 detonation. Three fractures develop in the white granite flour at 0.8 s and a larger opening releases a plume of gases to the right of the flour at 1.4 s.

Figure 74. Digitized still images of the Shot 3 denotation. From the hilltop camera, there were no observable surface effects other than dust.

Figure 75. Digitized still images of the Shot 4 denotation. This shot produced significantly more dust than Shots 1-3. There may be small amounts of gas release in the gravel pile after 0.8 s, but there were no large fractures observable on the video like for Shots 1 and 2.

Figure 76. Crack from Shot 4 observed while walking around the borehole.

Two sections of PVC pipe (~20') were ejected from a nearby borehole, used for cross-hole tomography, by the explosive gasses during Shot 5. This hole as well as its partner hole on the other side of Shot 5 ejected large volumes of the bentonite grout. Individual snapshots of the video from Shot 5 are provided in Figure 77. The pipe can be seen leaving the borehole and the grout being ejected beginning 0.6 s and 0.8 s, respectively, after the detonation. Calculations to determine the maximum height attained by the PVC pipe returned values ranging from 20.3 to 45.6 m. The pipe hit a guy line, attached to a quarry tower crane, on the way down (Figure 78) making exact determination of height difficult. Although, we believe it to be approximately 33 m. Gas can be seen shooting from the borehole under high pressure for 4-5 s after the detonation. This loss of containment will affect the amount of gas available for driving fractures in the granite and will have to be taken into account during analyses.

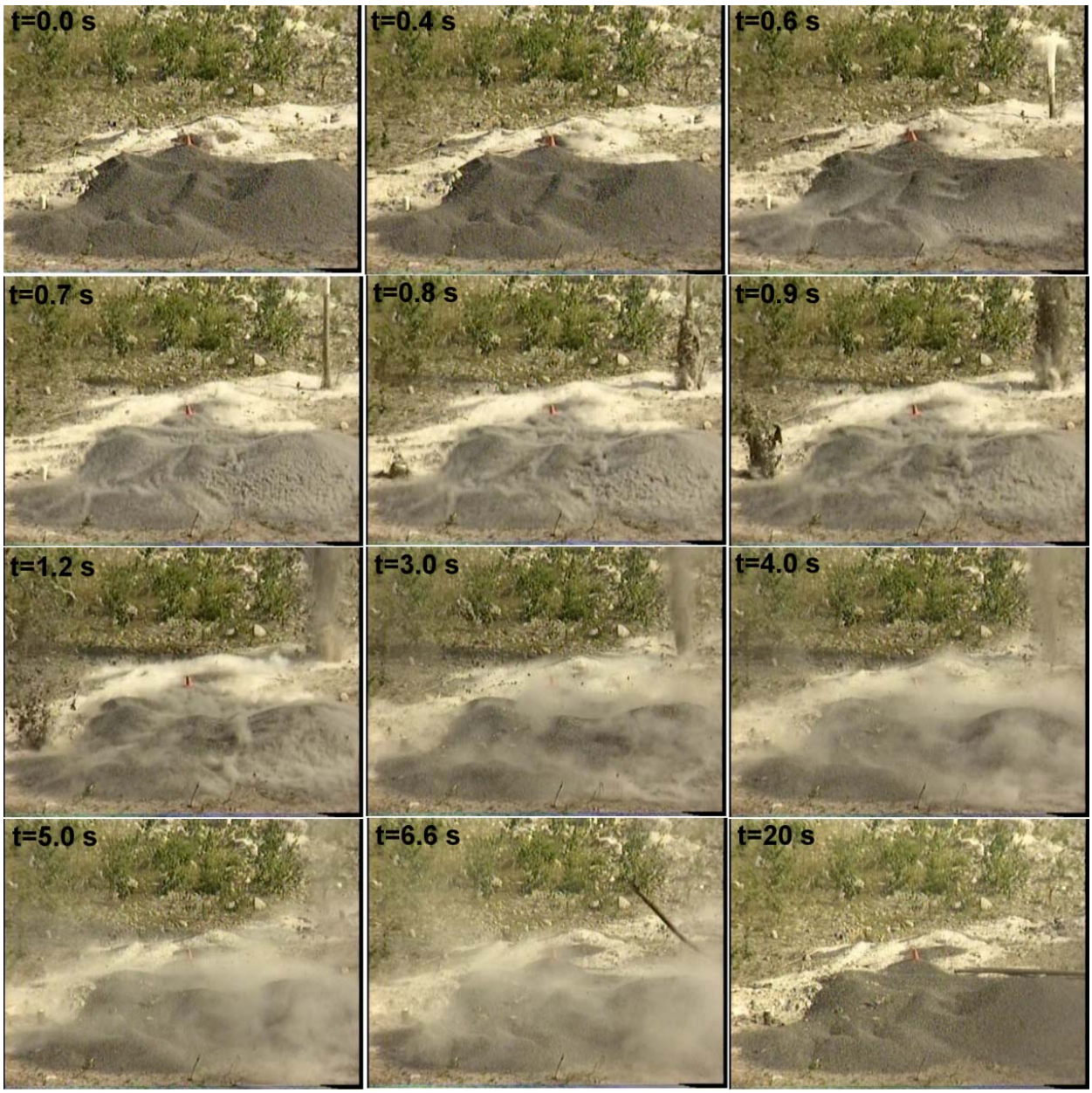

Figure 77. Digitized still images of the Shot 5 denotation. The PVC pipe begins to leave the borehole at 0.6 s and hits the ground at 6.6 s after detonation. No observable fractures were noted in the video.

Figure 78. PVC pipe breaking on guy line during free fall after being ejected from a nearby borehole during Shot 5.

4.3.4 Peak Particle Velocities

The proximity to nearby structures such as a cell/radio tower, the quarry high wall, and quarry cranes constrained the maximum size of the blasts we could conduct. The U.S. Bureau of Mines (USBM) sets peak particle velocity limits (U.S. Bureau of Mines RI 8507, 1980) that we followed. To allow for larger blasts, a second prospective test site was investigated in another region of the mine (Figure 52). Unfortunately, this site contained large xenoliths and the granite did not have a low fracture density (Figure 53).

The site in closer proximity to the tower and quarry structures was chosen due to the quality of granite. The predicted peak particle velocities were calculated to determine the maximum shot size using the following equation:

$$PPV=K*SD^{A},$$

where PPV is the peak particle velocity (in/s), K is a site constant (we used 605, the most conservative K value for an overly-confined explosion), SD is scaled distance ($ft/lb^{0.5}$), and A is another site constant (we used -1.6, a value based on low attenuation media).

The results of applying the planned shot sizes (either 200 or 400 lbs) and test site geometry in the above equation are shown in Figure 79. Also shown are the USBM limits for above and below 10 Hz and observed peak particle velocities from previous Weston Geophysical experiments. The values used in the above equation are very conservative and no prior observed data have exceeded the predicted values.

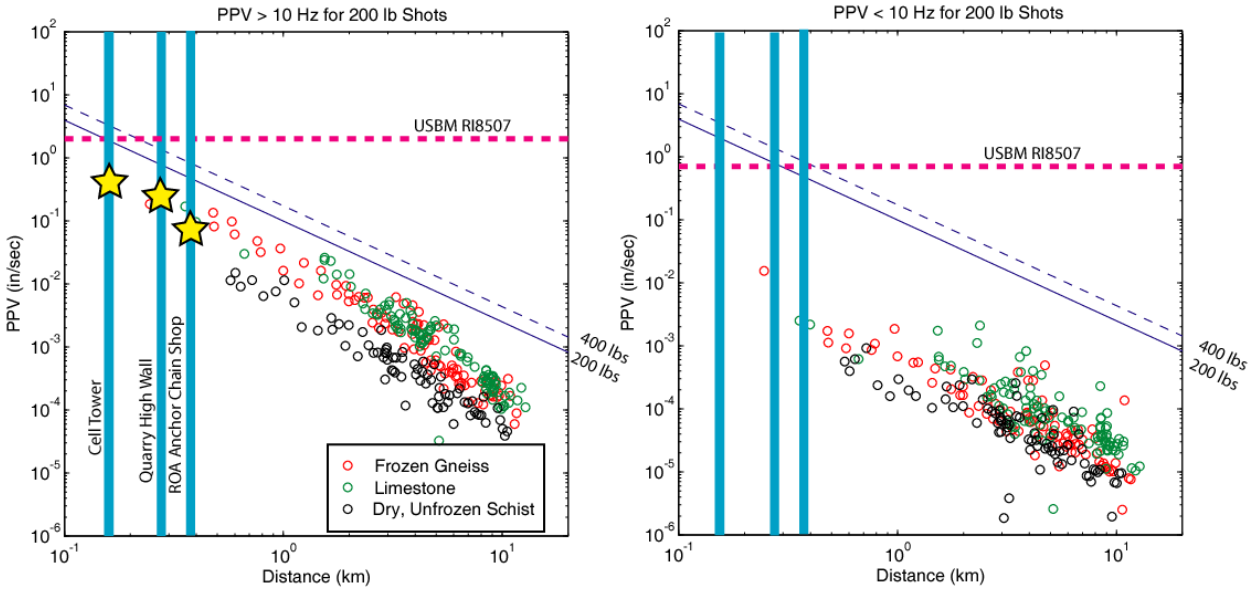

Figure 79. Vibration limits set by the U.S. Bureau of Mines (red dashed lines), the predicted values from our blasts (thin blue solid and dashed lines), distance to the nearby structures (thick vertical blue lines), and actual values from previous experiments (multi-colored circles). The peak particle velocities measured at the three structures from the NEDE blasts are shown as yellow stars.

Rob Haas of PreSeis, Inc. deployed "Instantel" seismic sensors at the cell/radio tower, quarry high wall, and the World War II anchor chain shop to provide rapid (and independent) measurements of PPV. The location of the WWII anchor chain shop was close to the nearest residential structure. Our plan was to shoot the smaller shots, measure the PPVs at each site, then decide whether or not to shoot the larger charges as planned or decrease their sizes. Figure 79 compares the observed maximum PPVs from the Instantels and the predictions. Table 17 shows which NEDE shot provided the maximum seismic vibration and acoustic signal at each structure. The values were all below the estimated PPVs and the USBM limits for safe vibration limits. The data seem to align along the trend of our measured values from previous explosion experiments.

Table 17. PPVs Measured by PreSeis, Inc

Location	Distance (ft)	Max PPV (in/sec)	Shot #	Max Acoustic (db)	Shot #
Cell/Phone Tower	403	0.420	2	114	4
Quarry Wall	875	0.290	5	114	4
Anchor Chain Shop	1192	0.060	3	105	2

4.4 Seismic Data Examples and Analyses

4.4.1 Near-Source

Below are a few examples of the near-source data recordings. In Figure 80 the vertical spall from all five shots is recorded on station N1B. Note the classic spall from Shot 5 with an impulsive shock wave arrival, 0.2 seconds of spall, and then a small spike from the slap down. Shot 4 has a double spike from the shock wave and a longer spall before three smaller slap downs. Shot 1 has a long duration shock wave arrival possibly caused by a "burning" of the explosives column instead of an instantaneous detonation. The origin times for the shots were determined from these data as well.

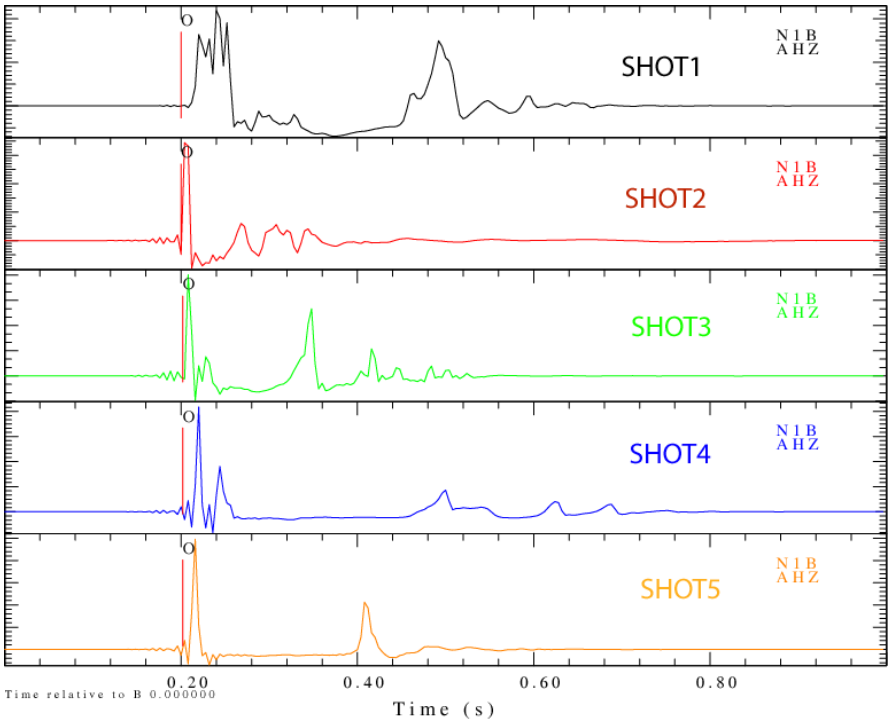

Figure 80. Near-source phenomenology for all five shots recorded on sensor N1B about 5 m from each blasthole collar. These data are not plotted on the same amplitude scales in order to better show the characteristics of the initial shock wave, the -1 g spall, and the spall slapdown(s). Figure 81 provides a better representation of the relative amplitudes between the shots.

Close-in vertical recordings of the shots look remarkably similar, particularly for shots 2, 3, 4, and 5 (Figure 81). Shot 1 appears to have lower frequency energy content in Figure 81. Three component data are shown in Figure 82 for the first three shots. It is interesting to note the large amplitude transverse components at these close-in distances, which have also been observed in prior experiments such as the Frozen Rock Experiment in Alaska.

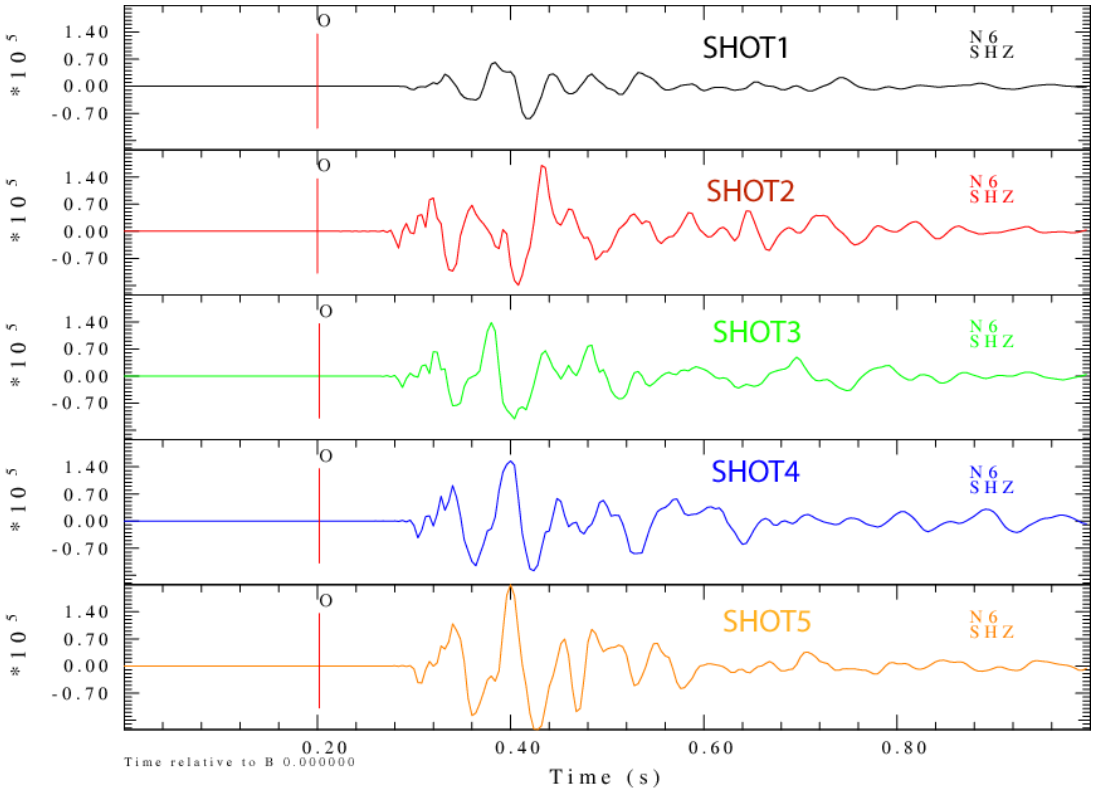

Figure 81. All five shots recorded on the L4-3D vertical channel of station N6. The data were scaled to the maximum amplitude on Shot 5.

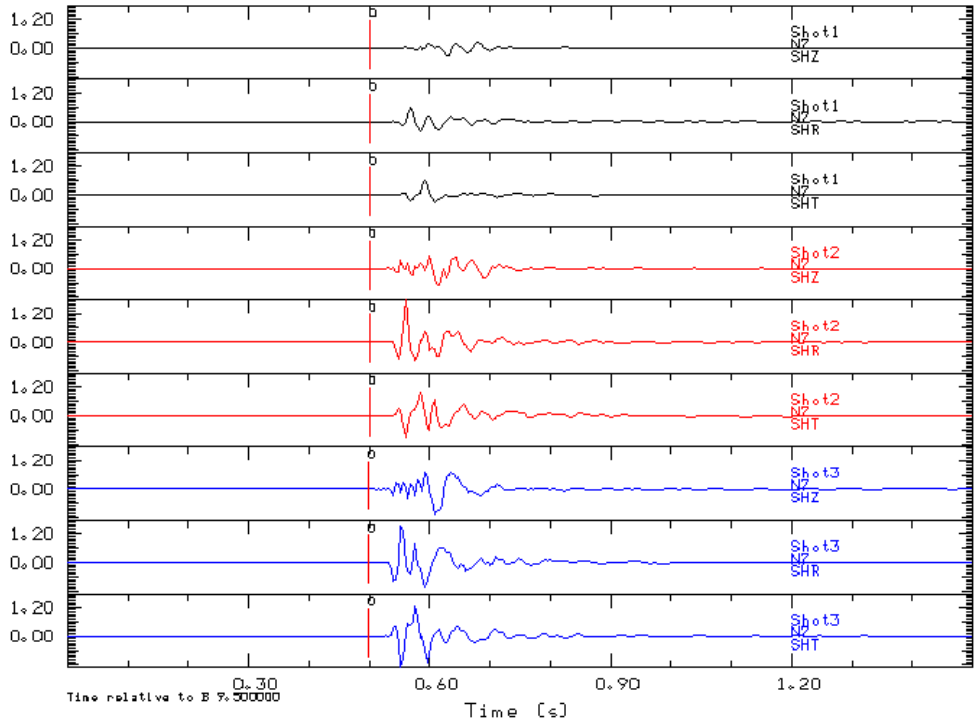

Figure 82. Vertical, radial, and transverse data of shots 1, 2, and 3 recorded on an L4-3D at station N7.

4.4.2 Short Period Linear Arrays

Band-passed, short-period linear array data is presented in Figures 90-92 highlighting the *P*, *S*(?), and surface waves. The pre-event noise data from NE08 (third from the top) are contaminated by the seismic response of a passing automobile.

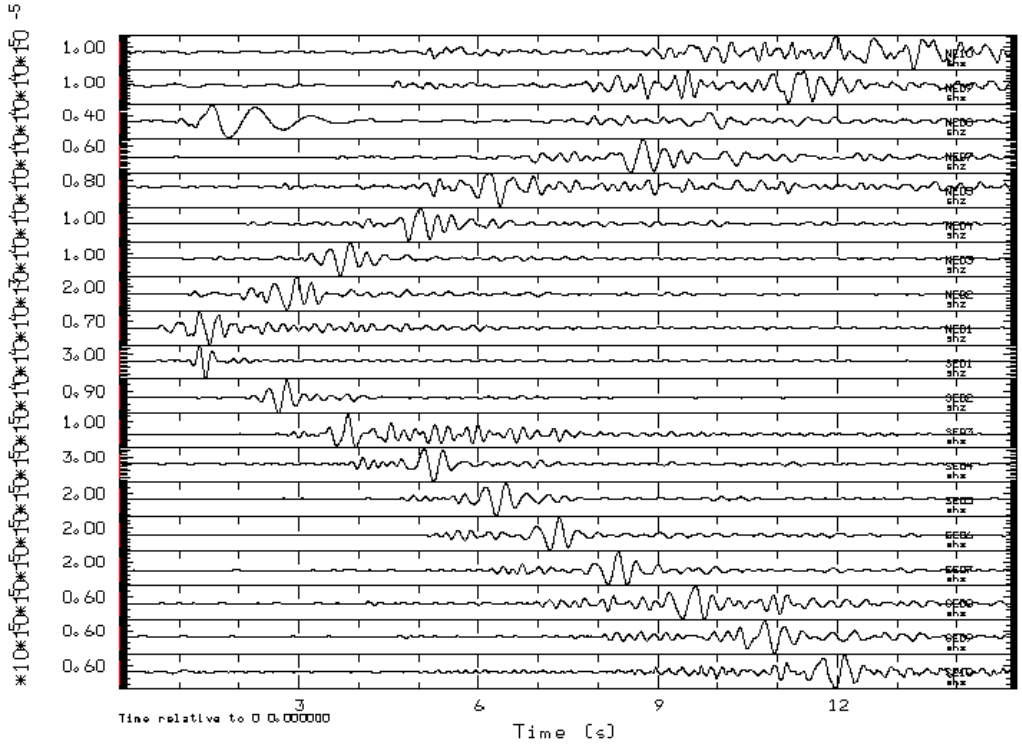

Figure 83. Shot 5 vertical recordings on the short period linear array from north (top) to south (bottom) band passed from 1-4 Hz showing the surface waves.

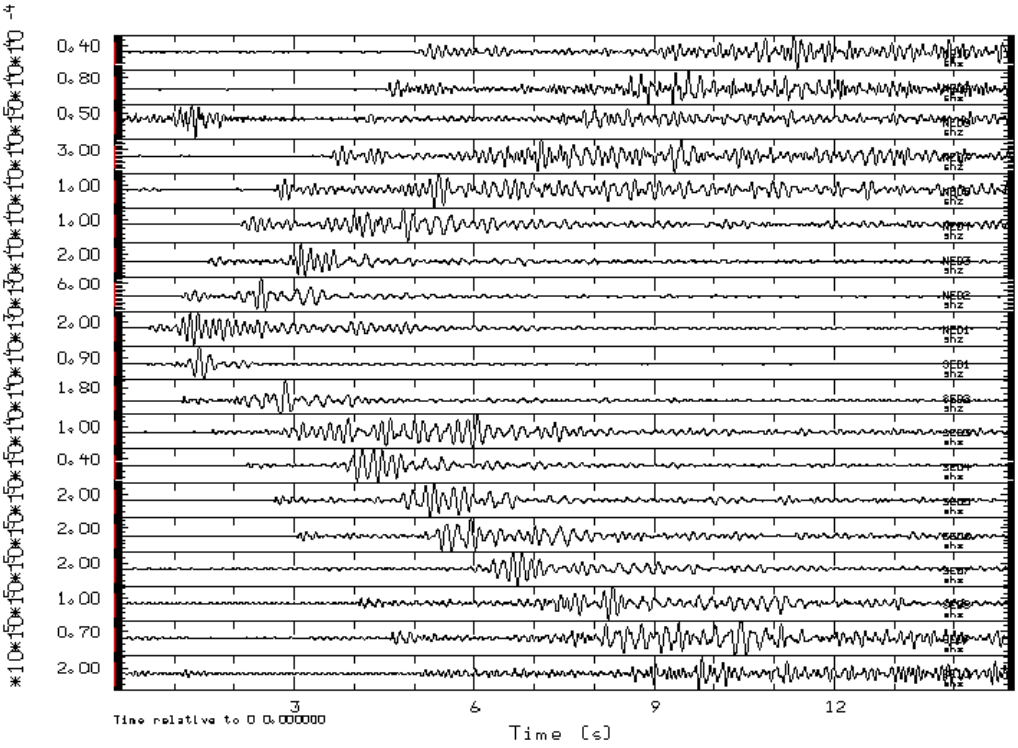

Figure 84. Shot 5 vertical recordings on the short period linear array from north (top) to south (bottom) band passed from 4-10 Hz showing the *P* and *S* (?) waves.

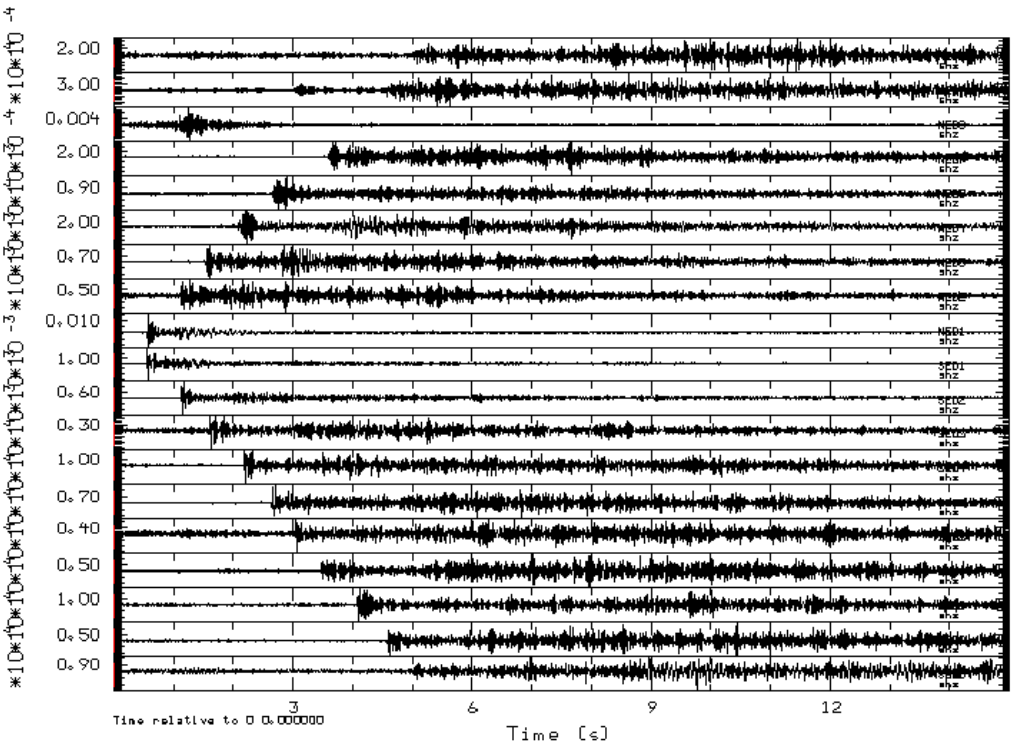

Figure 85. Shot 5 vertical recordings on the short period linear array from north (top) to south (bottom) high passed above 10 Hz showing the *P* waves and *P*- and *S*- coda.

In Figure 86, the Rayleigh waves from the five shots recorded at NE02 are plotted. At this station, the surface wave amplitudes are inversely related to the VOD of the explosives. This trend was observed at other stations. Combined with the observations that the slower VOD explosions generated more surface damage, these results may suggest that damage around the source was at least partly responsible for the generation of surface waves.

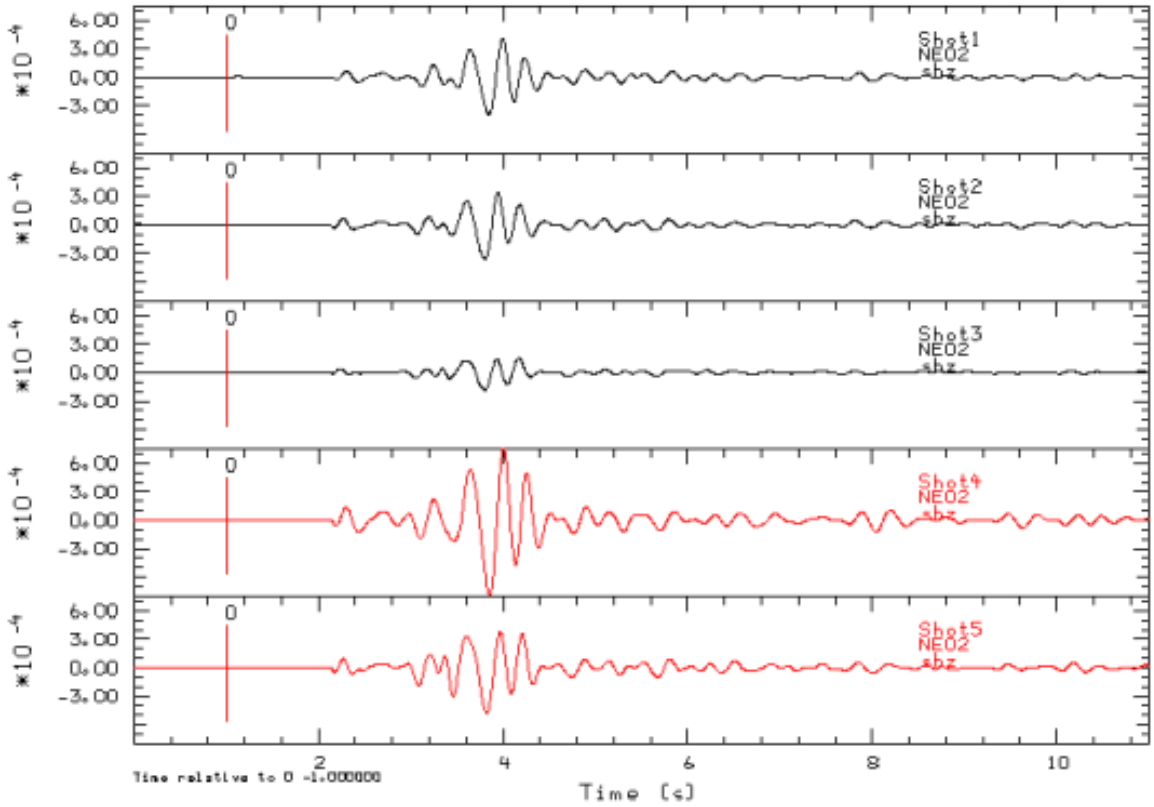

Figure 86. Rayleigh waves at station NE02 for all five shots. Vertical data are band passed between 0.5 and 4 Hz. Note decreasing amplitude of the Rayleigh waves from black powder (Shot 1) to ANFO/Emulsion (shots 2 and 4) to COMP B (shots 3 and 5). The waveforms are color coded by shot size, black=135 lbs, red=270 lbs.

4.4.3 Texans

Data from Shot 5, recorded on the two Texan profiles, are shown in Figure 87 and Figure 88. The data were band pass filtered between 4 and 10 Hz and plotted as a function of distance. The two Texans with either a bad cable connection or geophone are apparent in the plots. *P* and *S* arrivals are obvious in the data. The SE line of Texans appears to have a change in the shear wave arrival times around 13 km distance.

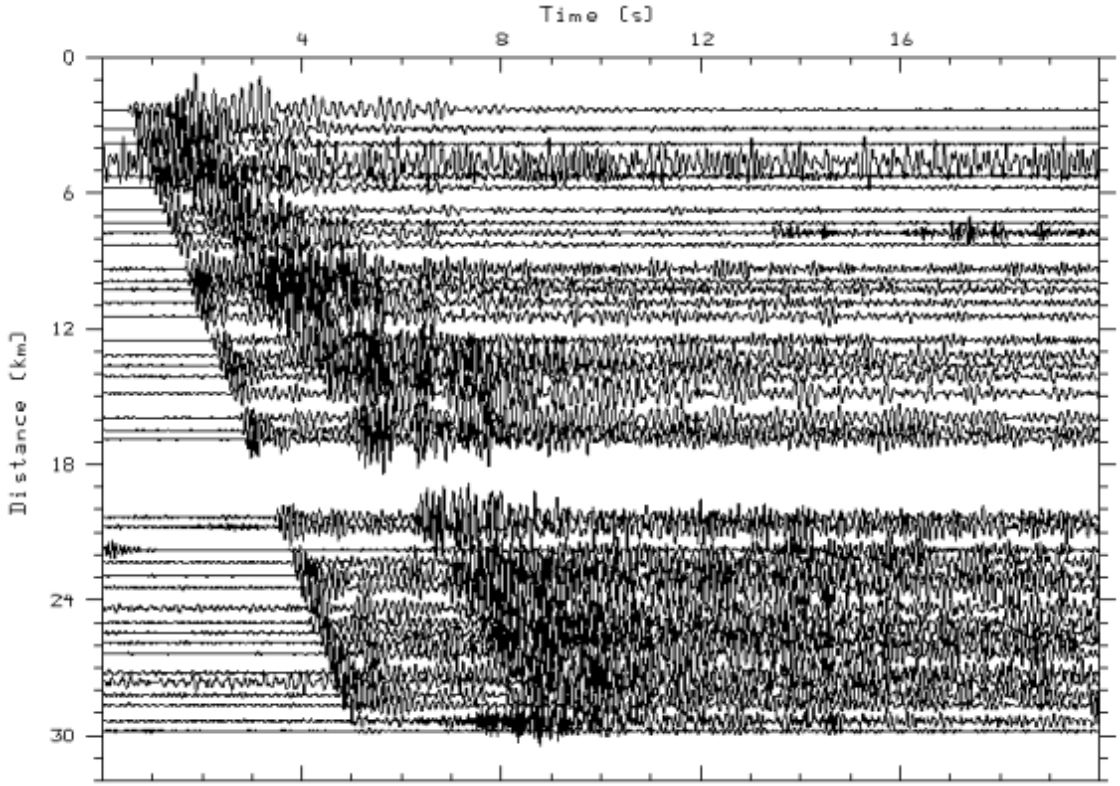

Figure 87. NE Texan line band passed from 4 to 10 Hz.

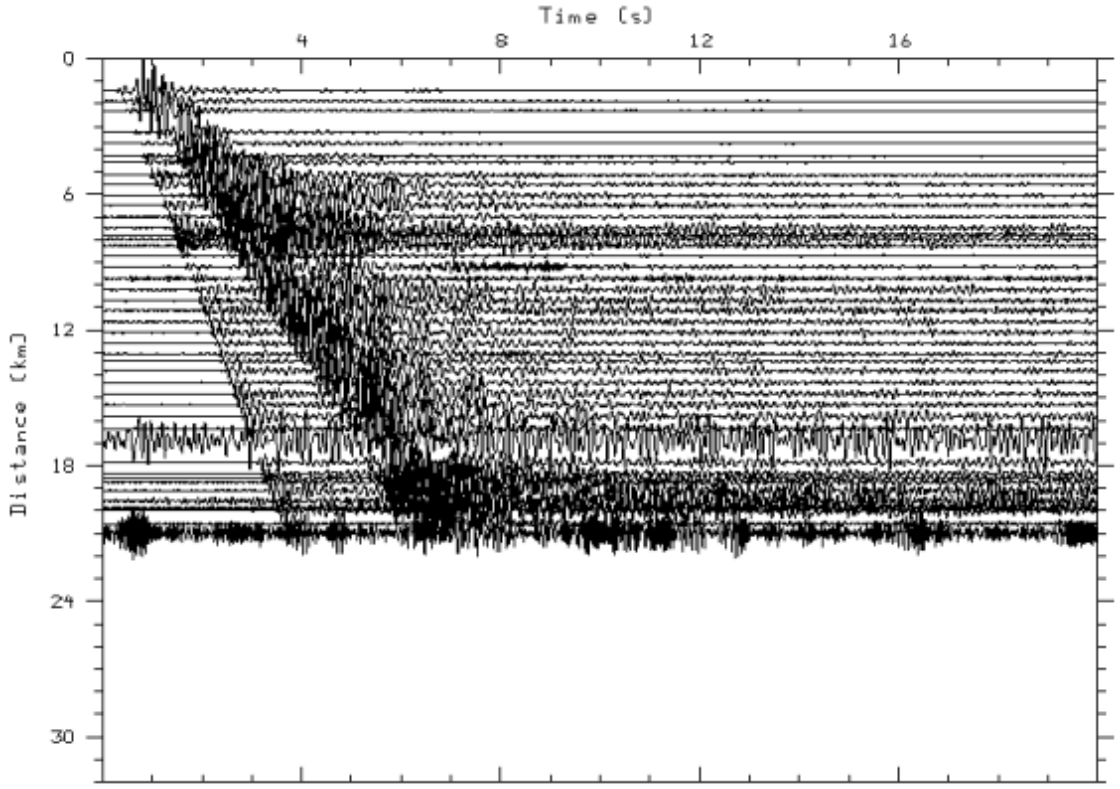

Figure 88. SE Texan line band passed from 4 to 10 Hz.

4.4.4 Regional

A number of regional stations in New England (Figure 89) recorded some or all of the NEDE shots. The signal-to-noise ratio (SNR) varies from fantastic at Lisbon, New Hampshire (LBNH) to not very good at most of the stations for Shots 1-3. With these data, our seismic data recording distance range varies from less than 5 meters (e.g., station N1B) to 281 km (174 miles as recorded at the USGS station in Peaks-Kenny State Park, Maine, PKME). The fact that the *Lg* phase from a 134 lb black powder explosion can be recorded over 280 km from the blast highlights both the low attenuation in New England and the quality of the PKME station. Examples of Love (Figure 90) and Rayleigh (Figure 91) waves from LBNH are plotted along with shots 4 and 5 recorded at PKME (Figure 92).

While the larger shots were recorded on the New England Seismic Network (NESN) stations HNH, QUA2, and FFD, the SNR is very low. HNH seems to be a very noisy station. QUA2 has harmonic noise dominating one of the components. The EHZ-only stations MDV and MIV of the Lamont-Doherty network have adequate SNR. The 3C station FRNY is probably the second-best recording (after LBHN) of the events from these permanent stations.

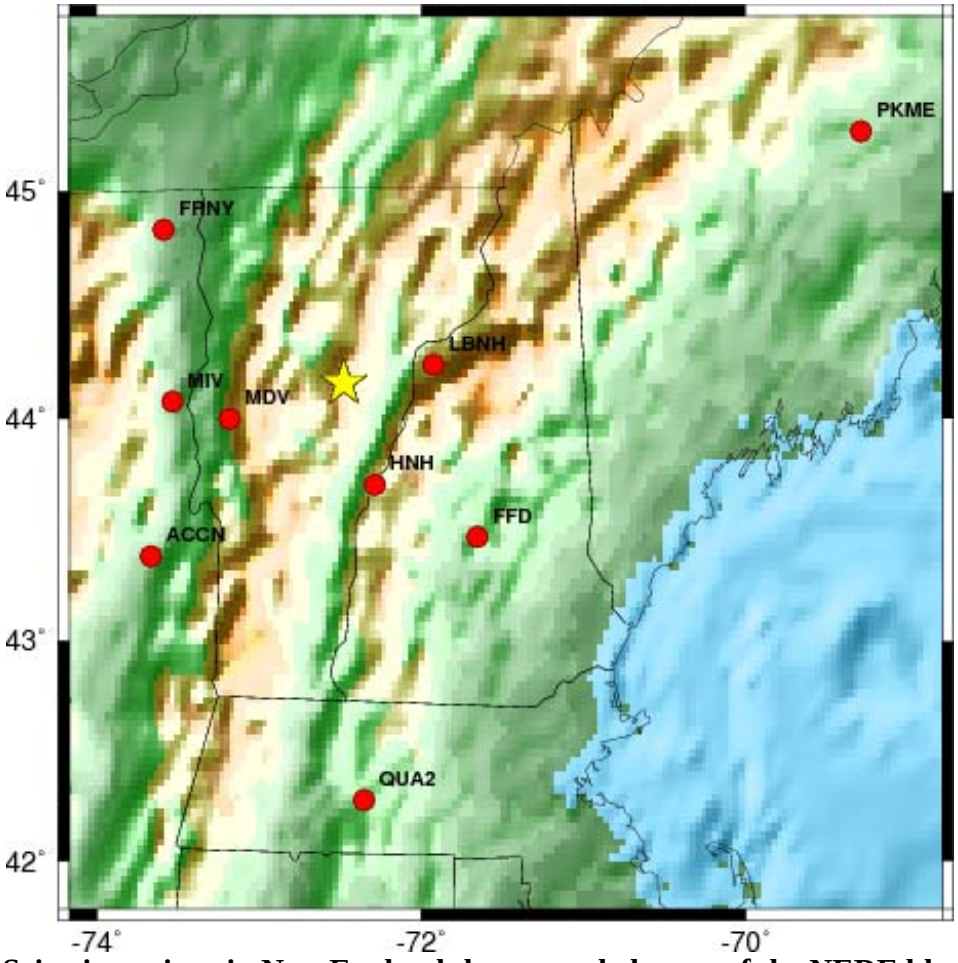

Figure 89. Seismic stations in New England that recorded some of the NEDE blasts (star).

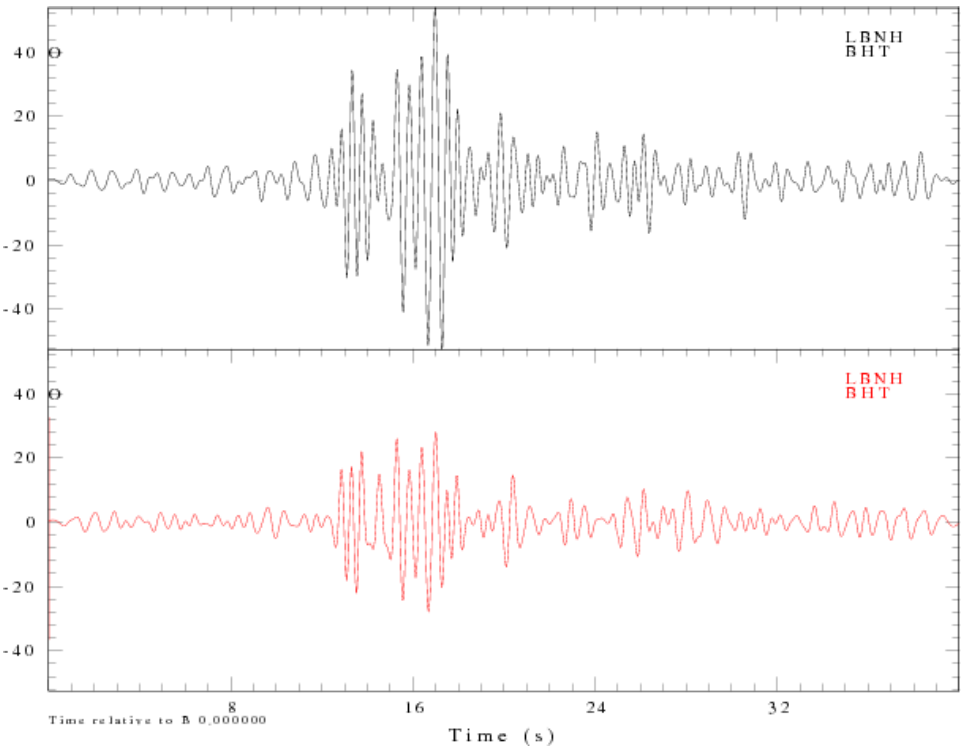

Figure 90. Love waves recorded on the BHT component of LBNH for Shot 4 (black) and Shot 5 (red). The later part of the wave train may be Rayleigh-waves that have scattered onto the transverse components. However, the first part of the wave train is definitely SH motion.

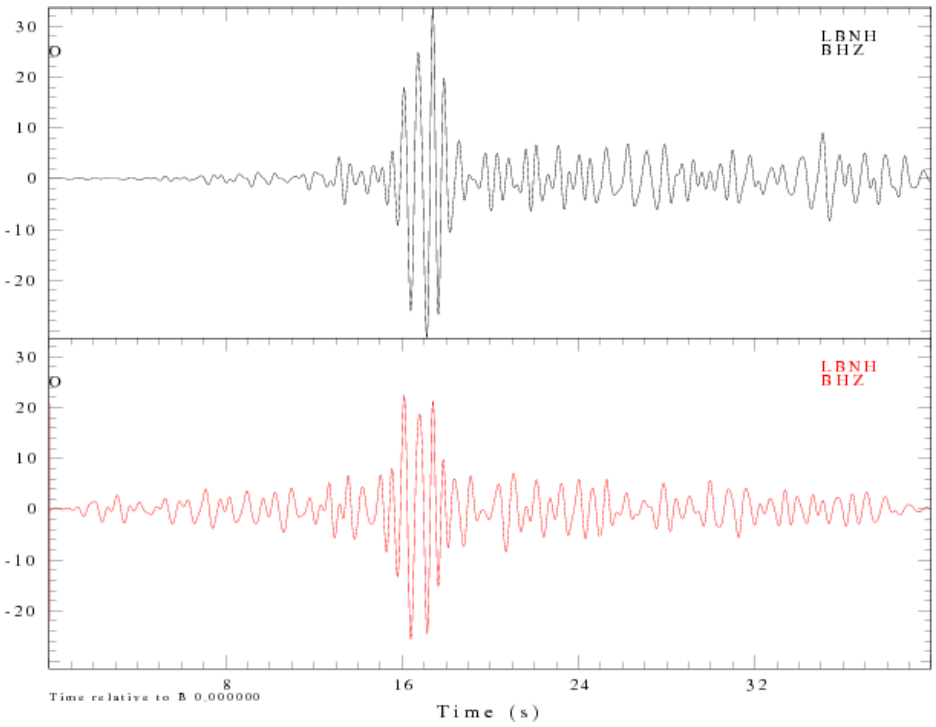

Figure 91. Rayleigh-waves recorded on the BHZ component at LBNH from Shots 4 (black) and 5 (red).

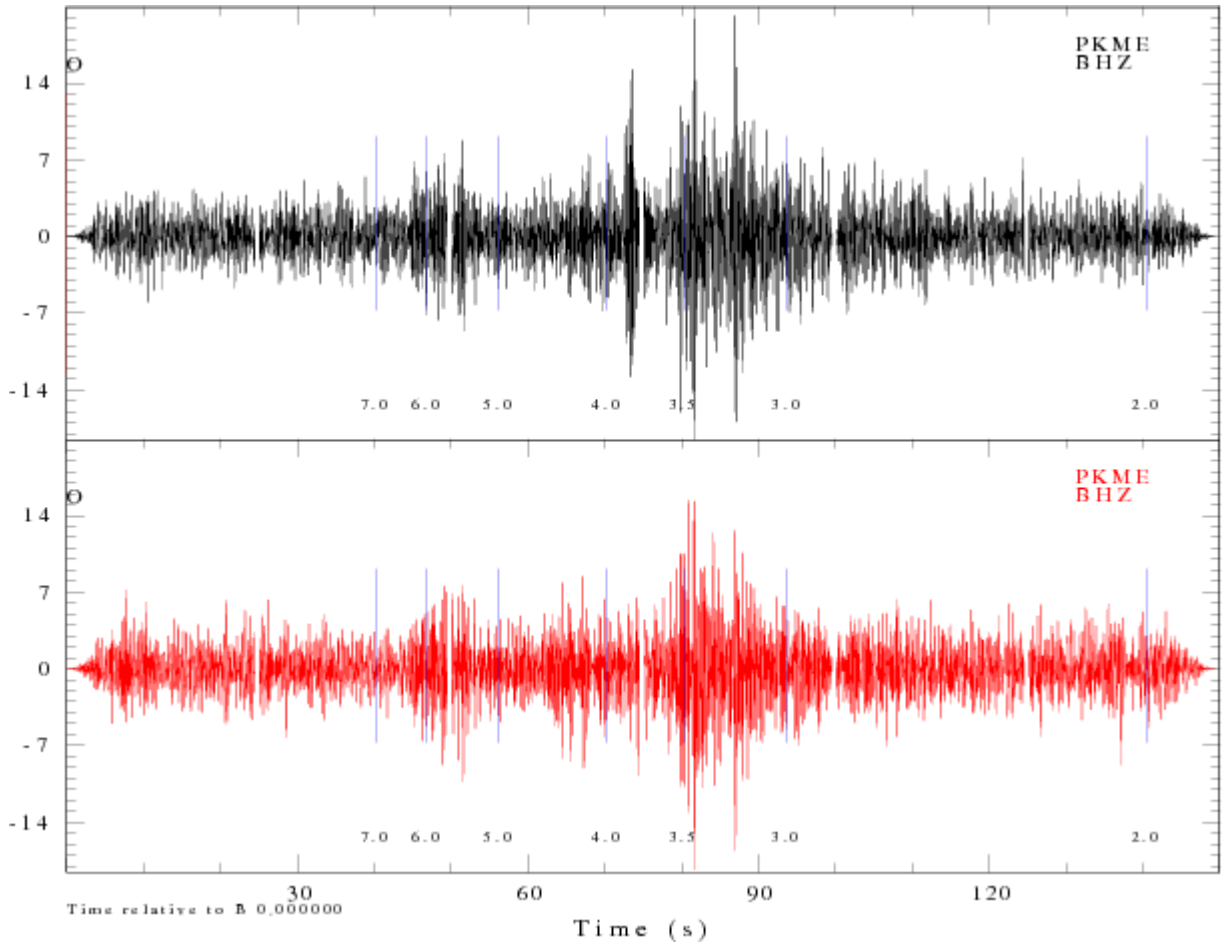

Figure 92. Shots 4 (black) and 5 (red) recorded at PKME (280 km). Note the impulsive arrival at group velocity 4 km/s only on the Shot 4 record.

4.5 Pre- and Post-Blast Source Rock Characterization

To quantitatively and qualitatively measure the damage caused by the blasts, geophysical studies were conducted on the source rock before and after (currently on-going) the explosions. Figure 93 shows initial planning for determining the damage to the source rock by drilling observational boreholes near the planned explosion. The pre-existing fractures and rock properties could be measured before the blast and then the fractures and damage could be observed in the boreholes after the explosions. This plan was modified for the actual experiment in that 2" diameter core was drilled near the explosion borehole and two boreholes were drilled on either side of the explosion borehole to perform a cross-hole tomography (Figure 94).

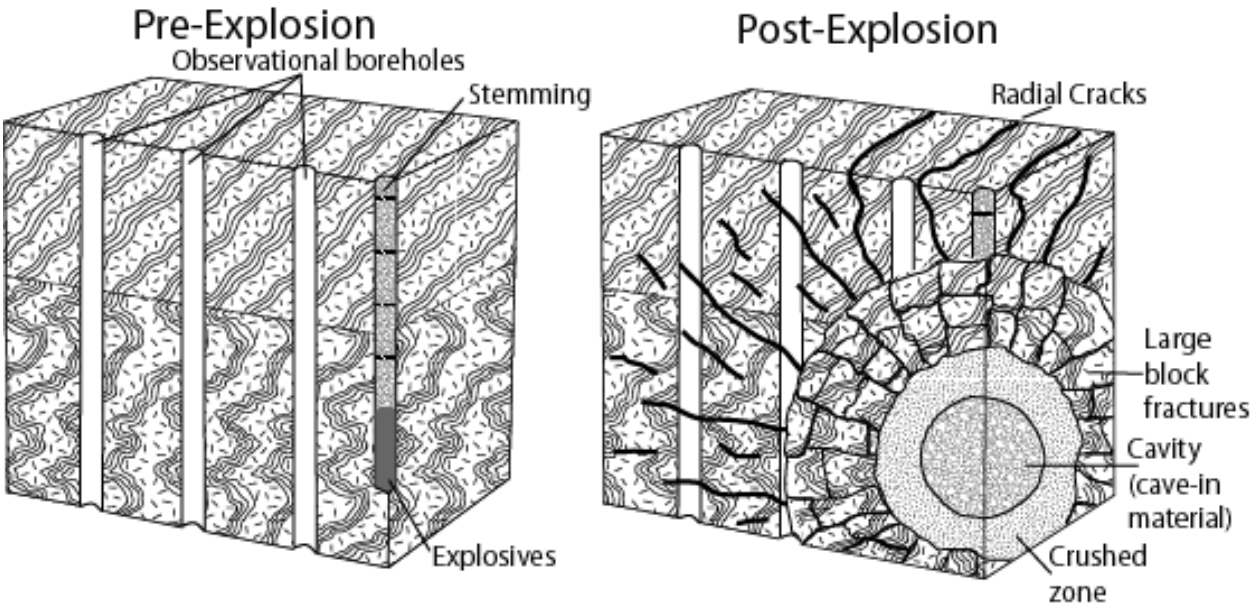

Figure 93. Diagram showing the initial planning for geophysical logging of the source rock before and after the explosions.

4.5.1 Core Samples

A photo of core taken from the test site is shown in Figure 95. The driller, Mike McGinley, had to break much of the core from the bottom of the hole due to the lack of natural fractures in the granite. Post-blast core samples are currently being extracted to compare to the pre-blast samples.

A velocity analysis of the core extracted from near Shot 2 was completed by Peter Boyd (New England Research, Inc). Figure 96 plots the compressional wave velocity as a function of depth in the core hole. The velocity increases with depth and has a change in slope at approximately 30 feet. The increase in compressional wave velocity with orientation, at a single depth, can approach 25 percent.

Figure 97 shows the diametrally-transmitted compressional wave velocity, as a function of chord orientation, in the core specimen recovered from near Shot 2. The “Fast” chord defines the strike of the rift plane in the Barre granite, which is N30E° at this site (Donald Murray, pers. comm. 2008). The rift plane is considered to be near-vertical and is the orientation that the granite blocks break cleanly when being quarried. The fastest compressional wave velocity is ~19 percent greater than the slowest velocity in this specimen.

4.5.2 Televiewer

Dorothy Richter, Rob Garfield, and Alexis Martinez of Hager-Richter Geoscience were responsible for performing optical and acoustic televiewer logging of the test site (Figure 98) before and after the blasts. The resulting images provide a 360° view of the borehole walls for mapping fractures (Figure 99). Table 18 lists the fractures found in core hole 1 (CH-1), and the rank defines the size and aperture of the fracture. This examination was carried out for all five core holes and is being conducted again after the explosions to determine the damage done to the granite by the blasting (assuming borehole stability).

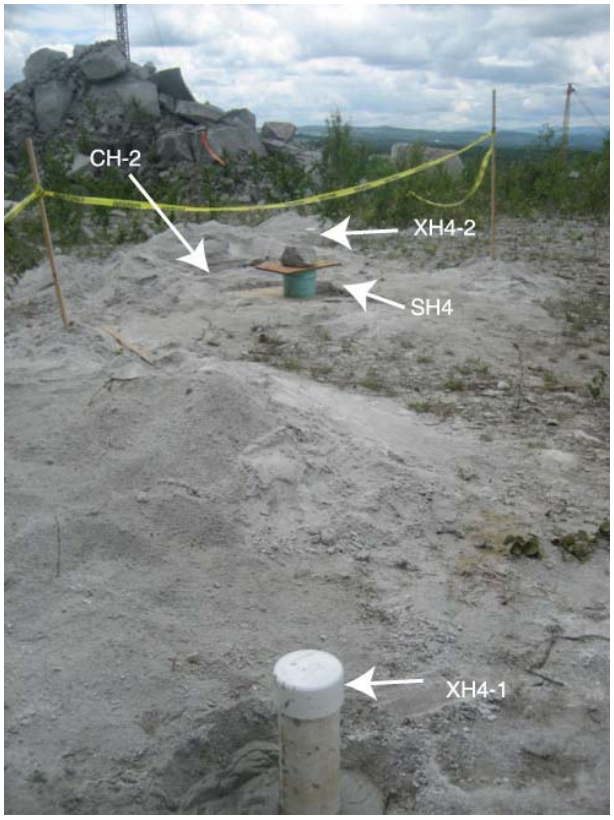

Figure 94. Typical layout of blast hole (SH4), core hole (CH-2), and cross-hole tomography holes (XH4-1 and XH4-2) for all five shots.

Figure 95. Example of unfractured core taken from the test site.

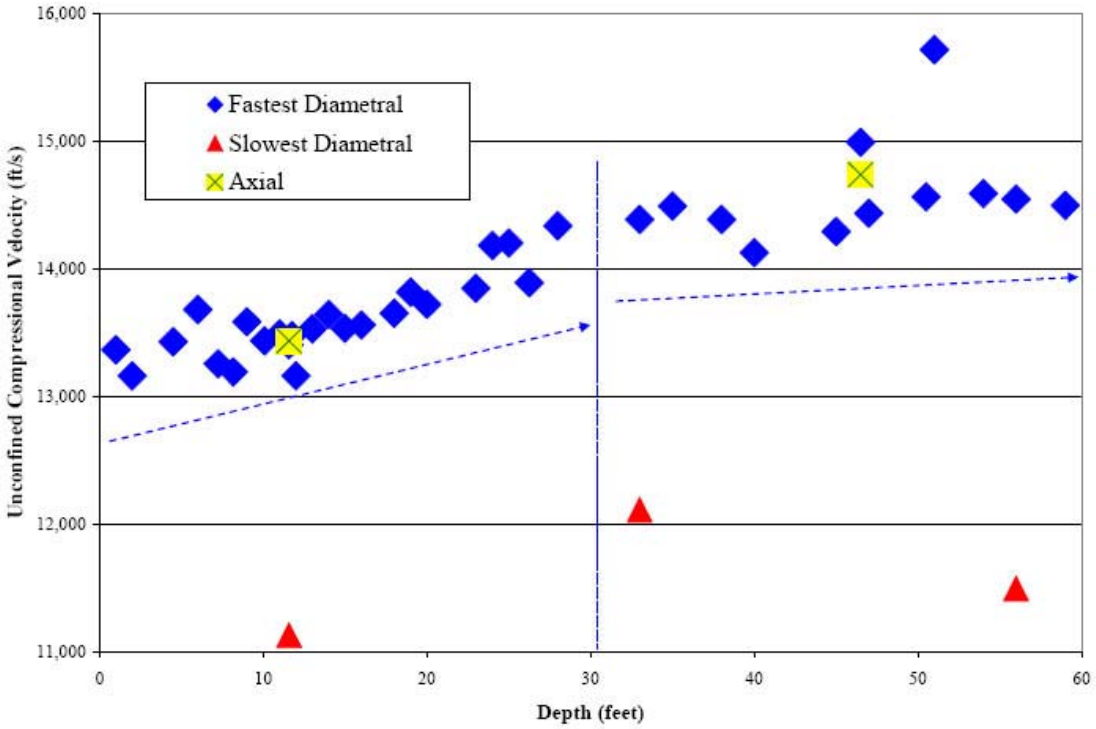

Figure 96. Compressional wave velocity determined in a laboratory study of core taken from near Shot 2. The diametrals indicate orientation in the core hole.

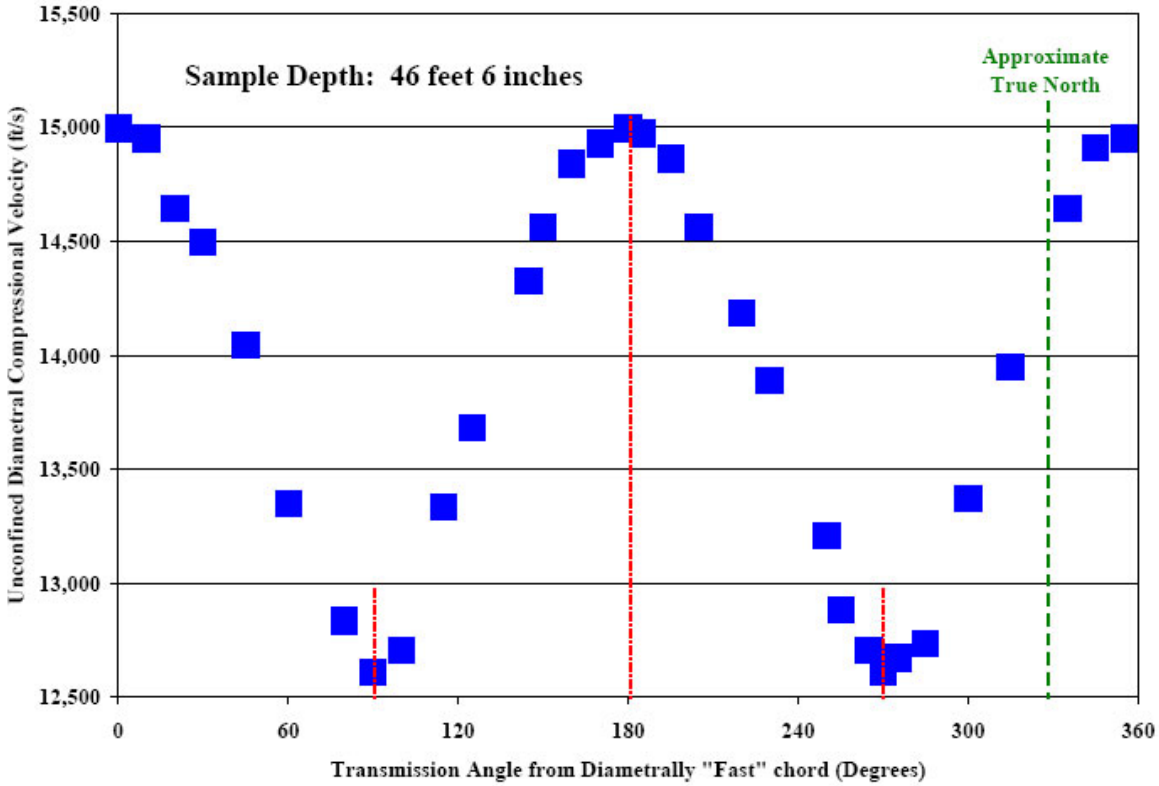

Figure 97. Compressional wave velocity as a function of azimuth in the Barre granite near Shot 2. The fast direction is oriented ~30° east of true north and is believed to follow the "rift" of the granite.

Figure 98. Logging with acoustic and/or optical televiewer.

Table 18. Structures in the Granite of Core Hole 1.

Depth (ft)	Dip Azimuth (°)	Dip Angle (°)	Bedrock Structure
6.5	187	82	Fracture Rank 1
7.7	101	4	Fracture Rank 3
8.3	185	17	Fracture Rank 2
8.4	265	14	Fracture Rank 2
8.5	263	19	Fracture Rank 2
9.9	179	67	Fracture Rank 1
10.1	195	7	Fracture Rank 2
10.2	172	20	Fracture Rank 2
11.9	82	41	Fracture Rank 1
11.9	260	16	Fracture Rank 2
13.2	353	45	Fracture Rank 1
13.6	224	39	Fracture Rank 2
14.6	65	48	Fracture Rank 2
21.1	241	68	Fracture Rank 2
39.6	105	26	Fracture Rank 2
50.8	105	26	Fracture Rank 2

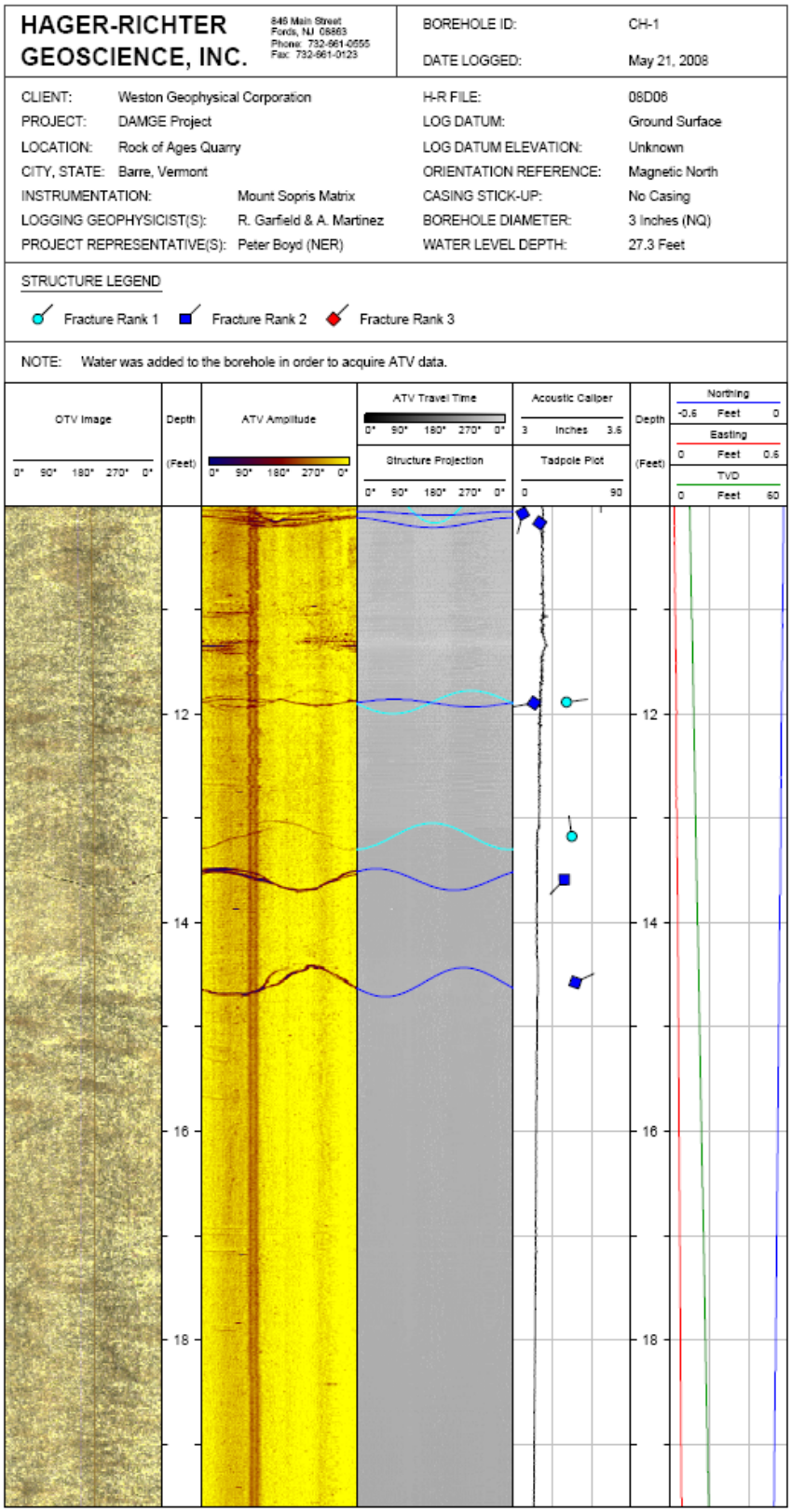

Figure 99. Optical and acoustic televiewer log documenting fractures in the granite.

4.5.2 Cross-hole Tomography

A cross-hole tomography was to be conducted prior to the blasting across each blast hole, but the grout used to hold the PVC pipe in the holes was bentonite-based instead of cement based. The result is shown in Figure 100. The grout did not solidify properly to secure the PVC pipe and "attach" it to the bore hole wall. It was therefore not possible to conduct the cross-hole tomography.

Figure 100. Grout collapsed around PVC pipe in a cross-hole tomography bore hole.

5. CONCLUSIONS

5.1 Year One

During the first year of this contract, we negotiated agreements with numerous mines and quarries in New England that were willing to participate and detonate small (100 to 2000 lbs) simultaneously-detonated explosions in addition to their routine mining explosions. We obtained permits to deploy seismic stations at state parks in Connecticut and Vermont with additional candidate sites located in New York and New Hampshire to record these blasts. In addition, a seismo-acoustic array was designed for deployment near the Hanscom Air Force Base near Bedford, MA in order to try and differentiate urban-generated seismic signals from mining and earthquake associated phenomena.

5.2 Year Two

We were not awarded any new funds to carry out the planned explosions during the second year of the project. Instead, we continued with our plan to deploy the Hanscom Seismo-Acoustic Array in order to develop a database of seismo-acoustic signals in an urban setting. The four element acoustic array with single broadband seismic station, code named HANS, was deployed and became operational in December 2006. In the initial year of operation, we recorded natural and manmade seismicity at local and near-regional distances. The database developed thus far includes seismic and acoustic waveforms from nearly co-located quarry blasts and earthquakes near the town of Littleton, MA. Additionally, we have a database of seismic and acoustic data from 16 construction explosions that include on-site instrumentation. The database is supplemented with blasting information as well as seismic data from other stations in New England. We also have an extensive number of acoustic signals in the database from known (military or commercial aviation) and unknown sources. We continued the development and analysis of this database in the final year of this project as well as accomplishing our goals of examining small explosion source phenomenology in hard and crystalline rock.

5.3 Year Three

During the final year of this contract, we conducted the New England Damage Experiment (NEDE) in Vermont to examine how rock damage affects surface and shear wave generation. We detonated five explosions using three explosive agents with dramatically different velocity of detonations. The homogeneous low fracture density source rock granite was characterized in-situ and in the laboratory before and after the blasting to quantify the fracturing and rock damage done by the explosions. Results from this experiment suggest that creating long fractures during blasting generates increased Rg and shear wave energy in the frequency range dominated by surface wave (<5 Hz). In addition, we continued operation of the HANS seismo-acoustic array.

REFERENCES

Ashby, M.F. and C. G. Sammis, (1990). The Damage Mechanics of Brittle Solids in Compressions. *Pure appl. Geophys*. **133**. 489-521.

Bassin, C., G. Laske, and G. Masters (2000). Current limits of resolution for surface wave tomography in North America, *EOS Trans AGU*, 81, F897.

Chiburus, E. F., and R.O. Ahner (1979). Northeastern U.S. Seismic Network Bulletin **15**, p. 7.

Doolan, B., (1996). The Geology of Vermont, *Rocks and Minerals Magazine*, Vol. 71, No. 4, pp. 218-225.

Geology of Korea (1996), Institute of Geology, State Academy of Sciences, DPR of Korea, Foreign Languages Books, Publishing House, Pyongyang.

Kadinsky-Cade, K. R.S. Jih, A. Dainty, D. Reiter, V. Hsu, R. Blandford, W. Walter, K. Mayeda (1996). Proceedings of the February 1996 Workshop on Seismic Location and Discrimination in Korea (U). PL-TR-96-2086. SR. No. 279.

Kafka, A.L., and M.F. Dolin (1985). Constraints on lateral variations in upper crustal structure beneath southern New England from dispersion of *Rg* waves, *Geophys. Res. Lett.*, **12**, 235-238.

Kafka, A.L., and J.W. McTigue (1985). The Avalonian terrane and Merrimack trough in southern New England: similarities and differences in upper crustal structure from dispersion of *Rg* waves, *Eos. Trans. AGU*, **66**, 987.

Kafka, A.L., and E.C. Reiter (1987). Dispersion of *Rg* waves in southeastern Maine: evidence for lateral anisotropy in the shallow crust, *Bull. Seism. Soc. Am*., 77, 925-941.

Kafka, A.L. (1990). *Rg* as a depth discriminant for earthquakes and explosions: a case study in New England, *Bull. Seism. Soc. Am.*, **80**, 373-394.

Jeon, J.S., M.S. Jun, J.W. Park, I. Che (2001). P-wave velocity model in South Korea, *Proceedings of the 3rd Workshop on IMS Location Calibration*, NORSAR, 23-27 April, 2001.

Luetgert, J. H. (1985). Depth to Moho and characterization of the crust in the northern Appalachians from 1984 Maine-Quebec seismic refraction data, *Earthquake Notes*, **43**, 31-39.

Melosh, H. J., (1979). Acoustic Fluidization: A New Geologic Process. *J. Geophys. Res*., **84**, 7513-7520.

Patton, H. J. and S. R. Taylor, (1995). Analysis of *Lg* Spectral Ratios from NTS Explosions: Implications for the Source Mechanism of Spall and the Generation of *Lg* Waves, *Bull. Seism. Soc. Am.* **85**, 220 - 236.

Patton, H., J. Bonner, and I. Gupta, (2005). *Rg* Excitation by Underground Explosions: Insights from Source Modeling the 1997 Kazakhstan Depth of Burial Experiments. *Geophys. J. Int*. doi:10.1111/j.1365-246X.2005.02752.x.

Peterson, J., (1993). Observations and modelling of background seismic noise. Open-file report 93-322, U. S. Geological Survey, Albuquerque, New Mexico.

Rodean, H.C., (1971). Nuclear-Explosion Seismology, U. S. Atomic Energy Commission, TID-25572, 156 pp.

Saikia, C.K., A. L. Kafka, S. C. Gnewuch, and J. W. McTigue (1990). Shear velocity and intrinsic Q structure of the shallow crust in southeastern New England from Rg wave dispersion. *J. Geophys. Res.* **95**, 8527-8541.

Sammis, C. G. (2002). Generation of High-Frequency *P* and *S* Wave Energy by Rock Fracture During a Buried Explosion: Its Effect on *P/S* Discriminants at Low Magnitude, Proceedings of the 24th Seismic Research Review – Nuclear Explosion Monitoring: Innovation and Integration, Sept. 17-19, 2002, Ponte Verde Beach, Florida, 542-551.

Schnerk, R., Agarwal, Y.P., Golisono, M. and F. England (1976). Regional seismological bulletin of the Lamont Doherty network: Palisades, New York, Lamont-Doherty Geological Observatory, 15 p.

Stevens, J.L., G. E. Baker, H. Xu, T.J. Bennett, N. Rimer, and S.M. Day, (2003). The Physical Basis of *Lg* Generation by Explosion Sources. *Proceedings of the 25th Annual Seismic Research Review on Nuclear Monitoring Technologies*, Tucson AZ.

Taylor, S.R. (1980). Crust and upper mantle structure of the northeastern United States [Ph.D Thesis]: Cambridge, Massachusetts Institute of Technology, 288 p.

Zen, E-an, (1968). Nature of the Ordovician Orogeny in the Taconic Area, in *Studies of Appalachian Geology – Northern and Maritime*, edited by E-an Zen, W.S. White, J.B. Hadley, and J.B. Thompson, Interscience Publishers, 129-139.

APPENDIX A. HUDDLE TEST PRIOR TO THE NEDE

We conducted a huddle test with all the near-source and linear short period array sensors in Lexington, MA, on 6 July 2008 prior to packing the equipment up and trucking it to Barre, VT. The two primary goals of this test were to assemble working stations with DAS, GPS clocks, hard drives, and sensors and to record the same signals on all the sensors so we could compare instrument response for correcting the NEDE blast data.

Figure 101 shows the Weston, PASSCAL, and Los Alamos National Laboratory (LANL) sensors with batteries and digitizers in close proximity to record the same signals at 250 sps. Table 19 lists the equipment used during the huddle test. The PASSCAL and LANL sensors did not have feet so it was a challenge to level them on the sloping parking lot.

Figure 101. Huddle test in the Weston Geophysical parking lot prior to the experiment.

Some of the old LANL sensors had bad channels and were not used for the actual experiment. For the short period equipment, a Weston RT130 power cable was found to have reversed polarity connectors. Reversing the connection to the battery fixed this problem. In addition, the parameter files did not upload properly to two DAS and the data were set to be downloaded to disk and ethernet. This caused the internal memory to fill and dump to disk once and then stop recording. Data were collected for the majority of the huddle test though. A PASSCAL RT130

would not boot so no data were collected. This DAS was repaired in the field and used for the experiment. We also found that leaving the new RT130 Palm controllers in the sun causes the screen and system to act erratically.

Table 19. Huddle Test Setup.

DAS	Disk	GPS	CH 1-3	CH 4-6	Notes
734	5715	663	Endevco 6	Endevco 2	All chans good
619	87	664	L4-3D 619	TerraTek 9	All chans good (TT hi-freq noise on Z and E)
716	5106	248	L4-3D 84	TerraTek 13	L4 bad E; TT has bad N
745	5236	299	L4-3D 37	TerraTek ??	Re-do test
739	5237	674	L4-3D 623	TerraTek 6	L4 bad E and N valid >30 Hz; TT good, Z may be enhanced
737	5180	670	L4-3D 189	TerraTek 4	Re-do test
744 (1768)	5713	244	L4-3D 257	TerraTek 7	Re-do test
733	5959	669	L4-3D 628		All chans good
9E4B	-	2514	L4-3D L41167		Good
9D8F	-	2661	L4-3D L41166		Good; 1 data dump
9DEA	-	2448	L4-3D L41169		Good
9E18	-	2565	L4-3D L41162		Good
9E1B	-	2711	L4-3D L41164		Good; 1 data dump
9D63	-	2665	L4-3D L41168		Good
9E42	-	2516	L4-3D L41161		Good
9E4F	-	2531	L4-3D L41165		Good
9DAA	-	2520	L4-3D L41170		Good
9E17	-	2809	L4-3D L41163		Good
939E	-	4194	L22 449L		Good
930E	-	3890	L22 643L		Good
9E45	-	4175	L22 642L		Good
9E40	-	4161	L22 468L		DAS would not boot; not tested
A198	-	4176	L22 462L		Good
9E50	-	4188	L22 720L		Good
940F	-	4196	L22 479L		Good
9312	-	4189	L22 496L		Good
9D42	-	4198	L22 494L		Good
9669	-	4179	L22 459L		Good

Data examples from the huddle test are shown in the following figures. The “flip test” (Figure 102 and Figure 103) for accelerometers involves turning the accelerometer upside down for a moment to record 1 g of acceleration. For the seismometers, various signals are examined to determine if all channels are working and how the signals vary from sensor to sensor (Figure 104, Figure 105, and Figure 106). Both the Weston L4-3D (Figure 107) and the PASSCAL L22 (Figure 108) sensors have self-similar responses. It is important to understand the response difference between the L4-3D and L22 sensors. Figure 109 compares the same vertical signal on the two types of sensor after the data have been converted to velocity (cm/s). The signals are almost identical. The polarity on the Weston L4-3D horizontal components needs to be reversed, but almost identical signals were produced for these components after correction as well.

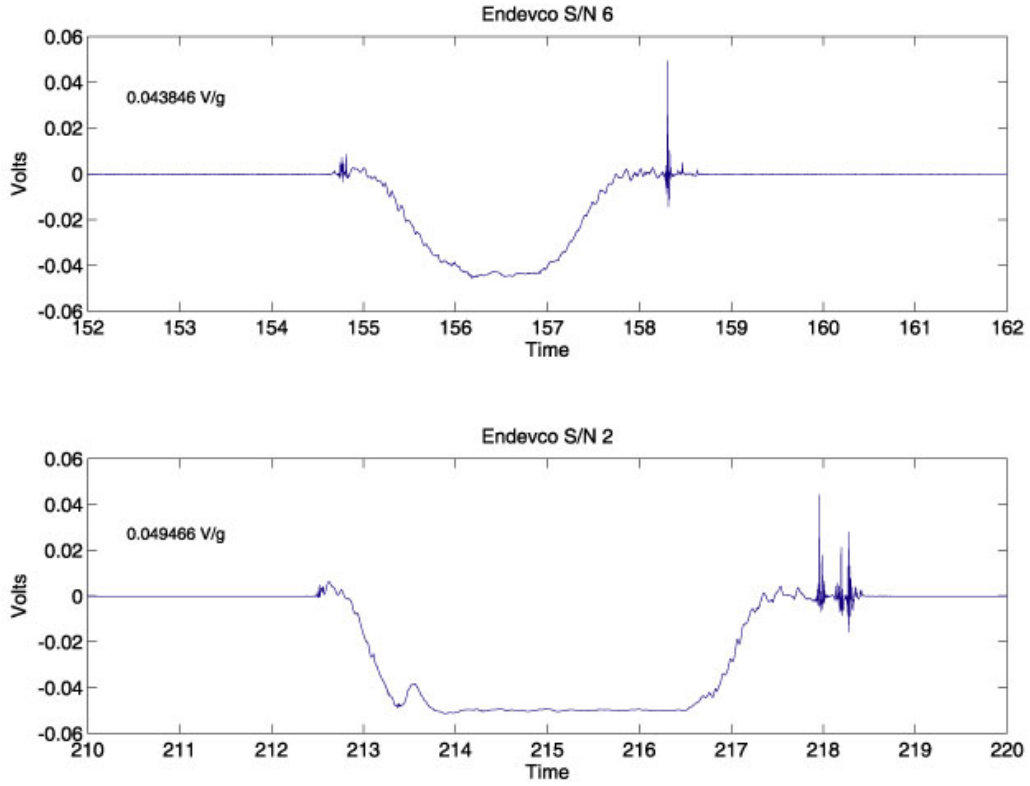

Figure 102. "Flip test" for Endevco sensors.

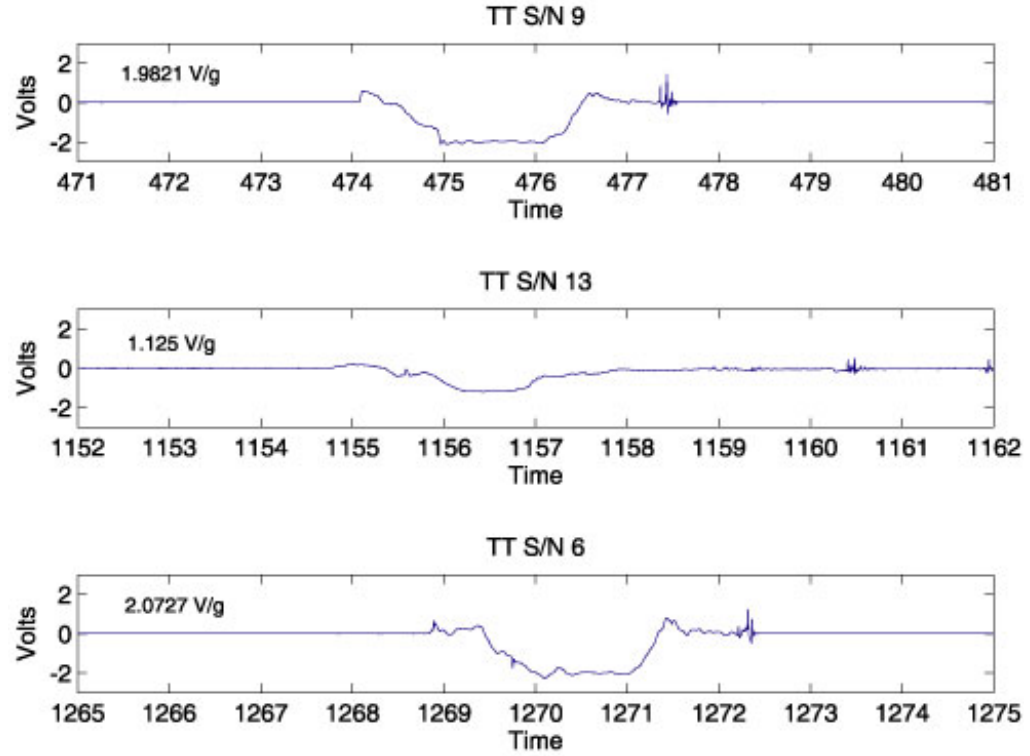

Figure 103. "Flip test" for TerraTek sensors.

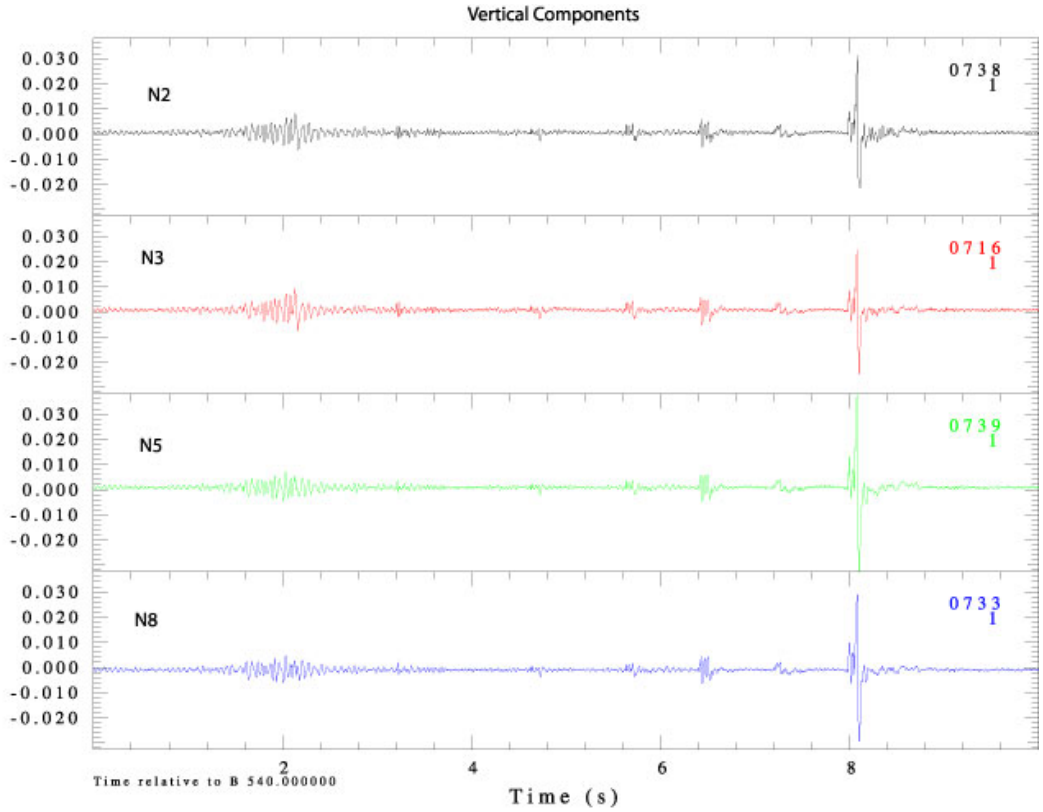

Figure 104. Near-source vertical L4-3D components.

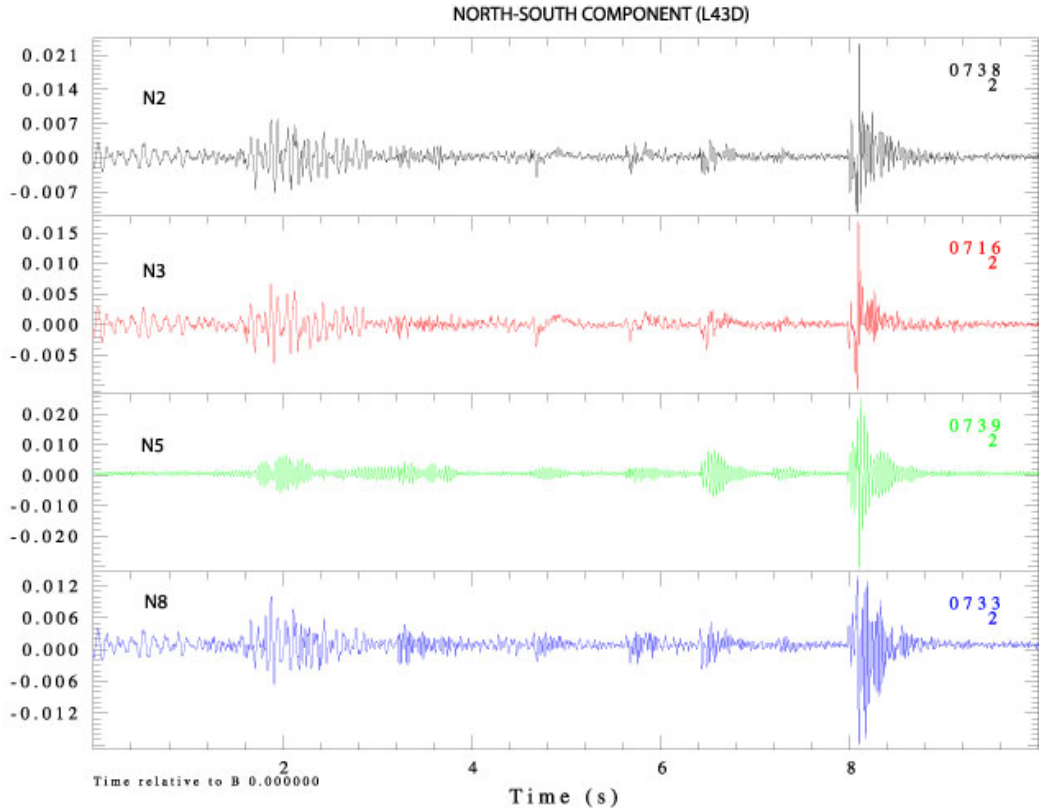

Figure 105. Near-source north/south L4-3D components.

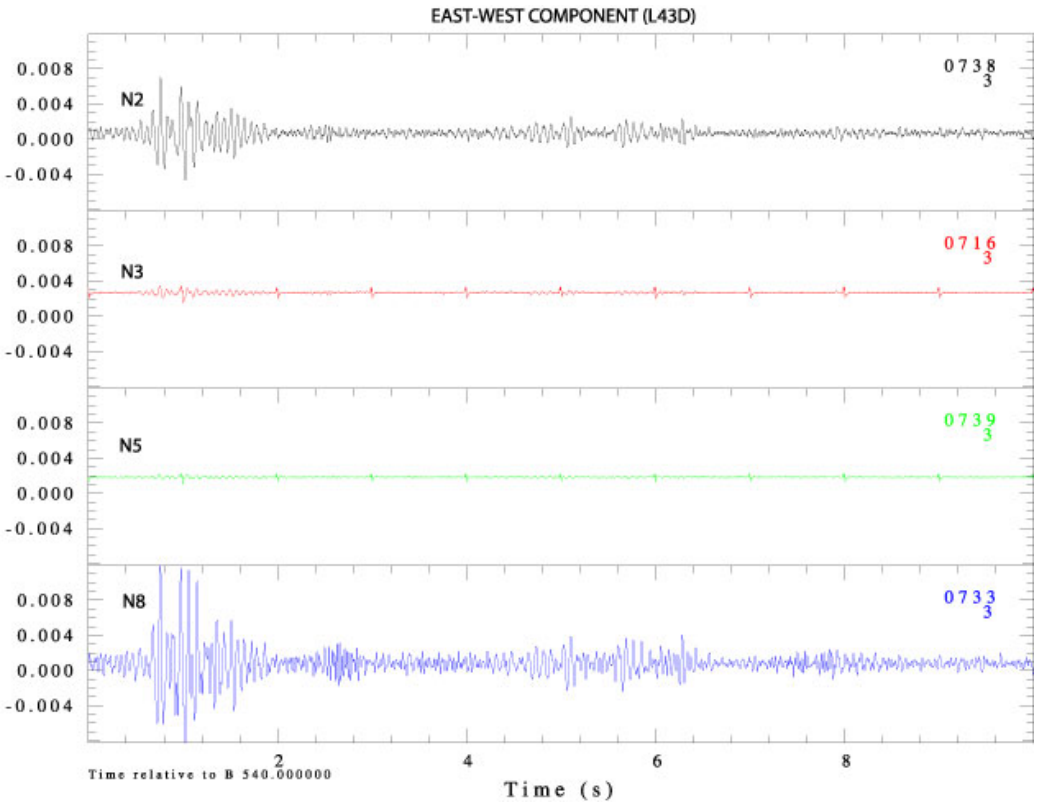

Figure 106. Near-source east/west L4-3D components.

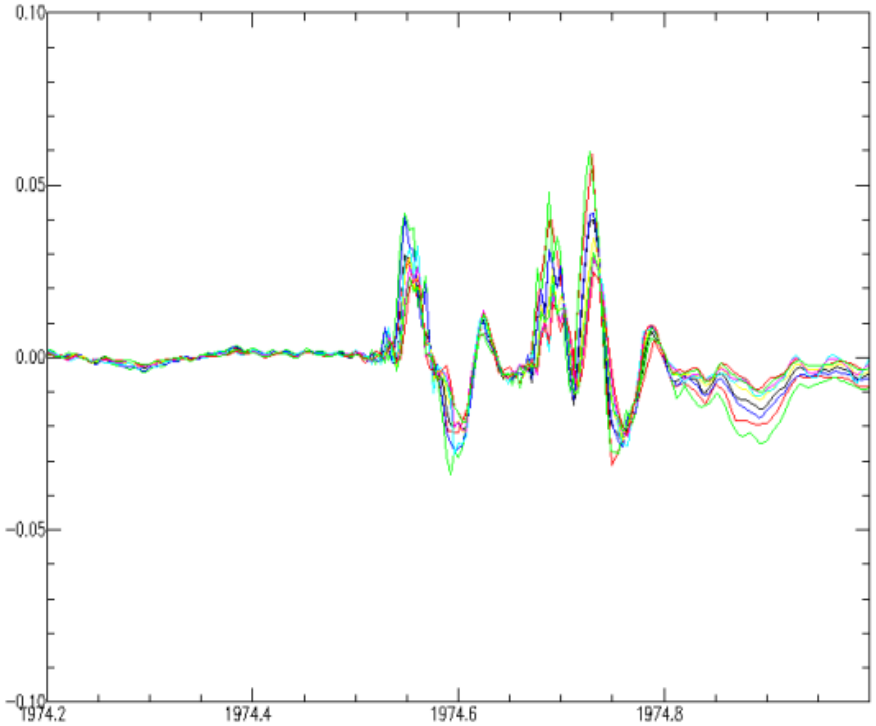

Figure 107. Weston L4-3D vertical component huddle data for all sensors.

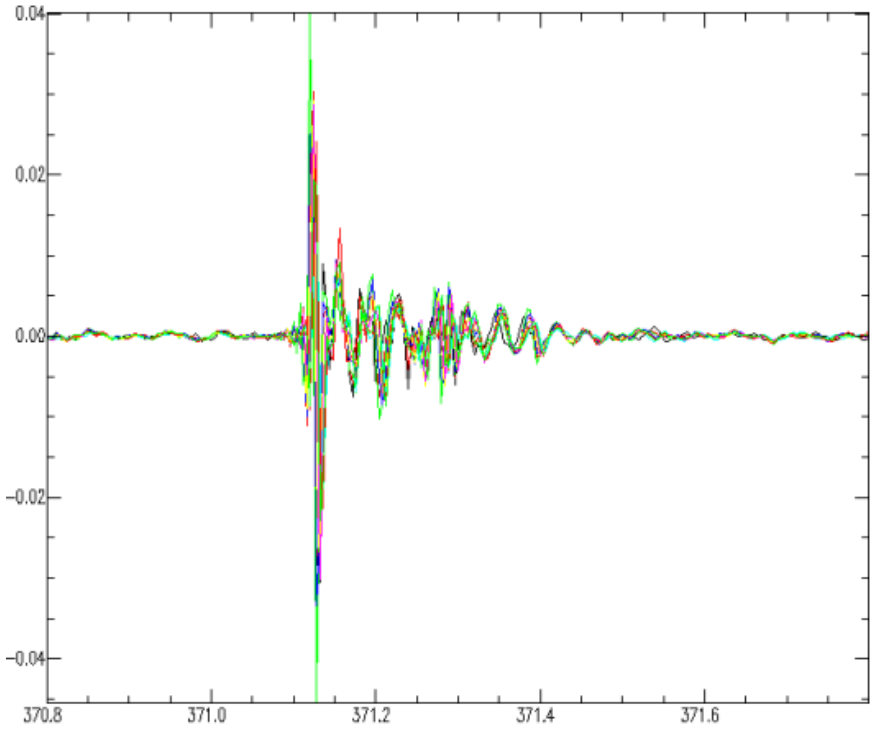

Figure 108. PASSCAL L22 vertical component huddle data for all sensors.

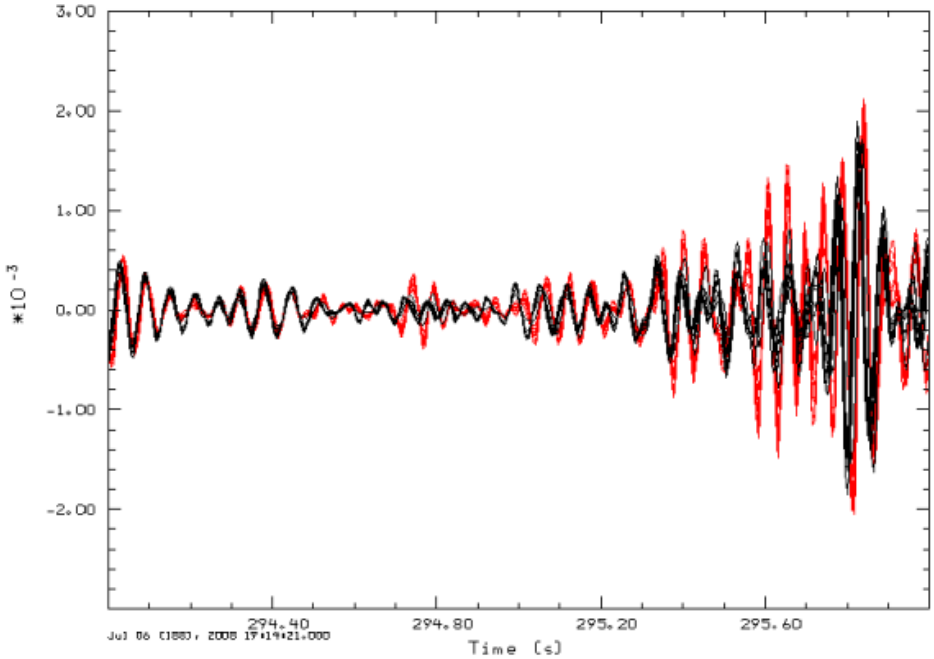

Figure 109. Comparison of Weston L4-3D (red) and PASSCAL L22 (black) vertical huddle data between 2 and 20 Hz after converting all data to velocity (cm/s).

APPENDIX B. PASSCAL L22 IN-SITU RESPONSE

Table 20. L22 Instrument Response.

Serial #	Channel	String	Frequency	Damping	Resistance	Sensitivity (V/cm/s)	Impedance	LoDrv Impedance	Distortion	Polarity	Leakage	GeoType
449L	1	Single	2.11	0.7	4501	0.893	5012.4	5017	0.05	0	0	L-22D-200804
449L	2	Single	2.07	0.728	4447	0.859	4989.2	4994	0	0	0	L-22D-200804
449L	3	Single	2.01	0.75	4442.6	0.935	4997.8	5002	0.17	0	0	L-22D-200804
459L	1	Single	2.17	0.765	4281	0.934	4927.1	4947	0.01	0	0	L-22D-200804
459L	2	Single	1.88	0.812	4300.9	0.872	4791.2	4795	0.12	0	0	L-22D-200804
459L	3	Single	2.1	0.702	4287.9	0.878	4787.9	4792	0.04	0	0	L-22D-200804
462L	1	Single	2.05	0.762	4344.1	0.919	4970.6	4975	0.08	0	0	L-22D-200804
462L*	2	Single	2.07	0.785	4392	0.9	5045	5049	0.14	0	0	L-22D-200804
462L*	3	Single	2.09	0.818	4403.9	0.989	5145.1	5150	0.14	0	0	L-22D-200804
479L	1	Single	2.23	0.633	4369.8	0.959	4946.2	4957	0.12	0	0	L-22D-200804
479L	2	Single	1.99	0.697	4258.8	0.806	4885.8	4894	0.55	0	0	L-22D-200804
479L	3	Single	1.97	0.804	4269.5	0.917	4884.3	4890	0.03	0	0	L-22D-200804
494L	1	Single	1.99	0.773	4532.2	0.906	5101.2	5105	0	0	0	L-22D-200804
494L	2	Single	2	0.752	4574	0.866	5074.8	5079	0	0	0	L-22D-200804
494L	3	Single	2.04	0.769	4489.7	0.938	5050.9	5056	0.23	0	0	L-22D-200804
496L	1	Single	1.96	0.745	4536	0.917	5026.7	5031	0.72	0	0	L-22D-200804
496L**	2	Single	-5.11	0.431	4470.6	1.194	4993.7	4998	0.03	0	0	L-22D-200804
496L	3	Single	2.01	0.727	4559.5	0.893	5058.5	5063	0.04	0	0	L-22D-200804
642L	1	Single	2.03	0.808	4465.7	0.99	5194.8	5199	0.36	0	0	L-22D-200804
642L	2	Single	2.02	0.818	4487.1	0.953	5161.3	5166	0.03	0	0	L-22D-200804
642L	3	Single	1.85	0.826	4340	0.844	4817.4	4822	0	0	0	L-22D-200804
643L	1	Single	2.13	0.733	4298.9	0.929	4919.5	4924	0	0	0	L-22D-200804
643L	2	Single	2.07	0.742	4169.7	0.915	4728.3	4733	0.18	0	0	L-22D-200804
643L	3	Single	2.5	0.623	4387.7	1.041	5073.2	5078	0.44	0	0	L-22D-200804
720L	1	Single	2.13	0.607	4434.1	0.89	4863.5	4869	0.33	0	0	L-22D-200804
720L	2	Single	2.32	0.683	4534.2	0.916	5188.1	5193	0.2	0	0	L-22D-200804
720L	3	Single	2.03	0.707	4299.3	0.939	4954.6	4960	0.46	0	0	L-22D-200804

*Note: For sensor 462L, channels 2 and 3 were swapped. This table reflects data as collected in the field and has not been modified to fix that problem.
** Response information for this channel appears incorrect.

APPENDIX C. WESTON GEOPHYSICAL L4-3D FACTORY REPSONSE

1. **General**
   - a) Serial Number: L41161
   - b) Tested at 78 ° F
   - c) Leakage to case >100 Megohms at 500 volts.

2. **Calibration Coils, In Series**
   - a) Resistance: 21.3 Ohms
   - b) Polarity: Negative voltage at socket A with respect to socket B when suspended mass moves toward to the case bottom

3. **Signal Coil (Vertical Detector)** Serial Number: L41171
   - a) Electrodynamic Constant: 7.09 V/in/sec
   - b) Resistance: 5652 Ohms
   - c) Calibration Constant: 40.1 KDynes/Ampere
   - d) Frequency (fo): 0.98 Hz
   - e) Open circuit damping (bo): 0.28 of critical damping
   - f) Suspended mass (m): 969.4 grams
   - g) Polarity: Negative voltage at socket E with respect to socket F when suspended mass moves toward to the case bottom

4. **Signal Coil (Longtitudinal Detector)** Serial Number: ∅508725
   - a) Electrodynamic Constant: 7.05 V/in/sec
   - b) Resistance: 5644 Ohms
   - c) Calibration Constant: 39.6 KDynes/Ampere
   - d) Frequency (fo): 0.96 Hz
   - e) Open circuit damping (bo): 0.285 of critical damping
   - f) Suspended mass (m): 969.9 grams
   - g) Polarity: Negative voltage at socket C with respect to socket D when suspended mass moves toward to the case bottom

5. **Signal Coil (Transverse Detector)** Serial Number: ∅508726
   - a) Electrodynamic Constant: 7.24 V/in/sec
   - b) Resistance: 5647 Ohms
   - c) Calibration Constant: 40.5 KDynes/Ampere
   - d) Frequency (fo): 0.99 Hz
   - e) Open circuit damping (bo): 0.274 of critical damping
   - f) Suspended mass (m): 968.4 grams
   - g) Polarity: Negative voltage at socket G with respect to socket H when suspended mass moves toward to the case bottom

Figure 110. L4-3D L41161 factory calibration specifications.

1. General

a)	Serial Number:	L41162	
b)	Tested at	76	° F
c)	Leakage to case	>100	Megohms at 500 volts.

2. Calibration Coils, In Series

a)	Resistance:	20.9	Ohms	
b)	Polarity: Negative voltage at socket	A	with respect to socket	B
	when suspended mass moves toward to the case bottom			

3. Signal Coil (Vertical Detector) Serial Number: L41172

a)	Electrodynamic Constant:	7.1	V/in/sec	
b)	Resistance:	5649	Ohms	
c)	Calibration Constant:	40.4	KDynes/Ampere	
d)	Frequency (fo):	0.98	Hz	
e)	Open circuit damping (bo):	0.287	of critical damping	
f)	Suspended mass (m):	966.8	grams	
g)	Polarity: Negative voltage at socket	E	with respect to socket	F
	when suspended mass moves toward to the case bottom			

4. Signal Coil (Longtitudinal Detector) Serial Number: 508727

a)	Electrodynamic Constant:	6.93	V/in/sec	
b)	Resistance:	5647	Ohms	
c)	Calibration Constant:	40.3	KDynes/Ampere	
d)	Frequency (fo):	0.98	Hz	
e)	Open circuit damping (bo):	0.288	of critical damping	
f)	Suspended mass (m):	971.3	grams	
g)	Polarity: Negative voltage at socket	C	with respect to socket	D
	when suspended mass moves toward to the case bottom			

5. Signal Coil (Transverse Detector) Serial Number: 508728

a)	Electrodynamic Constant:	7.27	V/in/sec	
b)	Resistance:	5645	Ohms	
c)	Calibration Constant:	39.2	KDynes/Ampere	
d)	Frequency (fo):	0.96	Hz	
e)	Open circuit damping (bo):	0.273	of critical damping	
f)	Suspended mass (m):	970.7	grams	
g)	Polarity: Negative voltage at socket	G	with respect to socket	H
	when suspended mass moves toward to the case bottom			

Figure 111. L4-3D L41162 factory calibration specifications.

1. **General**

a)	Serial Number:	L41163	
b)	Tested at	78	° F
c)	Leakage to case	>100	Megohms at 500 volts.

2. **Calibration Coils, In Series**

a)	Resistance:	20.2	Ohms	
b)	Polarity: Negative voltage at socket	A	with respect to socket	B
	when suspended mass moves toward to the case bottom			

3. **Signal Coil (Vertical Detector)** Serial Number: L41173

a)	Electrodynamic Constant:	7.14	V/in/sec	
b)	Resistance:	5638	Ohms	
c)	Calibration Constant:	41.4	KDynes/Ampere	
d)	Frequency (fo):	1	Hz	
e)	Open circuit damping (bo):	0.276	of critical damping	
f)	Suspended mass (m):	967.2	grams	
g)	Polarity: Negative voltage at socket	E	with respect to socket	F
	when suspended mass moves toward to the case bottom			

4. **Signal Coil (Longtitudinal Detector)** Serial Number: 508729

a)	Electrodynamic Constant:	7.29	V/in/sec	
b)	Resistance:	5636	Ohms	
c)	Calibration Constant:	41.2	KDynes/Ampere	
d)	Frequency (fo):	1.01	Hz	
e)	Open circuit damping (bo):	0.276	of critical damping	
f)	Suspended mass (m):	970.7	grams	
g)	Polarity: Negative voltage at socket	C	with respect to socket	D
	when suspended mass moves toward to the case bottom			

5. **Signal Coil (Transverse Detector)** Serial Number: 508730

a)	Electrodynamic Constant:	7.24	V/in/sec	
b)	Resistance:	5622	Ohms	
c)	Calibration Constant:	40.9	KDynes/Ampere	
d)	Frequency (fo):	1	Hz	
e)	Open circuit damping (bo):	0.275	of critical damping	
f)	Suspended mass (m):	966.7	grams	
g)	Polarity: Negative voltage at socket	G	with respect to socket	H
	when suspended mass moves toward to the case bottom			

Figure 112. L4-3D L41163 factory calibration specifications.

1. **General**
   a) Serial Number: L41164
   b) Tested at 79 ° F
   c) Leakage to case >100 Megohms at 500 volts.

2. **Calibration Coils, In Series**
   a) Resistance: 19.9 Ohms
   b) Polarity: Negative voltage at socket A with respect to socket B when suspended mass moves toward to the case bottom

3. **Signal Coil (Vertical Detector)** Serial Number: L41174
   a) Electrodynamic Constant: 7.26 V/in/sec
   b) Resistance: 5630 Ohms
   c) Calibration Constant: 41.5 KDynes/Ampere
   d) Frequency (fo): 0.99 Hz
   e) Open circuit damping (bo): 0.283 of critical damping
   f) Suspended mass (m): 974.5 grams
   g) Polarity: Negative voltage at socket E with respect to socket F when suspended mass moves toward to the case bottom

4. **Signal Coil (Longtitudinal Detector)** Serial Number: 508731
   a) Electrodynamic Constant: 7.28 V/in/sec
   b) Resistance: 5637 Ohms
   c) Calibration Constant: 39.2 KDynes/Ampere
   d) Frequency (fo): 0.96 Hz
   e) Open circuit damping (bo): 0.268 of critical damping
   f) Suspended mass (m): 971.6 grams
   g) Polarity: Negative voltage at socket C with respect to socket D when suspended mass moves toward to the case bottom

5. **Signal Coil (Transverse Detector)** Serial Number: 508732
   a) Electrodynamic Constant: 7.25 V/in/sec
   b) Resistance: 5636 Ohms
   c) Calibration Constant: 39.3 KDynes/Ampere
   d) Frequency (fo): 0.97 Hz
   e) Open circuit damping (bo): 0.283 of critical damping
   f) Suspended mass (m): 969 grams
   g) Polarity: Negative voltage at socket G with respect to socket H when suspended mass moves toward to the case bottom

Figure 113. L4-3D L41164 factory calibration specifications.

1. **General**
   a) Serial Number: L41165
   b) Tested at 78 ° F
   c) Leakage to case >100 Megohms at 500 volts.

2. **Calibration Coils, In Series**
   a) Resistance: 20.5 Ohms
   b) Polarity: Negative voltage at socket A with respect to socket B when suspended mass moves toward to the case bottom

3. **Signal Coil (Vertical Detector)** Serial Number: L41175
   a) Electrodynamic Constant: 7.05 V/in/sec
   b) Resistance: 5636 Ohms
   c) Calibration Constant: 41.2 KDynes/Ampere
   d) Frequency (fo): 0.98 Hz
   e) Open circuit damping (bo): 0.277 of critical damping
   f) Suspended mass (m): 970.2 grams
   g) Polarity. Negative voltage at socket E with respect to socket F when suspended mass moves toward to the case bottom

4. **Signal Coil (Longtitudinal Detector)** Serial Number: 508733
   a) Electrodynamic Constant: 7.21 V/in/sec
   b) Resistance: 5633 Ohms
   c) Calibration Constant: 39.6 KDynes/Ampere
   d) Frequency (fo): 0.98 Hz
   e) Open circuit damping (bo): 0.275 of critical damping
   f) Suspended mass (m): 972.5 grams
   g) Polarity: Negative voltage at socket C with respect to socket D when suspended mass moves toward to the case bottom

5. **Signal Coil (Transverse Detector)** Serial Number: 508734
   a) Electrodynamic Constant: 7.1 V/in/sec
   b) Resistance: 5613 Ohms
   c) Calibration Constant: 41.9 KDynes/Ampere
   d) Frequency (fo): 1 Hz
   e) Open circuit damping (bo): 0.274 of critical damping
   f) Suspended mass (m): 972.1 grams
   g) Polarity: Negative voltage at socket G with respect to socket H when suspended mass moves toward to the case bottom

Figure 114. L4-3D L41165 factory calibration specifications.

1. **General**
   a) Serial Number: L41166
   b) Tested at 79 ° F
   c) Leakage to case >100 Megohms at 500 volts.

2. **Calibration Coils, In Series**
   a) Resistance: 22 Ohms
   b) Polarity: Negative voltage at socket A with respect to socket B
   when suspended mass moves toward to the case bottom

3. **Signal Coil (Vertical Detector)** Serial Number: L41176
   a) Electrodynamic Constant: 7.15 V/in/sec
   b) Resistance: 5637 Ohms
   c) Calibration Constant: 40.2 KDynes/Ampere
   d) Frequency (fo): 0.98 Hz
   e) Open circuit damping (bo): 0.272 of critical damping
   f) Suspended mass (m): 969.3 grams
   g) Polarity: Negative voltage at socket E with respect to socket F
   when suspended mass moves toward to the case bottom

4. **Signal Coil (Longtitudinal Detector)** Serial Number: 508735
   a) Electrodynamic Constant: 7.33 V/in/sec
   b) Resistance: 5653 Ohms
   c) Calibration Constant: 39.7 KDynes/Ampere
   d) Frequency (fo): 1 Hz
   e) Open circuit damping (bo): 0.284 of critical damping
   f) Suspended mass (m): 971.9 grams
   g) Polarity: Negative voltage at socket C with respect to socket D
   when suspended mass moves toward to the case bottom

5. **Signal Coil (Transverse Detector)** Serial Number: 508736
   a) Electrodynamic Constant: 7.3 V/in/sec
   b) Resistance: 5646 Ohms
   c) Calibration Constant: 40.3 KDynes/Ampere
   d) Frequency (fo): 0.99 Hz
   e) Open circuit damping (bo): 0.273 of critical damping
   f) Suspended mass (m): 971.8 grams
   g) Polarity: Negative voltage at socket G with respect to socket H
   when suspended mass moves toward to the case bottom

Figure 115. L4-3D L41166 factory calibration specifications.

1. **General**

a)	Serial Number:	L41167	
b)	Tested at	81	° F
c)	Leakage to case	>100	Megohms at 500 volts.

2. **Calibration Coils, In Series**

a)	Resistance:	31.9	Ohms	
b)	Polarity: Negative voltage at socket	A	with respect to socket	B
	when suspended mass moves toward to the case bottom			

3. **Signal Coil (Vertical Detector)** Serial Number: L41177

a)	Electrodynamic Constant:	7.12	V/in/sec	
b)	Resistance:	5674	Ohms	
c)	Calibration Constant:	40.9	KDynes/Ampere	
d)	Frequency (fo):	1	Hz	
e)	Open circuit damping (bo):	0.28	of critical damping	
f)	Suspended mass (m):	971.6	grams	
g)	Polarity: Negative voltage at socket	E	with respect to socket	F
	when suspended mass moves toward to the case bottom			

4. **Signal Coil (Longtitudinal Detector)** Serial Number: 508737

a)	Electrodynamic Constant:	7.36	V/in/sec	
b)	Resistance:	5694	Ohms	
c)	Calibration Constant:	39.6	KDynes/Ampere	
d)	Frequency (fo):	0.99	Hz	
e)	Open circuit damping (bo):	0.279	of critical damping	
f)	Suspended mass (m):	972.8	grams	
g)	Polarity: Negative voltage at socket	C	with respect to socket	D
	when suspended mass moves toward to the case bottom			

5. **Signal Coil (Transverse Detector)** Serial Number: 508738

a)	Electrodynamic Constant:	7.13	V/in/sec	
b)	Resistance:	5676	Ohms	
c)	Calibration Constant:	41.6	KDynes/Ampere	
d)	Frequency (fo):	1	Hz	
e)	Open circuit damping (bo):	0.271	of critical damping	
f)	Suspended mass (m):	969.5	grams	
g)	Polarity: Negative voltage at socket	G	with respect to socket	H
	when suspended mass moves toward to the case bottom			

Figure 116. L4-3D L41167 factory calibration specifications.

1. **General**
   a) Serial Number: L41168
   b) Tested at 81 ° F
   c) Leakage to case >100 Megohms at 500 volts.

2. **Calibration Coils, In Series**
   a) Resistance: 22.4 Ohms
   b) Polarity: Negative voltage at socket A with respect to socket B
   when suspended mass moves toward to the case bottom

3. **Signal Coil (Vertical Detector)** Serial Number: L41178
   a) Electrodynamic Constant: 7.05 V/in/sec
   b) Resistance: 5646 Ohms
   c) Calibration Constant: 41.1 KDynes/Ampere
   d) Frequency (fo): 0.98 Hz
   e) Open circuit damping (bc): 0.289 of critical damping
   f) Suspended mass (m): 966.8 grams
   g) Polarity: Negative voltage at socket E with respect to socket F
   when suspended mass moves toward to the case bottom

4. **Signal Coil (Longtitudinal Detector)** Serial Number: Ø508739
   a) Electrodynamic Constant: 7.23 V/in/sec
   b) Resistance: 5676 Ohms
   c) Calibration Constant: 40.4 KDynes/Ampere
   d) Frequency (fo): 1 Hz
   e) Open circuit damping (bo): 0.266 of critical damping
   f) Suspended mass (m): 974.4 grams
   g) Polarity: Negative voltage at socket C with respect to socket D
   when suspended mass moves toward to the case bottom

5. **Signal Coil (Transverse Detector)** Serial Number: Ø508740
   a) Electrodynamic Constant: 7.25 V/in/sec
   b) Resistance: 5669 Ohms
   c) Calibration Constant: 41.8 KDynes/Ampere
   d) Frequency (fo): 1 Hz
   e) Open circuit damping (bo): 0.274 of critical damping
   f) Suspended mass (m): 971.3 grams
   g) Polarity: Negative voltage at socket G with respect to socket H
   when suspended mass moves toward to the case bottom

Figure 117. L4-3D L41168 factory calibration specifications.

1. **General**
   a) Serial Number: L41169
   b) Tested at 75 ° F
   c) Leakage to case >100 Megohms at 500 volts.

2. **Calibration Coils, In Series**
   a) Resistance: 23.8 Ohms
   b) Polarity: Negative voltage at socket A with respect to socket B
   when suspended mass moves toward to the case bottom

3. **Signal Coil (Vertical Detector)** Serial Number: L41179
   a) Electrodynamic Constant: 7.03 V/in/sec
   b) Resistance: 5594 Ohms
   c) Calibration Constant: 41 KDynes/Ampere
   d) Frequency (fo): 0.97 Hz
   e) Open circuit damping (bo): 0.28 of critical damping
   f) Suspended mass (m): 970 grams
   g) Polarity: Negative voltage at socket E with respect to socket F
   when suspended mass moves toward to the case bottom

4. **Signal Coil (Longtitudinal Detector)** Serial Number: Ø508741
   a) Electrodynamic Constant: 6.93 V/in/sec
   b) Resistance: 5672 Ohms
   c) Calibration Constant: 44.5 KDynes/Ampere
   d) Frequency (fo): 1 Hz
   e) Open circuit damping (bo): 0.257 of critical damping
   f) Suspended mass (m): 968.9 grams
   g) Polarity: Negative voltage at socket C with respect to socket D
   when suspended mass moves toward to the case bottom

5. **Signal Coil (Transverse Detector)** Serial Number: Ø508742
   a) Electrodynamic Constant: 7.23 V/in/sec
   b) Resistance: 5631 Ohms
   c) Calibration Constant: 41.1 KDynes/Ampere
   d) Frequency (fo): 1 Hz
   e) Open circuit damping (bo): 0.271 of critical damping
   f) Suspended mass (m): 972.7 grams
   g) Polarity: Negative voltage at socket G with respect to socket H
   when suspended mass moves toward to the case bottom

Figure 118. L4-3D L41169 factory calibration specifications.

1. General

a)	Serial Number:	L41170	
b)	Tested at	73	° F
c)	Leakage to case	>100	Megohms at 500 volts.

2. Calibration Coils, In Series

a)	Resistance:	23	Ohms	
b)	Polarity: Negative voltage at socket	A	with respect to socket	B
	when suspended mass moves toward to the case bottom			

3. Signal Coil (Vertical Detector) Serial Number: L41180

a)	Electrodynamic Constant:	L41180	V/in/sec	
b)	Resistance:	5600	Ohms	
c)	Calibration Constant:	41.1	KDynes/Ampere	
d)	Frequency (fo):	0.98	Hz	
e)	Open circuit damping (bo):	0.283	of critical damping	
f)	Suspended mass (m):	964.8	grams	
g)	Polarity: Negative voltage at socket	E	with respect to socket	F
	when suspended mass moves toward to the case bottom			

4. Signal Coil (Longtitudinal Detector) Serial Number: 0508743

a)	Electrodynamic Constant:	6.73	V/in/sec	
b)	Resistance:	5565	Ohms	
c)	Calibration Constant:	45.1	KDynes/Ampere	
d)	Frequency (fo):	1	Hz	
e)	Open circuit damping (bo):	0.257	of critical damping	
f)	Suspended mass (m):	972.8	grams	
g)	Polarity: Negative voltage at socket	C	with respect to socket	D
	when suspended mass moves toward to the case bottom			

5. Signal Coil (Transverse Detector) Serial Number: 0508744

a)	Electrodynamic Constant:	6.85	V/in/sec	
b)	Resistance:	5552	Ohms	
c)	Calibration Constant:	42.1	KDynes/Ampere	
d)	Frequency (fo):	0.98	Hz	
e)	Open circuit damping (bo):	0.283	of critical damping	
f)	Suspended mass (m):	972.2	grams	
g)	Polarity: Negative voltage at socket	G	with respect to socket	H
	when suspended mass moves toward to the case bottom			

Figure 119. L4-3D L41170 factory calibration specifications.

APPENDIX D. DATA RECORDS WITH HIGH NOISE OR CONTAMINATION

Near-source

No near-source data had issues with noise or signal contamination when the data were examined in a band pass of 1 to 20 Hz.

Short Period

The following short period stations had signal quality problems due to the listed issue when the data were examined in a band pass of 1 to 20 Hz. Filtering can help with noise issues.

Table 21. Short Period Data Quality Issues.

Shot 1	Shot 2	Shot 3	Shot 4	Shot 5
NE10-Noise	**NE08**-Car prior to shot arrival	**NE05**-Noise, possibly from lawn mower	**NE05**-Noise, possibly from lawn mower	**NE02**-Car prior to shot arrival
SE03-Noise	**NE09**-Car	**NE10**-Noise	**SE05**-Car?	**NE08**-Car
SE07-Noise	**SE05**-Car			
SE10-Noise	**SE09**-Car			
	SE10-Noise			

Texan

The following Texan stations had signal quality problems due to the listed issue when the data were examined in a band pass of 4 to 20 Hz. Filtering can help with noise issues.

Table 22. Texan Data Quality Issues.

Shot 1	Shot 2	Shot 3	Shot 4	Shot 5
ST11-Cont	**ST09**-Cont	**ST19**-Cont	**ST10**-Cont	**ST34**-Bad
ST20-Noise	**ST10**-Cont	**ST34**-Bad	**ST11**-Cont	**ST40**-Cont
ST22-Cont	**ST34**-Bad	**ST45**-Noise	**ST22**-Cont	**ST45**-Noise
ST23-Cont	**ST44**-Cont	**TN04**-Bad	**ST30**-Cont	**TN04**-Bad
ST34-Bad	**ST45**-Noise	**TN11**-Noise	**ST34**-Bad	**TN26**-Cont
ST40-Noise	**TN04**-Bad	**TN12**-Cont	**ST45**-Noise	**TN36**-Noise
ST41-Noise	**TN06**-Cont	**TN20**-Noise	**TN04**-Bad	**TN39**-Cont
ST42-Noise	**TN09**-Noise	**TN26**-Cont	**TN11**-Cont	**TN40**-Noise
ST43-Noise	**TN11**-Cont	**TN28**-Cont	**TN30**-Cont	
ST44-Noise	**TN30**-Noise	**TN39**-Cont	**TN38**-Cont	
ST45-Noise	**TN33**-Noise	**TN40**-Noise	**TN39**-Noise	
TN04-Bad	**TN34**-Cont		**TN40**-Noise	
TN11-Noise				
TN25-Cont				
TN28-Cont				
TN30-Noise				

TN32-Cont				
TN33-Noise				
TN40-Cont				

Noise=High noise levels; Cont=Contamination by other unspecified signals; Bad=Geophone or cable connection was bad

APPENDIX E. BLASTER'S LOG FOR 11 JULY 2008 PRODUCTION SHOT

GREEN MOUNTAIN EXPLOSIVES GME

UNIFORM BLASTER'S LOG

Location of Blast Rock of Ages — **GPS Information**

Street Address:		At shot
City: Barre VT		At protected structure
Date of Blast: 7-11-08	Time of Blast: 3:40 ☐ AM ☒ PM	Description of Blast: ☐ Construction ☐ Quarry ☐ Trench

Weather Conditions

Conditions: ☐ Cloudy ☒ Clear ☐ Rain ☐ Snow	Temperature: /Degrees F 80	Wind Velocity: /MPH and Direction:

Design Information

Face Height: /ft —	Over Burden: /ft 0'-2'	Burden: /ft 5'	Cubic yards 455
Type of Material Blasted: Granite	Hole Diameter: /in 3 1/2"	Spacing: /ft 5'	Tons: 1490
Hole Depth: /ft 7'-15'	Deck Stem: /ft —	Number of holes: 54 (78 Presplit)	lbs/yd³ 1.5
Sub Drill: /ft —	Type of Stemming: crushed stone	Collar Stem: /ft 5'-7'	Tons /Lb. 1.04
Blast Mat / Cover Used: none	Drill Co. Yankee	Face Direction:	Total Drill footage: 1001

Explosives Used

Type	1.	2.	3.	4.
	2 Boost	Presplit 2x6	Emgel 250 2x16	Emgel 250 2 3/4x16
Lbs.	54	55	220	990
Type	5.	6.	7.	8.
Lbs.				

Max. holes per 8ms delay: | Max. lbs.per 8ms delay: | Total lbs: 1349

Initiation System

Type of Initiation System ☐ Electric ☒ Non Electric ☐ Other: ☐ Sequential Machine ☐ CD ☐ Other:

ELECTRIC See attachments

Timer Setting Hole to Hole:	Nominal Cap Delay Hole to Hole:	Timer Setting Row to Row:	Cap Nominal Delay Row to Row:
Cap Delays per Circuit:	Number of Circuits:	OHMS: (Resistance each series or circuit)	

NON ELECTRIC (8 MS RULE) ☐ See attachments

Number of Rows:	7	Delay(s) parallel to free face along spacing:	12
Delay(s) Perpendicular to the face, in echelon or row to row:	7		

Nearest Protected Structure

Street Address:

Type of Structure:	Distance: /ft

Allowable Limits of Vibration

☐ OPTION 1 ☒ OPTION 2

Scaled Distance: ☐ 50 ☐ 55 ☐ 60 ☐ 65 ☐ Other:

(Conforms to M.G.L. c 14

Post-it® Fax Note 7671		Date 7/29	# of pages ▶ 1
To Jessie Bonner		From Don Murray	
Co./Dept.		Co.	
Phone #		Phone #	
Fax # 536 632 4226		Fax #	

List of Symbols, Abbreviations, and Acronyms

AFRL	Air Force Research Laboratory
ANFO	Ammonium Nitrate Fuel Oil Explosives
HANS	Hanscom Air Force Base Seismo-Acoustic Array
LANL	Los Alamos National Laboratory
NEDE	New England Damage Experiment
NEIC	National Earthquake Information Center
NESN	New England Seismic Network
PASSCAL	Program for Array Seismic Studies of the Continental Lithosphere
USGS	United States Geological Survey